AD________________

AWARD NUMBER: DAMD17-03-1-0067

TITLE: Microlocalization and Quantitation of Risk Associated Elements in Gleason Graded Prostate Tissue

PRINCIPAL INVESTIGATOR: Curtis D. Eckhert, Ph.D.

CONTRACTING ORGANIZATION: University of California
Los Angeles, California 90024

REPORT DATE: March 2006

TYPE OF REPORT: Annual

PREPARED FOR: U.S. Army Medical Research and Materiel Command
Fort Detrick, Maryland 21702-5012

REPORT DOCUMENTATION PAGE

Form Approved OMB No. 0704-0188

1. REPORT DATE *(DD-MM-YYYY)*	**2. REPORT TYPE**	**3. DATES COVERED** *(From - To)*
01-03-2006	Annual	1 Mar 2005 – 28 Feb 2006

4. TITLE AND SUBTITLE

Microlocalization and Quantitation of Risk Associated Elements in Gleason Graded Prostate Tissue

5a. CONTRACT NUMBER

5b. GRANT NUMBER
DAMD17-03-1-0067

5c. PROGRAM ELEMENT NUMBER

6. AUTHOR(S)

Curtis D. Eckhert, Ph.D.

E-Mail:

5d. PROJECT NUMBER

5e. TASK NUMBER

5f. WORK UNIT NUMBER

7. PERFORMING ORGANIZATION NAME(S) AND ADDRESS(ES)

University of California
Los Angeles, California 90024

8. PERFORMING ORGANIZATION REPORT NUMBER

9. SPONSORING / MONITORING AGENCY NAME(S) AND ADDRESS(ES)
U.S. Army Medical Research and Materiel Command
Fort Detrick, Maryland 21702-5012

10. SPONSOR/MONITOR'S ACRONYM(S)

11. SPONSOR/MONITOR'S REPORT NUMBER(S)

12. DISTRIBUTION / AVAILABILITY STATEMENT
Approved for Public Release; Distribution Unlimited

13. SUPPLEMENTARY NOTES

14. ABSTRACT

The objective of this proposal was to determine the concentration and location of elements in normal and tumor tissue. Specific aims included: (1) preparation of Gleason graded prostate tissue, (2) determination of tissue concentrations of: B, Ca, Cd, Se and Zn; and (3) determination of tissue and cellular distribution of these elements using a NanoSIMS ion microscope at Lawrence Livermore National Laboratory (LLNL). Completion of specific aims 1, 2 showed that the concentrations of the elements did not correlate with Gleason status. They also showed that B was unique in its variability. Aim 3 was accomplished in part, but imaging was impaired by ice crystal formation. We made progress in the 3rd year in both methodology to improve samples resolution and identifying subcellular B targets for B as a way around the resolution problem. These included: (1) Slam freezing samples to -196oC followed by vacuum dehydration <-80oC to avoid ice crystal formation and identification of two potential subcellular proteins CD38 on the plasma membrane and the ryanodine receptor on the endoplasmic reticulum.

15. SUBJECT TERMS
boron, selenium, zinc, calcium, cobalt, cancer prevention, risk factors

16. SECURITY CLASSIFICATION OF:			**17. LIMITATION OF ABSTRACT**	**18. NUMBER OF PAGES**	**19a. NAME OF RESPONSIBLE PERSON**
a. REPORT	**b. ABSTRACT**	**c. THIS PAGE**			USAMRMC
U	U	U	UU	54	**19b. TELEPHONE NUMBER** *(include area code)*

Table of Contents

Introduction

There is growing evidence that the elements boron, selenium and zinc reduce PCa risk whereas calcium and cadmium increase risk (1-12). The objective of this proposal was to determine if these elements differ in concentration and location between normal and tumor tissue and thus identify a fundamental underpinning of chemoprevention. Pathologically graded human prostate was analyzed to determine the elemental concentrations in these tissues and their relationship with Gleason scores. The results showed no significant differences in gross concentrations and Gleason scores (13). However, the variability of the element boron (B) was intriguing and so the chemopreventative properties of B were examined in human prostate cell lines resulting in a number of reportable outcomes (14-24). These studies showed B had strong chemopreventative properties and this was extended to populations using an ecological study (24). Analyzing the intracellular location of the elements was the most difficult task. The art and science of biological sample preparation for NanoSIMS analysis is primitive, but images were obtained that showed the elements were compartmentalized within cells. We are continuing to work with scientists at the Lawrence Livermore National Laboratory NanoSIMS microscopy to improve the resolution. A no-cost time extension has allowed this work to continue.

Research Accomplishments

Task 1. To identify and maintain a series of progressively dedifferentiated samples.

Accomplishments Project year 1: Unmatched and matched sets of normal and tumor prostate tissue were collected from the UCLA Human Tissue Research Center. Unmatched samples were used to establish the methods for elemental analysis. We had to use normal tissue from men with cancer because samples of normal tissue from normal men are nearly none existent. The vast majority of tissue samples available have Gleason scores in the range from 6 to 7.

Task 2. To utilize state of the art inductive coupled plasma mass spectrometry to determine the concentration of the B,Ca, Cd, Se and Zn in whole tissue samples. .

Accomplishments Project year 2: We analyzed matched pairs of normal and tumor tissue to determine the concentrations of B, Ca, Cd, Se and Zn in 23 different male donors. The mean, median, range and coefficient of variation of the concentrations are given in Table 1.

Table 1. Elemental Concentrations of Normal and Tumor Prostate Tissue in 23 Men						
Normal		Boron	Cadmium	Calcium	Selenium	Zinc
		ng/g	ng/g	μg/g	ng/g	μg/g
	Mean	291	71	313	471	86
	Median	90	58	300	480	73
	Range	28 - 3530	8 - 220	82 - 830	200 - 730	9 - 190

	Std Error	159	10	36	24	11
	CV	256%	66%	56%	25%	63%
Tumor						
	Mean	355	83	263	502	88
	Median	100	61	270	520	84
	Range	23 - 2360	20 - 250	80 - 430	15 - 820	110-180
	Std Error	129	12	18	34	9
	CV	170%	70%	33%	33%	50%

The concentrations in both normal and tumor tissue ranked as follows: Ca > Zn > Se > B > Cd. A statistical comparison of elemental concentrations in normal and tumor tissue did not reveal significant differences (Table 2). The coefficient of variation of the elements varied greatly between elements (Table 1). The magnitude of variation followed the same rank in normal and tumor tissue: B > Cd > Zn > Ca > Se. The high variation in boron concentrations was not expected. Boron is not known to activate or covalently bind to proteins. It's variability and 10 fold range in concentration suggests that prostate is able to accumulate boron. Examination of tissue using the NanoSIMS ion probe will determine where this occurs for boron and the other elements.

Table 2. Statistical Evaluation of Elemental Concentrations in Matched Normal and Tumor Tissue	
Element	Statistical Comparison between Normal and Tumor Tissue
Boron[1]	$p = 0.31$
Calcium[1]	$p = 0.46$
Cadmium[1]	$p = 0.58$
Selenium[1]	$p = 0.21$
Zinc[2]	$p < 0.09$

We then determined the strength of the relationship between whole tissue elemental concentrations and pathological tissue classification will be determined by statistical analysis.

Accomplishments: Table 3 shows there was no relationship between Gleason score and the concentration of any element.

Table 3. Statistical Evaluation of the Relationship between Gleason Scores and Elemental Concentrations in Tumor Tissue	
Element	Correlation Coefficient of Gleason Score versus Element Concentration

Boron[1]	R = 0.10
Calcium[1]	R = 0.13
Cadmium[1]	R = 0.08
Selenium[1]	R = 0.30
Zinc[2]	R = 0.21

Each of these elements had been positively or negatively associated with prostate cancer risk, but this did not show up as concentration differences at the gross tissue level. We were concerned that the variability may have come from dye contamination used in the Clinical Pathology Laboratory to mark regions of the organ. Dyes are applied to the outside of the prostate gland by clinical pathology laboratories to mark regions for technicians that subsequently prepare the gland for evaluation and Gleason grading. We analyzed the elemental composition of the three dyes used at UCLA. The results of triplicate measurements is given in the table below and show that element concentrations were too low to be a significant variable.

Table 4. Concentrations of elements in Pathology Laboratory Dyes

Clinical Pathology Marker Dye	Boron ng/g	Cadmium µg/g	Calcium µg/g	Selenium µg/g	Zinc µg/g
Black	ND; ND; ND	ND; ND; 4	ND; 17; 16	ND; ND; ND	ND; ND; ND
Blue	ND; ND; ND	0.37; 0.39; 0.4	41; 39; 40	0.42; 0.34; 0.37	1.6; 1.5; 1.6
Yellow	ND; ND; ND	ND; ND; ND	ND; ND; ND	ND; ND; ND	ND; ND; ND
Limit of Detection	60	0.002	10	0.2	0.3
LD = limit of detection; ND = not detectable					

The source of the variability is most likely due to natural biological variability.

Task 3. To determine the microlocation and microconcentrations of B, Ca, Cd, Se and Zn in graded series of samples.

Accomplishments (project years 2 and 3): The NanoSIMS ion microscope was installed at Lawrence Livermore in the Fall of 2004 and the two scientists who ran it worked with us to obtain images of the elements in prostate cells. Ion imaging of elements within prostate cells was accomplished using the ion microscope (NanoSIMS 50) located in the Analytical and Nuclear Chemistry Division of the Lawrence Livermore National Laboratory.

An very good image of human prostate epithelial cells taken by the NanoSIMS instrument is shown in figure 1. The image shows two cells with their dark elliptical nuclei and light nucleoli in the center of the cells. The This image maps the location of molecules with C-N polyatoms as a ratio of C atoms using dark to light shading to indicate increasing concentration. The concentration scale is shown in bar at the right of the image. The scale bar of 2 μm is at the bottom left.

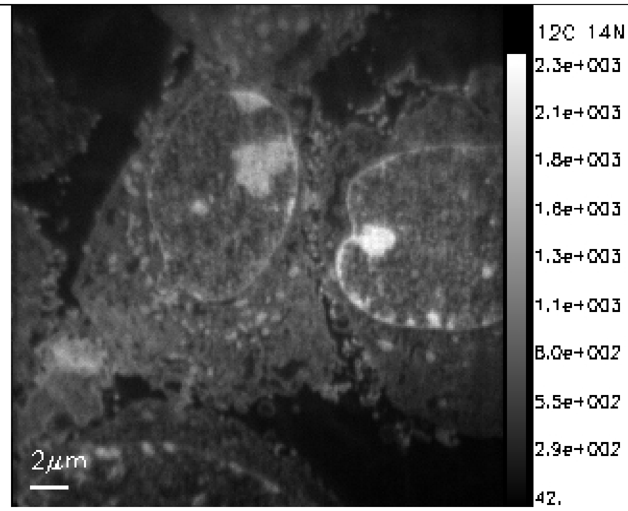

Figure 1. The light areas represent the origin of secondary carbon-nitrogen polyatomic ions sputtered from the sample by primary cesium ions rostered across the cells. The C-N atoms, which represent protein, are at their highest levels around the nucleus and within the nucleolus. The numbers to the right of the image indicate C-N polyatoms/per C atom emitted from the same region.

Problems:

Methodological advances in the field of biological imaging using dynamic secondary ion mass spectrometry have been slow because few instruments exist, the instruments in use are experimental, and method applications for animal tissue have not been perfected. Two NanoSIMS instruments exist in the U.S. and one is in use in Europe. To our knowledge, our application for use in studying prostate cancer is the only biomedical application focused on a human disease. In order to accomplish Task 3 we have had to work on the development of methods keep the subcellular structure intact for ion microscopy. This is not a problem in traditional electron microscopy because it does not image ions, as so does not need to preserve membrane structure.

Our initial approach to was to preparing cells and tissues was to use a Leica EM MM80 slam freezer to ultra-rapidly freeze prostate tissue and a Thermo Neslab CC-100 cold probe to regulate the dehydration phase. Briefly, the Leica slam freezer was prechilled by filling with liquid nitrogen. The tissue was slam frozen and transferred to a Dewar containing acetone chilled to – 83^{o}C. The temperature of the acetone bath was controlled using the Thermo Neslab CC-100 probe and refrigeration unit. Samples were slowly dehydrated and brought to room temperature over a period of 72 hours. The dehydrated tissue was fixed in osmium and embedded in Spurr Low Viscosity Resin. This procedure appeared successful using cultured prostate cells and the preparations looked good when evaluated by scanning electron microscopy. However, examination by NanoSIMS showed ion flow across membranes. We therefore turned to develop methods to fix and dehydrate cells and tissues without the use of membrane damaging agents.

The major obstacle in sample preparation without the use of acetone is the formation of ice crystals that disrupted subcellular architecture. If tissues are dropped into liquid nitrogen temperature conductance through the tissue is inefficient and crystals form before the tissue temperatures drop below -80^{o}C. We were successful in using slam freezing to prevent this. However, ice crystals also form when water is not removed before samples are brought back to room temperature, the temperature of the NanoSIMS instrument. We have purchased a Turbo Freeze Drier that holds sample temperatures down to -140^{o}C under vacuum during the warm-up phase when samples cross the -80^{0}C barrier a second time. We continue to work with scientists at Lawrence Livermore to perfect our technique.

Another problem was the need to change ion probes in the NanoSIMS instrument required removing the sample. This resulted in a loss of orientation in cells between ion measurements. This problem has been addressed by a reconfiguration of the NanoSIMS instrument at Lawrence Livermore. The goal is to have adjacent cross sections of a sample that can be evaluated using both electron microscopy and NanoSIMS so that the ion maps can be overlaid on electron micrographs. This would provide the best imaging of structure and ion concentrations.

During project year 3, the French group headed by Dr Croisy was successful in the development of a new approach that may provide a-work-around to the resolution problem in NanoSIMS imaging of biological material. This new approach requires knowledge of molecules that interact with the elements of interest. In 2005, Dr. Croisy and colleagues at the Laboratoire de Microscope Ionique, Institut Curie Recherche in Cedex France reported the successful subcellular localization of stable isotope labeled proteins using NanoSIMS (24). This approach was exciting and we moved quickly to identify proteins for B since next to Se, this element is the most promising for chemoprevention of prostate cancer.

In working on task 3 we have expanded our knowledge of boron biochemistry in several ways that are important for the development of fundamental underpinnings of cancer control. We previously determined that the plasma form of B, boric acid, inhibits the growth of prostate tumor cells at concentrations about 10 fold lower than non-tumor cells (16). This suggested to us that B localizes to targets that differ in structure or function in tumor and non-tumor cells. In determined that boric acid inhibits the release of calcium from the endoplasmic reticulum (19). We sought to determine if this could be explained by boric acid interfering with either the ADP-ribosyl cyclase active site of the multifunctional ectoenzyme CD38 present on the plasma membrane of prostate cancer cells or the ryanodine receptor on the endoplasmic reticulum, both proteins in the NAD/cADPR calcium release pathway (19). This year we demonstrated that boric acid is a competitive inhibitor of ADP-ribosyl cyclase using purified enzyme from *Aplasia* (21). We have preliminary evidence that boric acid inhibits ryanodine induced calcium release, but have not completed the kinetic analysis. Both these proteins offer opportunities for stable isotope labeling and co-localization of B with the NanoSIMS instrument. A “no cost time extension” was requested and approved to support the collaborative effort with the Lawrence Livermore NanoSIMS team to continue to work to obtaining high resolution image of B using direct imaging and stable isotope labeled proteins. A diagram of the NAD/cADPR calcium release pathway is provided in figure 2.

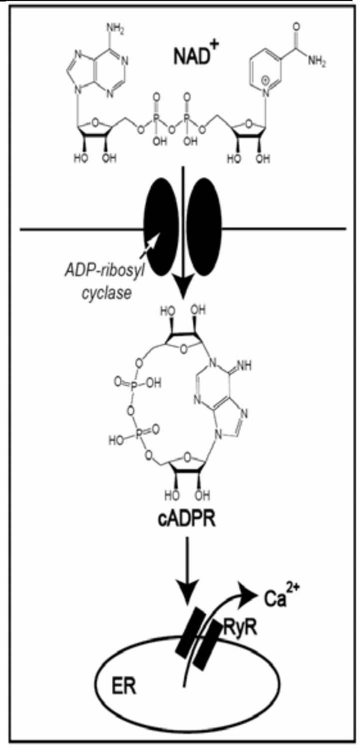

Figure 2. At physiological pH boron exists in human plasma as boric acid and inhibits the release of intracellular calcium from the endoplasmic reticulum. The cell cycle is stimulated by cell calcium release. We have reported that boric acid binds to the two ribose sugars of NAD^+ and the cyclic nucleotide cADPR. (Kim et al. 2004, 2006). Prostate cells have an extracellular enzyme called CD38 that contains 3 active sites. One site has ADP ribosyl cyclase activity and converts NAD^+ into cADPR an intracellular signaling molecule for calcium release. During the third project year we determined that boric acid inhibits purified Aplysia cyclase by non-competitive inhibition. We are in the process of determining if boric acid also inhibits the ability of agonists to activate the ryanodine receptor (RyR). This could also dampen the release of Ca^{+2} from the endoplasmic reticulum and inhibit cell proliferation. Preliminary results suggest that inhibition of RyR occurs at physiological concentrations of boric acid. It thus appears that RyR is a natural target protein for B. (Illustration from Kim et al. *J Chromatography A*, 2006)

Ecological Mapping of Se, B and Prostate Cancer

The data generated in this grant raised the possibility that the geographic disparity in prostate cancer incidence is in part due to difference in B exposures. We conducted an ecological study to assess if this was correct. For this we mapped the incidence and mortality of prostate cancer for Planning Regions in the State of Texas against the B concentrations of ground water for the same regions (23). In Texas, 60% of the drinking water comes from groundwater. Figure 3 shows a strong protective effect of boron exposure on both prostate cancer incidence and mortality.

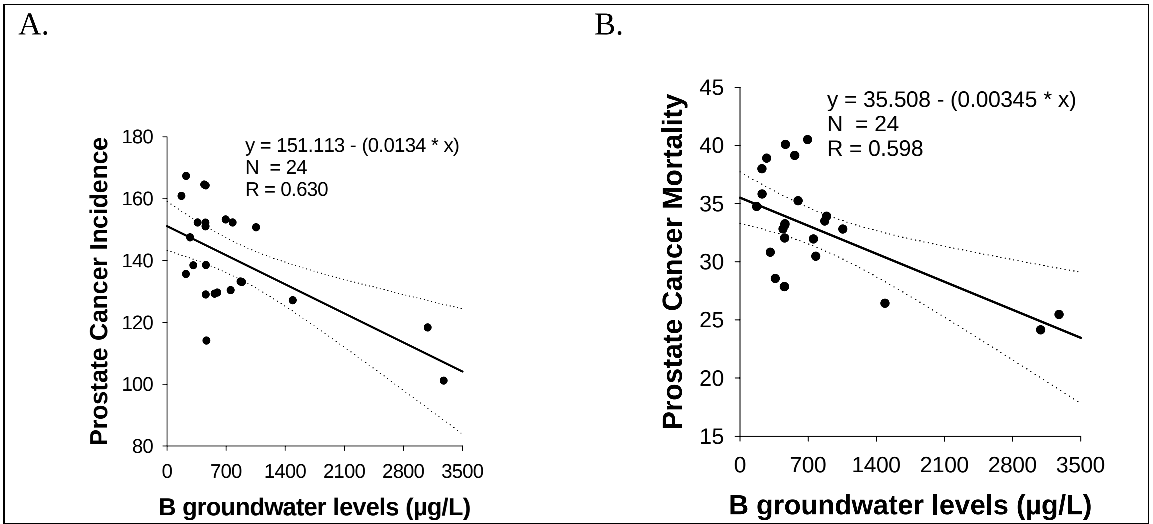

Figure 3. Incidence (A) and mortality (B) was plotted as a function of B groundwater levels for all Texas State Planning Regions. Dotted lines indicate 95% confidence intervals. Barranco, Hudak and Eckhert. *Cancer Causes Control*, In Press.

This strong inverse correlation between prostate cancer incidence and mortality is a very important discovery in the field of cancer prevention and one that could not have been predicted. Importantly, our progress at the ecological level is complemented by progress at the cellular level, thanks to this grant. Through a combination of imaging and biochemistry we have very high expectations that the underpinnings of part of the large geographical disparity in the occurrence in prostate cancer around the world can be explained at the molecular level.

KEY RESEARCH ACCOMPLISHMENTS

- Successful procurement of Gleason graded tissue classified as normal, Gleason grades 3, 5, 6, 7, 8.
- Analysis of matched sets of normal and tumor tissue obtained from 23 different men for the elements, boron, calcium, cadmium, selenium and zinc.
- Statistical analysis showed no difference between normal and tumor concentrations of these elements at the gross tissue level.
- Development of methods for NanoSIMS analysis for localizing elements within prostate cells.
- First ion microscope images of prostate cells obtained using the NanoSIMS instrument at Lawrence Livermore National Laboratory
- Progress made toward improving the preparation of prostate cells for higher resolution of the subcellular location of elements.
- Observed a 10 fold range of boron concentration in prostate tissue suggested the element differed significantly between individual men and maybe related to the risk of prostate cancer.
- Two potential molecular targets for B were identified in human prostate cells.
- Evaluation of the ecological and in vitro effects of boron on prostate cancer risk demonstrated that the incidence and mortality of prostate cancer in the Texas is

high correlated with groundwater B levels. This is a very significant observation in the field of cancer control.

REPORTABLE OUTCOMES

Manuscripts and Abstracts

Barranco WT, Stella Jr SL, Kim DH and Eckhert CD. NAD^+ and $NADP^+$-induced intracellular Ca^{2+} release in DU-145 prostate cancer cells and inhibition by boric acid. Submitted.

Barranco WT, Hudak PF and Eckhert CD. Evaluation of ecological and in vitro effects of boron on prostate cancer risk. *Cancer Causes Control*. In Press.

Kim DH, Que Hee S, Norris A, Faull KF and Eckhert CD. Boric acid inhibit ADP-ribosyl cyclase non-competitively. *J. Chromatography A.* 1115:246-252, 2006.

Barranco WT and Eckhert CD. Cellular changes in boric acid-treated DU-145 prostate cancer cells. *Brit J. Cancer* 94:884-890, 2006.

Henderson K and Eckhert CD. Boric acid induces ER stress in DU-145 and LNCAP prostate cancer cell lines. *Soc. Tox*. 2006.

Barranco WT and Eckhert CD. Inhibition of DU-145 Prostate Cancer Cell Proliferation by Boron and Selenium is Additive. *FASEB J.* 2005.

Barranco W.T. and Eckhert C.D. Boric acid inhibits human prostate cancer cell proliferation. *Cancer Letters* 216:21-29, 2004.

Kim D. H. S., Faull K. F., Norris A. J., Eckhert C. D. Borate-nucleotide complex formation depends on charge and phosphorylation state. *J. Mass Spectrometry* 39:743-751, 2004.

Barranco, W.T. Eckhert, C.D. Boric acid acts as a cADPR / RyR antagonist during inhibition of human prostate cancer cell proliferation. *FASEB J.* 2004; 18:A351.2 (352.2).

Kim, D.H, Faull, K.F., Eckhert, C.D. Determination of borate complex with cyclic ADP-ribose (cADPR) by electrospray ionization mass spectrometry (ESI-MS) *FASEB J.* 2004; 18: A351.4 (351.4).

Eckhert, C.D. Concentration and variation of boron, selenium and elements associated with cancer risk in non-tumor human prostate tissue. *FASEB J.* 2004; 18:A351.3 (351.3).

Employment and Research Opportunities

Support was provided for research training of the following students:

Kim Henderson (currently a Ph.D. working on imaging elements using the NanoSIMS ion microscope at Lawrence Livermore)
Joey Miller (currently a medical student)
Wade Barranco (currently a Post-doc at the Cancer Center at Southwestern Medical School in Houston, TX)
Danny Kim (Post-doc, UCLA)

Grants and Clinical Trial

Support provided data for an NIH R01 grant current under review by the NCI

Support provided data for the design of a Clinical Trial to examine the chemoprotective effect of boron on men at risk for prostate cancer. This is currently under review.

CONCLUSIONS

The project was designed to determine the relationship between elemental concentrations and the risk of prostate cancer. Our findings do not support a direct relationship between gross elemental concentrations in prostate tissue and pathological grading. The application of NanoSIMS technology to image the subcellular location of ions has taken longer than expected. The NanoSIMS instrument is an experimental instrument and there were many technical problems in setting it up at Lawrence Livermore. The post 9-11 requirement for increased security also delayed our access to the instrument. Finally, the absence of standard method for the preparation of biological material has resulted in much of the effort on Task 3 being devoted to methods development and optimizing the NanoSIMS instrument for our study. To get around this problem we have focused on identifying proteins that are involved in boron's a chemopreventative effect. We have been able to identify two proteins that may be labeled with stable isotopes and mapped along with B using the NanoSIMS. We have also conducted an ecological study using Cancer Registry and groundwater B data to map the occurrence of prostate cancer across the State of Texas. The results showed a strong inverse correlation between B and both incidence and mortality. This is a major observation in the field of cancer control and together with information from the co-mapping of B and proteins involved in its function will provide new fundamental knowledge in the field of cancer prevention.

References

1. Chan, JM, Stampfer MJ, Ma J, Gann, PH, Gaziano JM, Giovannucci EL. 2001. Dairy products, calcium, and prostate cancer risk in the Physicians' Health Study. Am. J. Clin Nut. 74:549-554.
2. Clark LC, Combs F, Turnbull BW, Slate EH, Chalker DK, et al. 1996. Effects of selenium supplementation for cancer prevention in patients with carcinoma of the skin. A randomized controlled trial. Nutritional Prevention of Cancer Study Group. JAMA 276:1957-63.
3. Coffey DS. New insights and methodologies are needed to solve the many epidemiologic enigmas of prostate cancer. 2001. Epidemiologic Reviews 23, 1)
4. Feustel A, Wennrich R, Steiniger D, Klauss P. 1982. Zinc and cadmium concentrations in prostatic carcinoma of different histological grading in comparison to normal prostate tissue and adenofibromyomatosis (BPH) Uro Res 10:301-303.
5. Feustel A, Wennrich R. 1984 Zinc and cadmium in cell fractions of prostatic cancer tissues of different histological grading in comparison to BPH and normal prostate. Urol Res 12:147-50.
6. Greenwald P. 2001. Clinical trials of breast and prostate cancer prevention. J. Nutr.131:176S-178S.
8. Hayes RB. 2001. Gene-Environmental interrelations in prostate cancer. Epidemiologic Rev. 23: 163-172.

9. Kantoff PW, Febbo PG, Giovannucci E, Krithivas K, Dahl DM, et al. 1997. Cancer Epidemio. Biomarkers Prev. 6, 189-92.
10. Lindegaard PM, Hansen SO, Christensen JEJ, Andersen BB, Andersen O. 1989. The distribution of cadmium with the human prostate. Bio. Trace Ele Res 25:97-104.
11. Oldereid NB, Thomassen Y, Purvis K. 1998. Selenium in human male reproductive organs. Human Repro. 13:2172-76.
12. Tvedt KE, Kopstad G, Haugen OA Halgunset J. 1987. Subcellular concentrations of calcium, zinc, and magnesium in benign nodular hyperplasia of the human prostate: X-ray microanalysis of freeze-dried cryosections. Cancer Res 47:323-328.
13. Zhang Z-F, Winton MI, Rainey C Eckhert CD. 2001. Boron is associated with decreased risk of human prostate cancer. FASEB J 15:A834.4.
14. Eckhert, C.D. Concentration and variation of boron, selenium and elements associated with cancer risk in non-tumor human prostate tissue. *FASEB J.* 2004; 18:A351.3 (351.3).
15. Cui Y. Winton M.I., Zhang, Z.F, Rainey C., Marshall J., deKernion J. B., Eckhert, C.D. Dietary Boron Intake and Reduced Risk of Prostate Cancer. *Oncology Reports* 11:887-892, 2004.
16. Barranco W.T. and Eckhert C.D. Boric acid inhibits human prostate cancer cell proliferation. *Cancer Letters* 216:21-29, 2004.
17. Kim D. H. S., Faull K. F., Norris A. J., Eckhert C. D. Borate-nucleotide complex formation depends on charge and phosphorylation state. *J. Mass Spectrometry* 39:743-751, 2004.
18. Barranco WT and Eckhert CD. Inhibition of DU-145 Prostate Cancer Cell Proliferation by Boron and Selenium is Additive. *FASEB J.* 2005.
19. Barranco, W.T. Eckhert, C.D. Boric acid acts as a cADPR / RyR antagonist during inhibition of human prostate cancer cell proliferation. *FASEB J.* 2004; 18:A351.2 (352.2).
20. Kim, D.H, Faull, K.F., Eckhert, C.D. Determination of borate complex with cyclic ADP-ribose (cADPR) by electrospray ionization mass spectrometry (ESI-MS) *FASEB J.* 2004; 18: A351.4 (351.4).
21. Kim DH, Que Hee S, Norris A, Faull KF and Eckhert CD. Boric acid inhibit ADP-ribosyl cyclase non-competitively. *J. Chromatography A.* March, 2006.
22. Barranco WT and Eckhert CD. Cellular changes in boric acid-treated DU-145 prostate cancer cells. *Brit J. Cancer* 94:884-890, 2006.
23. Henderson K and Eckhert CD. Boric acid induces ER stress in DU-145 and LNCAP prostate cancer cell lines. *Soc. Tox*. 2006.
24. Barranco WT, Hudak PF, Eckhert CD. Evaluation of ecological and in vitro effects of boron on prostate cancer risk. *Cancer Causes Control*, In Press.
25. Guerquin-Kern JL, Wu TD, Quintana C, Croisy A. Biochim Biophys Acta 1724:228-238, 2005

Appendices (published journal articles)

1. Barranco W.T. and Eckhert C.D. Boric acid inhibits human prostate cancer cell proliferation. *Cancer Letters* 216:21-29, 2004.

2. Kim D. H. S., Faull K. F., Norris A. J., Eckhert C. D. Borate-nucleotide complex formation depends on charge and phosphorylation state. *J. Mass Spectrometry* 39:743-751, 2004.

3. Barranco WT and Eckhert CD. Cellular changes in boric acid-treated DU-145 prostate cancer cells. *Brit J. Cancer* 94:884-890, 2006.

4. Kim DH, Que Hee S, Norris A, Faull KF and Eckhert CD. Boric acid inhibit ADP-ribosyl cyclase non-competitively. *J. Chromatography A.* 1115:246-252, 2006.
5. Barranco WT, Hudak PT, Eckhert CD. Evaluation of ecological and in vitro effects of boron on prostate cancer risk. Cancer Causes Control. In Press.

Available online at www.sciencedirect.com
SCIENCE DIRECT®
Cancer Letters 216 (2004) 21–29
CANCER Letters
www.elsevier.com/locate/canlet

Boric acid inhibits human prostate cancer cell proliferation

Wade T. Barranco, Curtis D. Eckhert*

Department of Environmental Health Sciences, University of California, Box 951770, Los Angeles, CA 90095-1772, USA

Received 17 December 2003; received in revised form 1 June 2004; accepted 2 June 2004

Abstract

The role of boron in biology includes coordinated regulation of gene expression in mixed bacterial populations and the growth and proliferation of higher plants and lower animals. Here we report that boric acid, the dominant form of boron in plasma, inhibits the proliferation of prostate cancer cell lines, DU-145 and LNCaP, in a dose-dependent manner. Non-tumorigenic prostate cell lines, PWR-1E and RWPE-1, and the cancer line PC-3 were also inhibited, but required concentrations higher than observed human blood levels. Studies using DU-145 cells showed that boric acid induced a cell death-independent proliferative inhibition, with little effect on cell cycle stage distribution and mitochondrial function.

Keywords: Boron; LNCaP; DU-145; PC-3; Necrosis; Prostate cancer

1. Introduction

Boron has been shown to be beneficial for many species, but its cellular processing in animals remains obscure. The boron atom has a high affinity for oxygen and in nature is present in the form of borates [1]. Soluble forms include boric acid $B(OH)_3$ and the monovalent anion $B(OH)_4^-$, with the presence of the dominant form dependent upon solvent pH. In plasma, boric acid predominates and its concentration reflects dietary intake and respiratory exposure [2].

Boron is known to be important for animal cell replication and development, but the underlying mechanisms remain obscure. Boric acid stimulates embryonic growth in trout [3] and is essential during the pre-blastula cleavage stage of zebrafish [4]. In frogs (*Xenopus*), boron deficiencies interfere with normal oocyte maturation, embryonic growth and morphogenesis [5]. Deficiencies in *Xenopus* also lead to inhibition of oocyte germinal vesicle breakdown, possibly due to an alteration in progesterone receptor binding [6].

Evidence leading to the hypothesis that boric acid may be anti-carcinogenic was derived from epidemiological screening, where the risk of prostate cancer was observed to be inversely proportional to dietary intake of boron in a dose responsive manner [7,8]. Boric acid has also been reported to inhibit the growth of LNCaP prostate tumors in nude mice [9]. In the present paper, we report that boric acid

* Corresponding author. Tel./fax: +1-310-825-8429.
E-mail address: ceckhert@ucla.edu (C.D. Eckhert).

0304-3835/$ - see front matter © 2004 Elsevier Ireland Ltd. All rights reserved.
doi:10.1016/j.canlet.2004.06.001

inhibits the proliferation of human prostate cancer cell lines in a dose-dependent manner. The mechanism of inhibition was investigated by examining the impact of boric acid on the cell cycle, apoptosis, and mitochondrial activity of the DU-145 cell line.

2. Materials and methods

2.1. Cell culture

Cell lines were cultured in media that support maximum proliferation. Prostate cancer cells (DU-145, LNCaP, and PC-3) were obtained from Dr Allan Pantuck and cultured in RPMI 1640 (Invitrogen) supplemented with 10% FBS, penicillin/streptomysin (100 U/ml; 100 μg/ml), and L-glutamine (200 mM) (Gemini Bioproducts, Woodlands, CA). Non-tumorigenic prostate cell lines (RWPE-1 and PWR-1E) were acquired from the American Type Culture Collection (ATCC, Manassas, VA) and cultured in Keratinocyte-SFM supplemented with 50 μg/ml bovine pituitary extract, 5 ng/ml human recombinant epidermal growth factor, and 1× antibiotic/antimycotic mixture (100 U/ml penicillin, 100 μg/ml streptomycin, 0.25 μg/ml Fungizone) (Invitrogen). All cells were cultured at 37 °C, 5% CO_2 and were removed from culture plates via trypsinization (0.53 mM EDTA, 0.05% trypsin).

2.2. Culture media

Boron-depleted media was prepared by treatment with the boron-specific ionic exchange resin, Amberlite IRA-743 (Sigma). The resin was added to supplemented media and agitated by rotation on a Koala-Ty rotator at 80 rpm, overnight, at 4 °C. Resin-treated media was then transferred to sterile 250 ml centrifuge tubes (Corning). Boric acid solutions were prepared using ultra-pure boric acid in ion exchange treated water [10]. Experimental media was prepared by the addition of concentrated boric acid solutions to provide a range of concentrations (0, 100, 250, 500 and 1000 μM B). Low boron exposures were also performed using concentrations from 15 to 100 μM B. Boron was quantified by inductively coupled plasma mass spectrometry (ICPMS) as previously described [10].

2.3. Experimental culture

Cells were plated, using non-resin treated media, on culture plates (Fisher) at densities to prevent confluence and to maintain a proliferative state throughout the duration of exposure. LNCaP, DU-145, and PC-3 cells were plated onto six-well culture plates at densities of 300, 1000 and 2000 cells/cm^2. RWPE-1 and PWR-1E cells were plated onto 24-well culture plates at a density of 4100 cells/cm^2. Because of the expense associated with media preparations, non-tumorigenic lines were cultured on smaller plates to reduce the volume of media used during exposures. Following an overnight incubation, non-treated media was removed and replaced daily with boric acid-supplemented media. Cells were cultured, in the presence of boric acid supplemented media, for 8 days and were counted using a hemocytometer with the aid of Trypan Blue for exclusion of non-viable cells (Invitrogen).

2.4. Cell cycle analysis

DU-145 cells were seeded on 100×20 mm tissue culture plates at 178 cells/cm^2 and were cultured for 8 days in the presence of boric acid (0–1000 μM B), with daily media replacement. After 8 days of exposure, and at 50% confluence, adherent cells were washed once with cold PBS and scraped from the plates with a rubber policeman. Cells were suspended in PBS and centrifuged at 1200 rpm for 5 min. Following centrifugation, PBS was aspirated and the cell pellets were re-suspended in a hypotonic propidium iodide DNA staining buffer (1 mg/ml sodium citrate, 0.3% Triton-X100, 100 μg/ml propidium iodide, 20 μg/ml ribonuclease A) and allowed to incubate for 30 min at 4 °C, protected from light. Cell cycle analysis was then performed with a FACS Calibur flow cytometer, while Modfit LT 3.0 software was used for data analysis. Analysis of each sample was performed on greater than 10,000 events and coefficients of variation never exceeded 5%.

2.5. Treatment of G_0 arrested cells with boron

DU-145 cells were cultured on 75 cm^2 culture plates for 3 days in RPMI 1640 serum-free media, supplemented with penicillin/streptomysin

(100 U/ml; 100 μg/ml) and L-glutamine (2 mM), to induce G_0 arrest. Arrested cells were trypsinized and plated onto six-well culture plates, at a density of 3×10^5 cells/well, and treated daily with serum-free media, supplemented with boric acid (0–1000 μM B). Following 8 days of exposure, cells were trypsinized and counted using a hemacytometer, with the aid of Trypan Blue to exclude non-viable cells (Invitrogen).

2.6. Caspase-3 analysis via Western blot and PhiPhiLux assay

DU-145 cells were cultured in the presence of boric acid (0–1000 μM B), for 8 days, on 100×20 mm tissue culture plates, with daily media replacement. Cell monolayers were washed with PBS, scraped off with a rubber policeman, and centrifuged at 1200 rpm for 5 min. Protein was extracted from pellets with lysis buffer (250 mM NaCl, 0.1% NP40, 50 mM HEPES (pH 7.0), 5 mM EDTA, 1 mM dithiothreitol (DTT), 10% protease inhibitor mixture (Sigma #P8340)), sonication, and a 40 min incubation at 4 °C. Two hundred microgram of protein from each sample was separated on 12% polyacrylamide-sodium dodecyl sulfate gels (SDS-PAGE) and transferred to nitrocellulose membranes. Immunoblotting was performed with polyclonal antibodies to caspase-3 (sc-7148, Santa Cruz) using actin (sc-1616, Santa Cruz) as a control. Secondary antibodies were anti-goat (sc-2033, Santa Cruz) and anti-rabbit (sc-2317, Santa Cruz). Protein expression was detected with the ECL detection kit (Amersham Int., Arlington Heights, IL).

PhiPhiLux (G_1D_2), a cell-permeable fluorogenic substrate containing the caspase-3 cleavage site GDEVDG, was utilized to monitor caspase-3 activity, according to the manufacturer's instructions (OncoImmunin, Inc., Kensington MD). Briefly, DU-145 cells were cultured on six-well culture plates for 8 days, using a range of boric acid concentrations (0–1000 μM B), with daily media replacement. Cells were removed from the plates, with the aid of a rubber policeman in the presence of PBS, and suspended in 50 μl of substrate solution and 5 μl of FBS. Suspensions were allowed to incubate for 60 min at 37 °C, in the absence of light. Following incubation, cells were washed once with flow cytometry dilution buffer (1 ml), centrifuged, aspirated, and then re-suspended in dilution buffer (1 ml). Fluorescence emission was measured on a FACS Calibur flow cytometer, utilizing an FL1 channel, with greater than 8000 events per sample. Cell Quest 3.3 software was used for data analysis.

2.7. DNA fragmentation assay

For DNA fragmentation detection, DU-145 cells were cultured for 8 days, in the presence of boric acid (0–1000 μM B) on 100×20 mm tissue culture plates, with daily media replacement. Positive controls of DNA fragmentation were cultured for 24 h in the presence of 5 and 10 μM sodium selenite [11]. Following treatment, cells were trypsinized from plates and washed with PBS, transferred to 1.5 ml microcentrifuge tubes and centrifuged at 1200 rpm for 5 min. Pellets were digested in lysis buffer (10 mM Tris–HCl (pH 8.0), 100 mM EDTA, 0.5% SDS, 0.5 mg/ml proteinase K) and allowed to incubate overnight at 37 °C. DNA was extracted from digest with an equal volume of phenol:chloroform (1:1), centrifuged at 14,000 rpm for 15 min until phases resolved, and then the supernatant was transferred to a fresh tube for precipitation. DNA-containing elution was precipitated with 7.5 M ammonium acetate (1/2× vol) and 100% ethanol (2× vol) overnight. The precipitate was centrifuged at 14,000 rpm for 15 min the following day, and the DNA was solubilized in TE buffer (10 mM Tris–Cl, 1 mM EDTA, pH 7.5). Ten microgram of DNA was loaded per well in a 1.8% agarose gel containing ethidium bromide (1 μg/ml). The gel was run in 1× TAE buffer for 2.5 h at 75 V, visualized under UV light, and photographed.

2.8. Assessment of mitochondrial activity and cell proliferation with the MTT assay

To assess mitochondrial activity, DU-145 cells were plated onto 96-well culture plates, at a density of 10^4 cells/well, and allowed to incubate overnight. Cells were then exposed to 200 μl of boric acid supplemented media (0–1000 μM B) for 2.5 or 7.5 h. (The 7.5-h exposure involved supplementing the MTT solution with boric acid in the subsequent 5-h step.) After 2.5 h, boric acid supplemented media

Table 1
MTT assay absorbance among 2.5 and 7.5 h, boric acid-exposed DU-145 cells

BA (μM)	Exposure time (h)	
	2.5	7.5
0	0.441 ± 0.009	0.555 ± 0.029
100	0.409 ± 0.014	0.571 ± 0.015
250	0.448 ± 0.037	0.479 ± 0.027
500	0.557 ± 0.011	0.563 ± 0.016
1000	0.411 ± 0.021	0.493 ± 0.024

Following 2.5 and 7.5 h exposures to boric acid (0–1000 μM), mitochondrial activity of DU-145 cells was detected via the MTT assay, indicative of mitochondrial conversion of MTT to formazan. Absorbance values measured at 590 nm, mean ± SEM, $n=6$.

were removed and replaced with 200 μl of MTT-supplemented media (1.25 mg/ml) and allowed to incubate for 5 h. Following incubation, the MTT solution was removed and replaced with 200 μl of DMSO and 25 μl of Sorenson's buffer (0.1 M glycine, 0.1 M NaCl, pH 10.5) and mixed thoroughly to dissolve the formazan crystals. Optical density of the MTT formazan product was read on a microplate reader at 590 nm (Table 1).

To assess cell proliferative activity, DU-145 cells were plated onto 96-well culture plates at a density of 100 cells/well, and allowed to incubate overnight. Cells were then exposed to 200 μl of boric acid supplemented media (0–1000 μM B) every 24 h, for 8 days. MTT analysis was performed identically as in the mitochondrial activity assay (with a boron-free MTT solution) and the number of cells quantified.

2.9. Statistical evaluation of proliferation values

Proliferation values were compared by ANOVA, followed by Bonferroni and Holme tests for determination of statistical differences.

3. Results

3.1. Proliferative inhibition

A dose-dependent, anti-proliferative relationship was observed in all cancer cell lines exposed to boric acid, with the hormone-independent DU-145 line showing the highest sensitivity to boric acid. At day 8, proliferation was depressed 32, 62, 87 and 98% at concentrations of 100, 250, 500, and 1000 μM B, respectively (Fig. 1A). This inhibition, in the DU-145 cell line, was also observed with the aid of MTT conversion analysis (Fig. 1B). In addition, these doses significantly depressed proliferation in the hormone-dependent, LNCaP cell line by 40, 51, 59 and 77% and the PC-3 line by 29% at 500 μM, and 52% at 1000 μM B (Fig. 1). Sub-100 μM B concentrations were evaluated in the DU-145 cell line and statistically significant proliferative inhibition occurred as low as 60 μM B (data not shown).

Non-tumorigenic prostate cells displayed reduced sensitivity to boron relative to DU-145 and LNCaP, but not PC-3. After 8 days of exposure, the HPV-18 immortalized prostate epithelial cell line, RWPE-1, displayed statistically significant reductions in proliferation of 26 and 76% at 500 and 1000 μM B exposure levels (Fig. 1). At 8 days, PWR-1E prostate epithelial cells, immortalized with Ad12-SV40 adenovirus, exhibited a 41% reduction in proliferation only at 1000 μM B level of exposure (Fig. 1).

3.2. Cell cycle analysis with propidium iodide

The impact of boric acid on the cell cycle was examined in the most sensitive cell line, DU-145. Propidium iodide is an intercalating dye with a specific affinity for DNA. Its quantitation, in permeabilized cells, measures DNA content and is used to estimate the cell cycle distribution in populations of cells. A small, but significant dose-dependent shift, in cell cycle stage distribution, was detected in cells exposed for 8 days to 500 and 1000 μM B, with a 2.2 and 4.5% shift from G_0/G_1 to G_2. A 50% reduction in proliferation, observed at 250 μM B for DU-145 cells, occurred with no significant cycle stage shift (Fig. 2).

3.3. Boron toxicity in G_0 arrested cells

Cells enter a state of growth arrest, accompanied by a shift to the G_0 cell cycle stage, when serum starved. An exposure study was performed, on growth arrested DU-145 cells, in order to evaluate boron induced proliferative inhibition in non-cycling cells. Cycling DU-145 cells have a population doubling time of 24 h, while manual cell counts indicated that only one cell division occurred over the 8-day

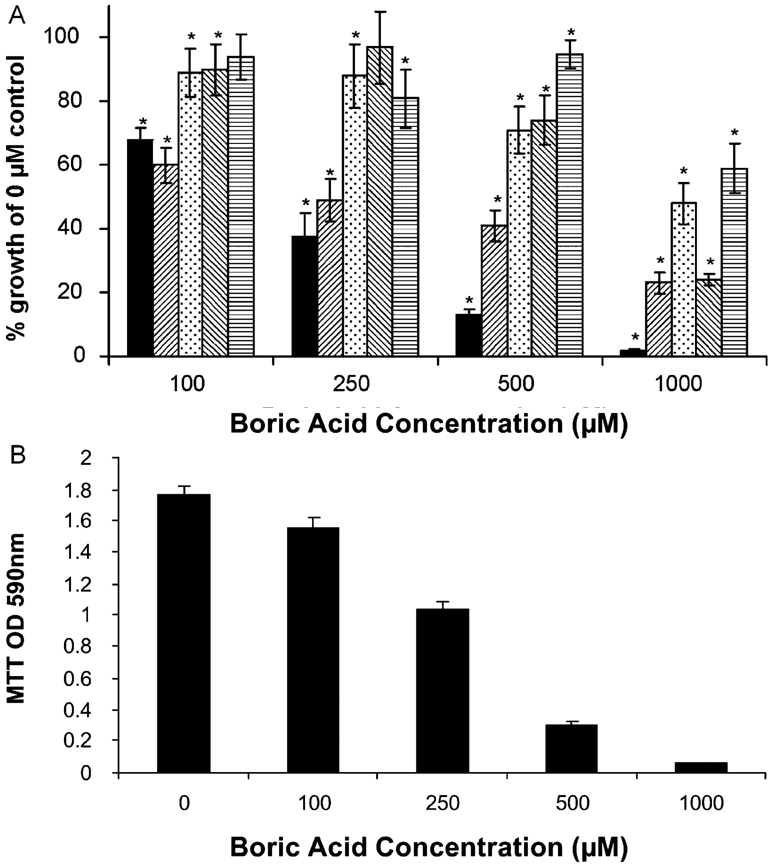

Fig. 1. A dose-dependent shift in proliferation of prostate cancer (DU-145 ■, LNCaP ▨ and PC-3 ▩) and non-tumorigenic prostate cell lines (RWPE-1 ▧ and PWR-1E ▤), relative to unexposed (control) cells, is displayed. Boric acid (0–1000 μM boron) was administered for 8 days. Values are presented as the mean of six independent measurements ± SEM. *Asterisk represents statistically significant means as compared to the 0 μM boron control ($P<0.05$) (A). Dose-dependent shift of MTT conversion, in DU-145 cells, in response to boric acid exposure. Absorbance values was measured at 590 nm ± SEM, $n=6$ (B).

exposure period, in the serum-free, zero-boron treated control cells. It is often the case that apoptotic and necrotic cells detach from culture plate surfaces, yet the strongly growth inhibiting 1000 μM B concentration had no effect on cell adherence, and exposed cells maintained their initial seeding value of 30×10^4 cells, throughout the 8 day exposure (Fig. 3).

3.4. Apoptosis analysis with PhiPhiLux, Western blot, and DNA fragmentation assay

Caspase-3 is an aspartate-specific, cysteine protease expressed during apoptotic cell death and was used as an indicator of apoptosis. The absence of a population shift into the R2 (Region 2) gated area showed that boric acid did not increase caspase-3 activity relative to the 0 μM B exposed DU-145 cells (Fig. 4A). This was reinforced by the Western blot analysis showing the absence of caspase-3 protein in exposed cell extracts (Fig. 4B).

During apoptosis, DNA is degraded into fragments of unique lengths, known as a ladder, in contrast to necrosis, where a wide range of fragment sizes are apparent in electrophoresis gels. A dose-dependent fragmentation was not detected in the genomic DNA isolated from DU-145 cells, relative to the 8 day boric acid exposure concentrations, yet was present in the positive controls (Fig. 5).

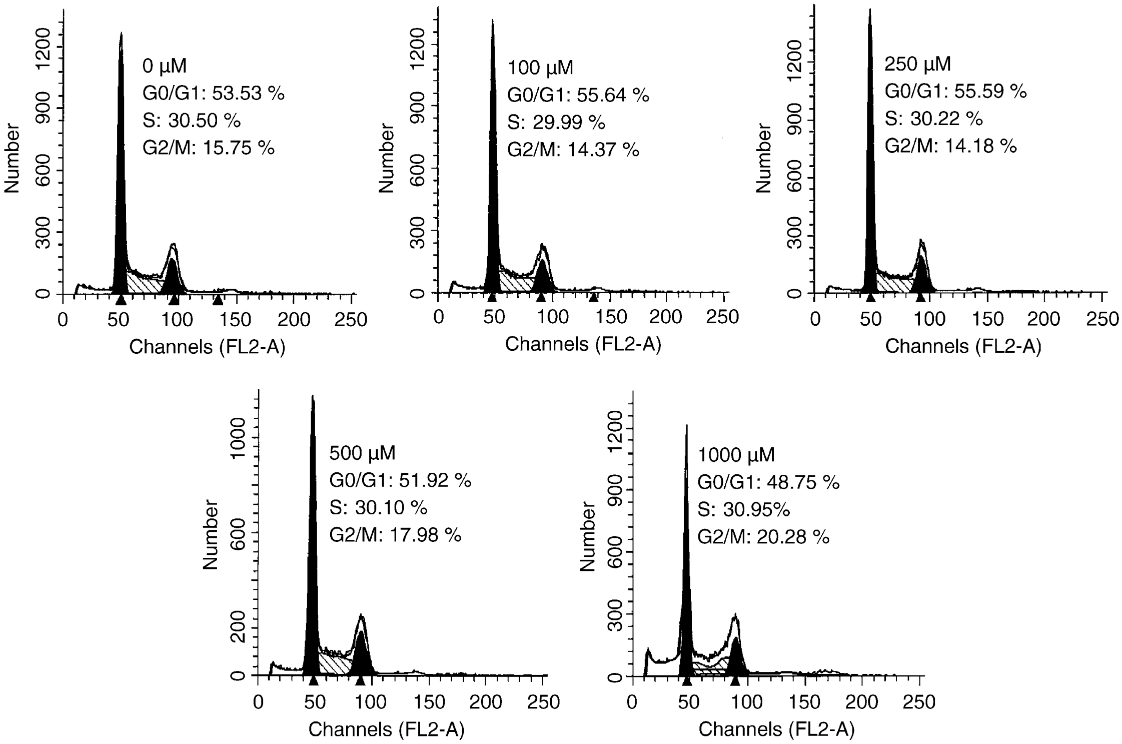

Fig. 2. Flow cytometry analysis of DNA content with propidium iodide, in DU-145 cells, following an 8-day exposure to boric acid (0–1000 μM boron). The *y*-axis represents the number of cells detected and the *x*-axis propidium iodide fluorescence intensity. Displayed are the exposure doses, followed by the percentage of cell populations in each phase. Values represented as mean (%), $n=6$.

3.5. Mitochondrial activity analysis via MTT assay

Mitochondrial viability can be assessed through detection of formazan, at 590 nm, derived from the reduction of MTT (3[4,5-dimethylthiazol-2-yl]-2, 5-diphenyl-tetrazolium bromide) by mitochondrial dehydrogenase. No differences occurred in formazan concentrations, in DU-145 cells exposed to boric acid (0–1000 μM B) at 2.5 and 7.5 h (Table 1).

3.6. Boron analysis

Boron concentrations were determined by ICPMS. The detection limit of the ICPMS for boron was 0.001 mg B/l and ultra-pure water below this limit was used to perform all dilutions. Analysis of cell culture media treated with the ionic exchange resin Amberlite IRA-743 and supplemented with boric acid showed boron concentrations slightly higher than their theoretical level of supplementation. The concentrations of boric acid in the 0, 100, 250, 500 and 1000 μM supplemented media were determined to be 4.1 ± 0.4, 109.0 ± 0.9, 276 ± 1.2, 565.6 ± 4.5 and 1149 ± 2.2 μM B, respectively. Since a molecule of boric acid contains one atom of boron the molar

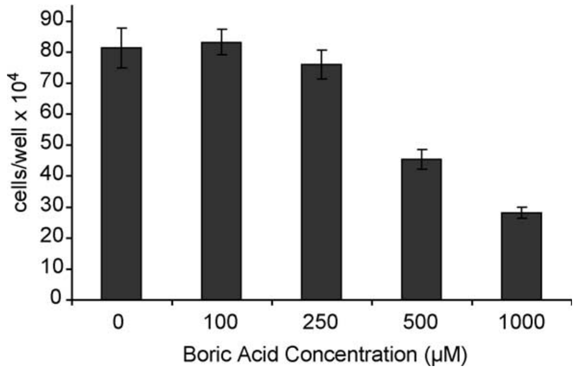

Fig. 3. DU-145 cells were arrested in G_0, through culturing in serum-free media, and then exposed to a range of boron concentrations (0–1000 μM). Cells were counted after 8 days of exposure and recorded as the number of adherent cells/well. Error bars represent mean $\pm$ SEM, $n=6$.

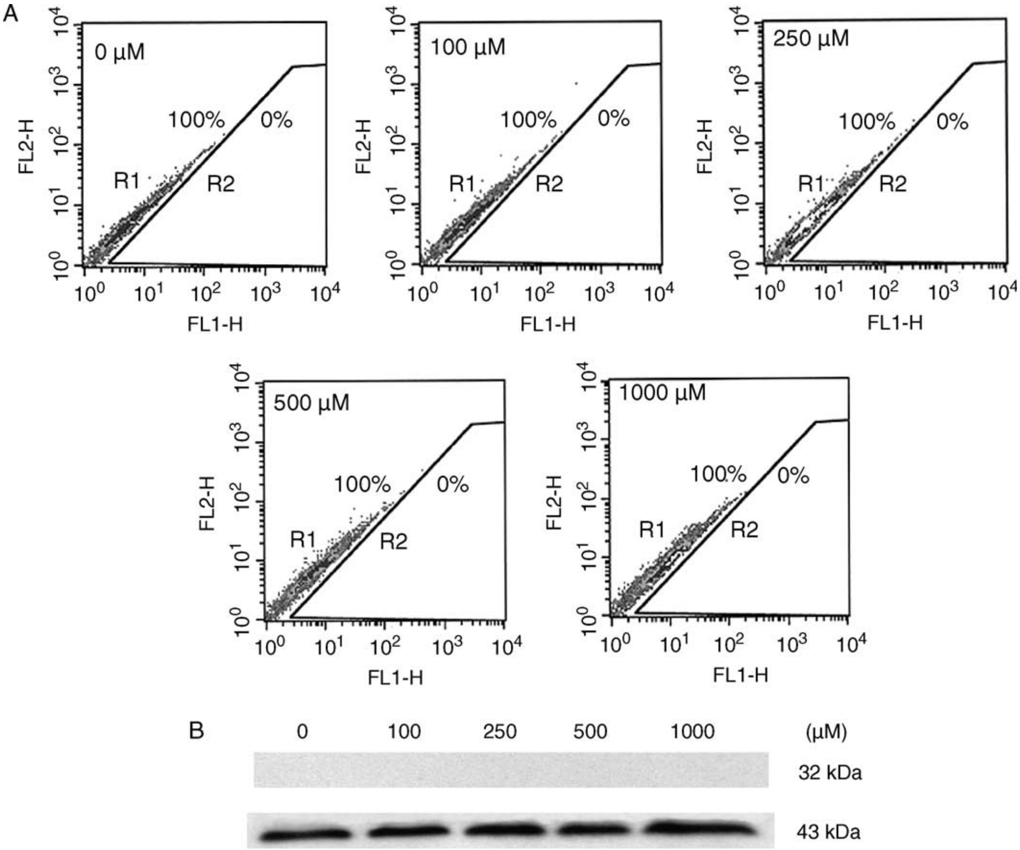

Fig. 4. Flow cytometry analysis of caspase-3 activity through PhiPhiLux-G_1D_2 probe cleavage, among DU-145 cells exposed to boric acid (100–1000 μM B), relative to 0 μM exposure. The *y*-axis represents fluorescence detected with the FL1 channel (PhiPhiLux) while the *x*-axis represents FL-2 channel-detected fluorescence. Region 1 (R1) represents baseline fluorescence among non-exposed cells, while region 2 (R2), set in the 0 μM exposure output, encompasses a gated area that displays cells expressing higher PhiPhiLux fluorescence. Values of cell population percentages in both regions are indicated, along with the boric acid exposure concentration. Values represented as mean (%) ± SEM, $n = 6$ (A). Western blot analysis of caspase-3 (32 kDa) presence in DU-145 cells exposed to boric acid (0–1000 μM B) for 8 days, while actin (43 kDa) was used as a control (B).

concentrations of boron are equivalent to those of boric acid.

4. Discussion

In this paper we examined the impact of boric acid on cell proliferation using three prostate cancer and two non-tumorigenic prostate cell lines. These were LNCaP cells derived from a lymph node metastasis that retained the androgen-responsive phenotype and two cell lines displaying the androgen-independent phenotype: DU-145, derived from a brain metastasis, and PC-3, derived from a lower lumber skeletal metastasis [12]. Proliferation of both the hormone-dependent (LNCaP) and independent (DU-145) cancer lines was reduced by boric acid in a dose-dependent manner, thus providing evidence that the mechanism responsible for the inhibition did not require the androgen receptor. Fourfold higher concentrations of boric acid were required to achieve 50% growth inhibition in PC-3 and the non-tumorigenic cell lines, PWR-1E and RWPE-1. This suggests that the sensitivity to boric acid was dependant on cellular mechanism(s) that are more highly expressed in LNCaP and DU-145 than the other cell lines.

Cell cycle analysis of DU-145 cells using propidium iodide showed that boric acid induced proliferative

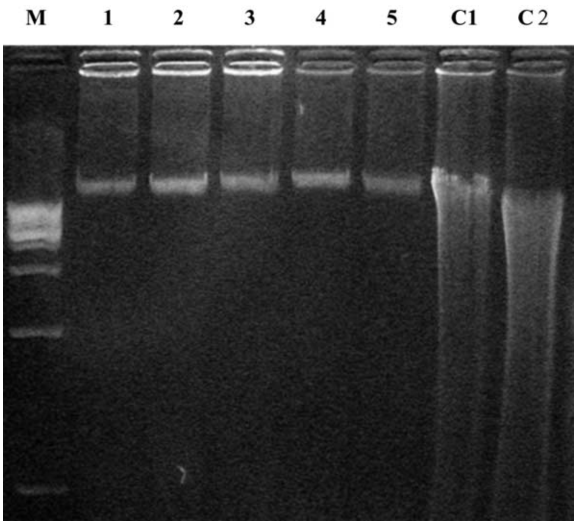

Fig. 5. DNA fragmentation was detected among the DU-145 cells exposed for 8 days to varying concentrations of boric acid: 0 (lane 1), 100 (lane 2), 250 (lane 3), 500 (lane 4) and 1000 μM (lane 5). Marker DNA (lane M) and positive controls, displaying 24-h exposures to 5 (Lane C1) and 10 μM (Lane C2) sodium selenite.

inhibition did not cause a pronounced cell cycle stage shift. Since apoptosis is often accompanied by a cycle stage shift, this suggested that the inhibition of cell proliferation occurred in the absence of cell death. Further, study showed that boric acid did not effect the adherence of G_0 arrested cells, nor did it induce detectable caspase-3 expression or activity, both indicators of apoptosis. Support for a death-independent, proliferative inhibition was also obtained from fragmentation analysis that showed intact, non-degraded DNA, regardless of exposure concentration. The absence of MTT reduction also indicated that mitochondrial activity was not affected during acute boric acid exposures. Together, these results support the interpretation that boric acid reduced growth by proliferative inhibition, rather than through the induction of cell death.

In the present study, proliferative inhibition by boric acid occurred at levels as low as 60 μM B in the DU-145 cell line. Although this concentration is high relative to pharmacological anti-cancer drugs, boron blood levels in this range have been reported in human dietary and pharmacological studies. Human blood levels reflect dietary intake and have been reported to vary from 13 to 70 μM B [13]. Drinking water boron concentrations of 2683 μM B in Turkey have not been shown to cause deleterious effects in humans populations exposed over many generations [14]. Serum levels of 0.9 M and 2.4 M B were reported in human infants accidentally fed infant formula prepared with medicinal boric acid that provided 30.4 and 94.7 mg B/kg BW, respectively [15]. These very high levels produced vomiting, diarrhea and temporary skin rashes, but no permanent damage. However, chronic toxicological oral doses of 26 mg B/kg BW causes atrophy of the seminiferous epithelium and testes in the rat [16].

The best characterized interaction of boric acid with cellular constituents is with nucleotides. Boric acid binds to *cis*-diols on the ribose moiety of nucleotides forming nucleotide–borate complexes including NAD^+ and *S*-adenosylmethione [17,18]. Direct measurements using mass spectrometry gave relative affinities for boric acid that ranked: $NAD^+ > AMP \approx CMP \approx GMP \approx UMP$ with binding affinities greatly reduced by phosphorylation [18,19]. The affinity of boric acid for hydroxyl groups underlies its ability to inhibit serine proteases, including prostate specific antigen (PSA), a marker for prostate cancer [20]. However, this affect on PSA cannot explain the inhibition of proliferation in the DU-145 cell line because it does not express PSA [21]. Given the available information, the most probable explanation for boric acid's anti-proliferative effect is through the formation of nucleotide–borate complexes that changes the function or utilization of the nucleotides.

Diets rich in fruits and vegetables, and low in fats, are widely recommended for cancer prevention [22]. Vegetables, nuts, fruits and their beverage by-products are also the primary source of boron exposure in humans. In men 31–70 years, the mean US intake is 1.42 mg/d with a wide range from 0.57 to 3.01 mg/d between the first and 99th percentiles of intake [23]. This information, taken together with the epidemiological evidence [7,8], mouse tumor suppression study [9], and the present cell culture study suggest that boron is an unrecognized natural anti-cancer agent present in the human diet. Future investigations are needed to elucidate the mechanism of boron's effect on proliferation and the relative importance of boron compared to dietary selenium, vitamin E and lycopene in the prevention and control of prostate cancer [24].

Acknowledgements

The work for this grant was funded in part by the US Army Medical Research and Material Command, The Prostate Cancer Research Program DAMD 17-03-1-0067 and the Ann Fitzpatrick Alper Program in Environmental Genomics at the Jonsson Comprehensive Cancer Center, UCLA and the UC Toxic substances Research and Teaching Program. We thank Dr Allan Pantuck, Randy Caliliw, and David Nguyen for their expertise concerning the culturing of prostate cancer cells. With the help of Michael Gulrajani, flow cytometry was performed in the UCLA Jonsson Comprehensive Cancer Center (JCCC) and Center for AIDS Research Flow Cytometry Core Facility, which is supported by National Institutes of Health awards CA-16042 and AI-28697, and by the JCCC, the UCLA AIDS Institute, and the David Geffen School of Medicine at UCLA.

References

[1] P. Argust, Distribution of boron in the environment, Bio. Trace Element Res. 66 (1998) 131–143.

[2] W.G. Woods, An introduction to boron: history, sources, uses, and chemistry, Env. Health Perspect. 102 (Suppl. 7) (1994) 5–11.

[3] C.D. Eckhert, Boron stimulates embryonic trout growth, J. Nutr. 128 (1998) 2488–2493.

[4] R.I. Rowe, C.D. Eckhert, Boron is required for zebrafish embryogenesis, J. Exp. Biol. 1999; 1649–1654.

[5] D.J. Fort, T.L. Propst, E.L. Stover, F.J. Murray, P.L. Strong, Adverse effects from low dietary and environmental boron exposure on reproduction, development, and maturation in *Xenopus laevis*, J. Trace Elem. Exp. Med. 12 (1999) 175–186.

[6] D.J. Fort, Boron deficiency disables *Xenopus laevis* oocyte maturation events, Biol. Trace Elem. Res. 85 (2002) 157–169.

[7] Z.F. Zhang, J.I. Winton, C. Rainey, C.D. Eckhert, Boron is associated with decreased risk of human prostate cancer, Fed. Am. Soc. Exp. Biol. J. 15 (A1089) (2001) 834.3.

[8] Y. Cui, M.I. Winton, Z.F. Zhang, C. Rainey, J. Marshall, J.B. De Kernion, C.D. Eckhert, Oncol. Rep. 11 (4) (2004) 887–892.

[9] M.T. Gallardo-Williams, R.E. Chapin, P.E. King, G.J. Moser, T.L. Goldsworthy, J.P. Morrison, R.R. Maronpot, Boron supplementation inhibits the growth and local expression of IGF-1 in human prostate adenocarcinoma (LNCaP) tumors in nude mice, Toxicol. Pathol. 32 (2004) 73–78.

[10] A. Bennett, R.I. Rowe, N. Soch, C.D. Eckhert, Boron stimulates yeast (*Saccharomyces cerevisiae*) growth, J. Nutr. 129 (1999) 2236–2238.

[11] C. Jiang, Z. Wang, H. Ganther, J. Lu, Caspases as key executioners of methyl selenium-induced apoptosis (anoikis) of DU-145 prostate cancer cells, Cancer Res. 61 (2001) 3062–3070.

[12] N.M. Navone, C.J. Logothetis, A.C. von Eschenbach, P. Troncoso, Model systems of prostate cancer: uses and limitations, Cancer Metastasis Rev. 17 (1999) 361–371.

[13] N.L. Ward, The determination of boron in biological materials by neutron irradiation and prompt gamma-ray spectrometry, J. Radioanal. Nucl. Chem. 110 (1987) 633–639.

[14] B.S. Sayli, E. Tuccar, A.H. Elhan, An assessment of fertility in boron-exposed Turkish subpopulations, Rep. Toxicol. 12 (1998) 297–304.

[15] M.D. Baker, Ingestion of boric acid by infants, Am. J. Emerg. Med. 4 (1986) 358–361.

[16] R.E. Chapin, W.W. Ku, The reproductive toxicity of boric acid, Environ. Health Perspect. 102 (Suppl. 7) (1994) 87–91.

[17] N.V.C. Ralston, C.D. Hunt, Diadenosine phosphates and *S*-adenosylmethione: novel boron binding biomolecules detected by capillary electrophoresis, Biochim. Biophys. Acta 1527 (2001) 20–30.

[18] D.H. Kim, B.N. Marbois, K.F. Faull, C.D. Eckhert, Esterification of borate with NAD^+ and NADH as studied by electrospray ionization mass spectrometry and ^{11}B NMR spectroscopy, J. Mass Spectrom. 38 (2003) 632–640.

[19] D.H. Kim, A. Norris, K.F. Faull, C.D. Eckhert, Borate–nucleotide complex formation depends on charge and phosphorylation state, J. Mass Spectrom. 2004; in press.

[20] M.T. Gallardo-Williams, R.R. Maronpot, R.N. Wine, S.H. Brunssen, R.E. Chapin, Inhibition of the enzymatic activity of prostate specific antigen by boric acid and 3-nitrophenyl boronic acid, Prostate 54 (2003) 44–49.

[21] D.D. Mickey, K.R. Stone, H. Wunderli, G. Mickey, D.F. Paulson, Characterization of a human prostate adenocarcinoma cell line (DU-145) as a monolayer culture and a solid tumor in athymic mice, in: G.P. Murphy, (Ed.), Models for Prostate Cancer Progr. Clin. Biol. Res. 37 (1980) 67–84.

[22] J.H. Cohen, A.R. Kristal, J.L. Stanford, Fruit and vegetable intakes and prostate cancer risk, J. Natl Cancer Inst. 92 (2000) 61–68.

[23] Dietary reference intakes for vitamin A, vitamin K, arsenic, boron, chromium, copper, iodine, iron, manganese, molybdenum, nickel, silicon, vanadium, and zinc. A Report of the Panel on Micronutrients, Subcommittees on Upper Reference Levels of Nutrients and of Interpretation and Use of Dietary Reference Intakes, and the Standing Committee on the Scientific Evaluation of Dietary Reference Intakes. Food and Nutrition Board, Institute of Medicine, National Academy Press, Washington, DC, 2001.

[24] S.K. Clinton, E. Giovannucci, Diet, nutrition, and prostate cancer, Annu. Rev. Nutr. 18 (1998) 413–440.

British Journal of Cancer (2006) 94, 884–890

www.bjcancer.com

Cellular changes in boric acid-treated DU-145 prostate cancer cells

WT Barranco[1] **and CD Eckhert***[,1]

[1]Department of Environmental Health Sciences, University of California, Los Angeles, Box 951770, CA 90095-1772, USA

Epidemiological, animal, and cell culture studies have identified boron as a chemopreventative agent in prostate cancer. The present objective was to identify boron-induced changes in the DU-145 human prostate cancer cell line. We show that prolonged exposure to pharmacologically-relevant levels of boric acid, the naturally occurring form of boron circulating in human plasma, induces the following morphological changes in cells: increases in granularity and intracellular vesicle content, enhanced cell spreading and decreased cell volume. Documented increases in β-galactosidase activity suggest that boric acid induces conversion to a senescent-like cellular phenotype. Boric acid also causes a dose-dependent reduction in cyclins A–E, as well as MAPK proteins, suggesting their contribution to proliferative inhibition. Furthermore, treated cells display reduced adhesion, migration and invasion potential, along with F-actin changes indicative of reduced metastatic potential. Finally, the observation of media acidosis in treated cells correlated with an accumulation of lysosome-associated membrane protein type 2 (LAMP-2)-negative acidic compartments. The challenge of future studies will be to identify the underlying mechanism responsible for the observed cellular responses to this natural blood constituent.

British Journal of Cancer (2006) **94,** 884–890. doi:10.1038/sj.bjc.6603009 www.bjcancer.com
Published online 21 February 2006

Keywords: boric acid; prostate cancer; DU-145; migration; senescence; acidosis

The element boron is nearly completely absorbed from drinking water and plant-derived foods in the gastrointestinal tract, and circulates in blood as boric acid (BA) (Price *et al*, 1997). Cells were once thought incapable of processing the element, yet this has since been disproved. Boron is utilised by bacteria in the structure of several antibiotics and autoinducer-2, a signalling molecule utilised during interspecies quorum sensing (Chen *et al*, 2002; Semmelhack *et al*, 2004). Plants require the element for growth, flowering and seed formation, and obtain boron from soil pore water using a borate transporter, BOR1, expressed in root pericycle cells (Takano *et al*, 2002). A human homologue, the electrogenic, voltage-regulated, Na^+-coupled borate transporter NaBC1, was recently identified in human kidney tubular cells and may function to maintain plasma BA levels (Park *et al*, 2004).

There are several reports supporting boron as a chemopreventative agent against prostate cancer. An epidemiological study using data from the NHANES III database reported that the risk of prostate cancer in US men is inversely proportional to dietary intake of boron (Cui *et al*, 2004). The biological plausibility of this observation has been supported by cell culture and animal studies. Treatment of nude mice, injected with androgen-sensitive LNCaP prostate cancer cells, with BA caused a reduction in tumour growth of 25–38%, along with a reduction in plasma PSA levels of 88% (Gallardo-Williams *et al*, 2004). BA inhibits the activity of serine proteases, including prostate-specific antigen (PSA), presumably by binding to its active site (Bone *et al*, 1987; Gallardo-Williams *et al*, 2003). In culture, BA has been shown to inhibit the proliferation of LNCaP and the androgen-independent prostate cancer cell lines DU-145 and PC-3, in a dose-dependent manner (Barranco and Eckhert, 2004). Since DU-145 cells do not synthesise PSA, BA's mode of inhibiting proliferation is likely not to occur by inhibiting the conversion of IGFBP-3 to IGF-1, as proposed in LNCaP tumours (Gallardo-Williams *et al*, 2004; Sobel and Sadar, 2005). The present investigation was initiated to define morphological and molecular responses of DU-145 prostate cancer cells to BA, which might lead to an explanation of its antiproliferative properties.

In the current report, we examined the effects of pharmacological concentrations of BA on cell morphology and molecular markers of proliferation, senescence, metastasis and motility. We show that prolonged exposure to BA causes DU-145 cells to develop a flattened, angular phenotype with numerous vesicles appearing in the cytoplasm. These changes occur coincident with a decrease in the expression of cyclin proteins, p21 and P-MEK1/2, as well as a reduction in cell motility and invasion capacity. Finally, increased β-galactosidase activity reflects a conversion of DU-145s to a senescence-like cell.

MATERIALS AND METHODS

Experimental culture

DU-145, LNCaP, and PC-3 PCa cells, donated by Dr Allan Pantuck, were cultured in RPMI 1640 media (Invitrogen, USA) supplemented with 10% FBS, penicillin/streptomysin (100 U ml^{-1}; 100 μg ml^{-1}), and L-glutamine (200 mM) (Gemini Bioproducts,

*Correspondence: Dr CD Eckhert; E-mail: ceckhert@ucla.edu
Received 12 September 2005; revised 4 January 2006; accepted 17 January 2006; published online 21 February 2006

USA). Experimental media was prepared as previously published in Barranco and Eckhert (2004). Cells were plated directly onto culture plates or glass coverslips and allowed to settle overnight in nontreated media. After 24 h, media was aspirated and replaced daily, for 7–8 days, with BA-supplemented media (0–1000 μM). Cell counts were performed using a hemacytometer and Trypan Blue (Invitrogen) for identifying nonviable cells.

Flow cytometry

Following 8 days in culture with BA (0, 250, and 1000 μM), DU-145 cells were trypsinised, resuspended as 1 ml aliquots (10^6 cells ml^{-1}) in loading buffer (RPMI 1640 w/o phenol red), and incubated in 12×75 mm polystyrene test tubes for 30 min, at 37°C, 5% CO_2. Following incubation, forward light scatter and side light scatter analysis (serving as measures of cell size and granularity, respectively) were determined using a Becton Dickinson BD-LSR analytic flow cytometer on samples of 10 000 cells. Data analysis was performed with FLOWJO. Loading buffer was supplemented with Indo-1 AM (1 μM) (Sigma, USA), a cell-permeable Ca^{2+} fluorescent probe, for concordant measurements of intracellular calcium.

β-galactosidase assay

Detection of β-galactosidase activity was determined using a previously published procedure (Dimri *et al*, 1995). DU-145 cells (8-day exposed), cultured on glass coverslips, were washed in PBS and fixed in 3% formaldehyde for 5 min. Fixed cells were washed with PBS and incubated overnight at 37°C (low CO_2) with fresh β-Gal stain solution (1 mg ml^{-1} 5-bromo-4-chloro-3-indoyl β-D-galactopyranoside (X-Gal), 40 mM citric acid/40 mM sodium phosphate (pH 4.0 & 6.0), 5 mM potassium ferrocyanide, 5 mM potassium ferricyanide, 150 mM NaCl, 2 mM $MgCl_2$). The percentage of cells testing positive for β-galactosidase activity (appearing blue) in four randomly selected optical fields were determined under light microscopy.

Western blot

DU-145 cells were cultured for 1, 2, and 7 days in the presence of BA (0–1000 μM), on 100×20 mm tissue culture plates, with daily media replacement. Following treatment, monolayers were washed with PBS, removed with a rubber policeman, and centrifuged at 1200 rpm for 5 min. For protein extraction, pellets were submerged in lysis buffer (250 mM NaCl, 0.1% NP40, 50 mM HEPES (pH 7.0), 5 mM EDTA, 1 mM DTT, 10% protease inhibitor mixture (Sigma)), sonicated, and incubated for 40 min at 4°C. Wells of 10% stacking, 12% separating (SDS–PAGE) gels were loaded with 30 μg of protein per sample and separated for 30 min at 100 V, followed by 1 h at 200 V. Separated proteins were transferred to nitrocellulose membranes for 4 h at 40 V, 4°C. Membranes were blocked overnight (Nonfat dry milk 4 g, 38 mM Tris base, 125 mM NaCl 2.5, 100 μl Tween 20, ddH_2O 100 ml). The 2-h primary antibody exposure (1/200–1/800 dilution) was followed by a 10 min wash in PBS/Tween 20 (0.1%) and 1-h secondary antibody exposure (1/1000 dilution) was followed by 3×10 min washes in PBS/Tween 20 (0.1%). Probed membranes were submerged in ECL detection reagent, (Amersham, USA), wrapped in cellophane, and exposed to X-ray film (Fuji). All primary and secondary antibodies were purchased from Santa Cruz Biotechnology (Santa Cruz, CA, USA).

Fluorescent probe detection of actin and acidic compartments

For actin probing (F-actin, fluorescein phalloidin; G-actin, fluorescent deoxyribonuclease I conjugate) (Molecular Probes, USA), 8-day BA-treated DU-145 cells were washed $2\times$ with PBS and fixed in PBS containing 3.7% formaldehyde, for 10 min at room temperature. Fixed cells were washed $2\times$ with PBS before being extracted with acetone (−20°C) for 5 min. $2\times$ wash with PBS followed before cells were loaded with phalloidin (0.16 μM in 1% BSA/PBS) or deoxyribonuclease I (0.3 μM in glycerol/PBS) for 20 min, at 37°C. Loaded cells were washed $2\times$ with PBS, mounted on slides, and viewed under confocal microscopy (Fluorescein: ex 496, em 516).

For intracellular acidic compartment labelling, 8-day BA-exposed DU-145 cells were loaded with a nonspecific lysosome marker (LysoTracker Green) (Molecular Probes). Cells were submerged in prewarmed media containing LysoTracker (1 μM) for 1 h, at 37°C. Following incubation, loading medium was aspirated, replaced with PBS, and cells were viewed under confocal microscopy (ex 504, em 511). All fluorescent images, along with light images, were recorded using an Axioskop 2 FS confocal microscope and brightened using Photoshop 6.0.

Cell attachment, migration, and invasion assays

For cell attachment efficiency calculations, DU-145 cells were cultured in the presence of BA (0, 250, and 1000 μM) for 8 days on 100×20 mm tissue culture plates, trypsinised and replated onto six-well polystyrene culture plates (Fisher, USA) at 2.5×10^5 cells well^{-1}. Following a 24-h incubation, nonadherent cells and media were aspirated, while attached cells were trypsinised and counted.

The migration analysis protocol was identical to the attachment assay's, except that 2.5×10^5 cells were loaded in the upper migration chamber of a Corning transwell permeable support (24-well transwell, 8-μM polycarbonate membrane) in 0.1 ml of serum-free RPMI-1640 media. RPMI-1640 (0.6 ml) supplemented with 10% FBS, serving as a chemo-attractant, was deposited in the lower chamber. Plates were covered and incubated for 24 h at 37°C, 5% CO_2. Following incubation, cells remaining on the upper filter were removed with a cotton swab, while the migrated population on the filter underside was washed with PBS, fixed in methanol, stained with Giemsa stain, rinsed with PBS, and deionised water, and allowed to air-dry. Cells in four random optical fields were counted to determine the number of migratory cells.

The invasion assay procedure was identical to that used in the migration analysis, except that each filter, prior to loading, was coated with 20 μg of growth factor reduced-matrigel (BD biosciences) in 100 μl of cold, serum-free RPMI-1640 media, and subsequently allowed to air-dry overnight in a sterile culture hood.

Since plating efficiency varied among BA-treated cells on matrigel-treated and untreated polycarbonate membranes, test cells were cultured alongside experimental cells and after incubation were trypsinised from filters, counted on a haemacytometer and used to determine the motility fraction.

Media pH measurements

Following 8-day BA (250 and 1000 μM) exposures to DU-145 cells, with daily media refreshment, media used for the 24 h period between day 7 and 8 was removed and the pH was measured using a Pinnacle 530 pH meter (Corning). Cell counts were performed on the adherent cells from corresponding plates and utilised for calculating the pH shift per cell:

$$\text{Acidic pH shift per cell} = \frac{7.4 - \text{observed pH}}{\text{Cells per plate}(\times 10^6)}.$$

Statistics

SigmaStat 3.1 statistical software (Systat Software, Point Richmond, CA, USA) was utilised for paired *t*-test. All experiments were performed in triplicate.

RESULTS

BA alters cell morphology, while inducing cellular senescence

Flow cytometry and light microscopy were used to assess morphological alterations resulting from BA exposure. Following an 8-day exposure to BA (0, 250, and 1000 μM), flow cytometry analysis showed a dose-dependent increase in cellular granularity (side light scatter) and a decrease in cell size (forward light scatter) (Figure 1A). No differences in cell morphology were apparent between confocal images of treated and untreated cells during the first 2 days. By day 8, treated DU-145 cells became flattened and contained numerous vesicles (Figure 1B).

BA's ability to inhibit cell proliferation without cell-death inspired our investigation to determine its effects on markers of senescence. The activity of β-galactosidase at pH 4.0, a marker of senescence, increased with BA exposure in a dose-dependent manner (Figure 1C). Enzyme activity was not detected at pH 6.0 (data not shown).

BA alters proliferation-relevant protein expression

DU-145 cells were exposed to BA (0–1000 μM) for 1, 2, or 7 days. No changes were apparent at 1 or 2 days, but at 7 days, the protein expression of cyclins A, B1, C, D1, E, and the phosphorylated form of MAPK signaler MEK (P-MEK1/2) decreased at 500 and 1000 μM concentrations (Figure 2A–F). Phosphorylated ERK (P-ERK1/2) increased at intermediate exposures (100 and 250 μM), relative to control, but was reduced by higher concentrations of BA (Figure 2B). The tumour suppressor gene p53 expression remained stable, but p21 decreased following 7-day exposures (Figure 2H).

BA induces cytoskeletal alterations, while inhibiting cell attachment, migration, and invasion

Measurements were taken to assess cell attachment, migration, invasion, and intracellular cytoskeletal actin distribution to determine if BA (250 and 1000 μM) exposure for 8 days had an effect on metastasis-related aspects of cancer cells. Staining for filamentous (F)-actin, a marker for intercellular connections and extensions such as filopodia, was decreased in cells exposed to high levels of BA. A total of 1000 μM-treated cells had smooth-edges and were angular in appearance (Figure 3A). Intracellular globular (G)-actin expression was unaltered by BA exposure.

BA-treated cells show a reduction in attachment efficiency to polystyrene culture dishes, with a drop in plating efficiency of 34% at 1000 μM (Figure 3B). With 10% FBS serving as a chemo-attractant, the capacity of DU-145 cells to migrate across an 8 μm polycarbonate permeable membrane was reduced by 28 and 89%, by 250 and 1000 μM BA, respectively (Figure 3C). The same trend was observed with invasion potential, where 250 and 1000 μM BA pretreatments reduced matrigel invasion by 82 and 97% (Figure 3C).

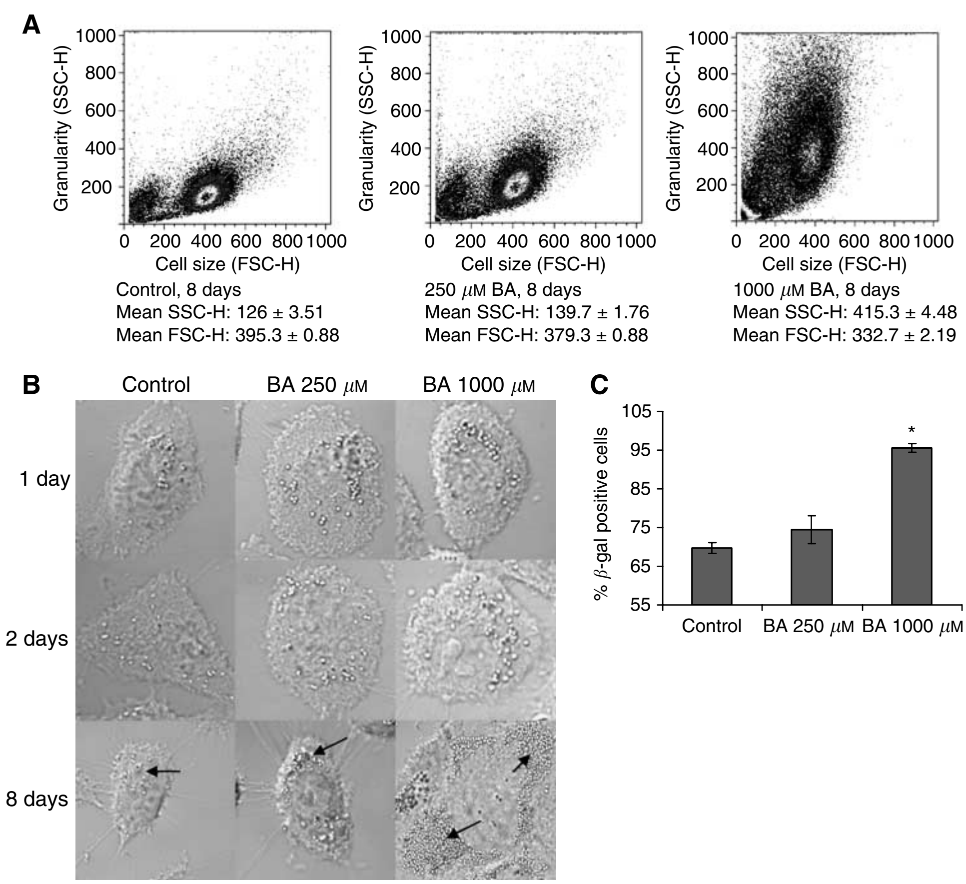

Figure 1 BA-induced morphological and senescent effects, following 8-day exposure, in DU-145 cells. (**A**) Dose-dependent increase in granularity, by way of forward light scatter (FSC-H), and decrease in cell size, by way of side light scatter (SSC-H), from BA (0–1000 μM) exposure, as presented on density plot; mean $\pm$ s.e.m., $n = 3$. (**B**) Confocal images (63 $\times$) showing dose-dependent intracellular vesicle accumulation, as indicated by arrows, and flattened appearance at 8 days of exposure; whereas at 1 and 2 days cells remain unaltered. (**C**) Dose-dependent β-galactosidase activity (pH 4.0) increase in DU-145 cells; mean $\pm$ s.e.m., $n = 4$. * Statistically significant from control exposures (P-value < 0.001).

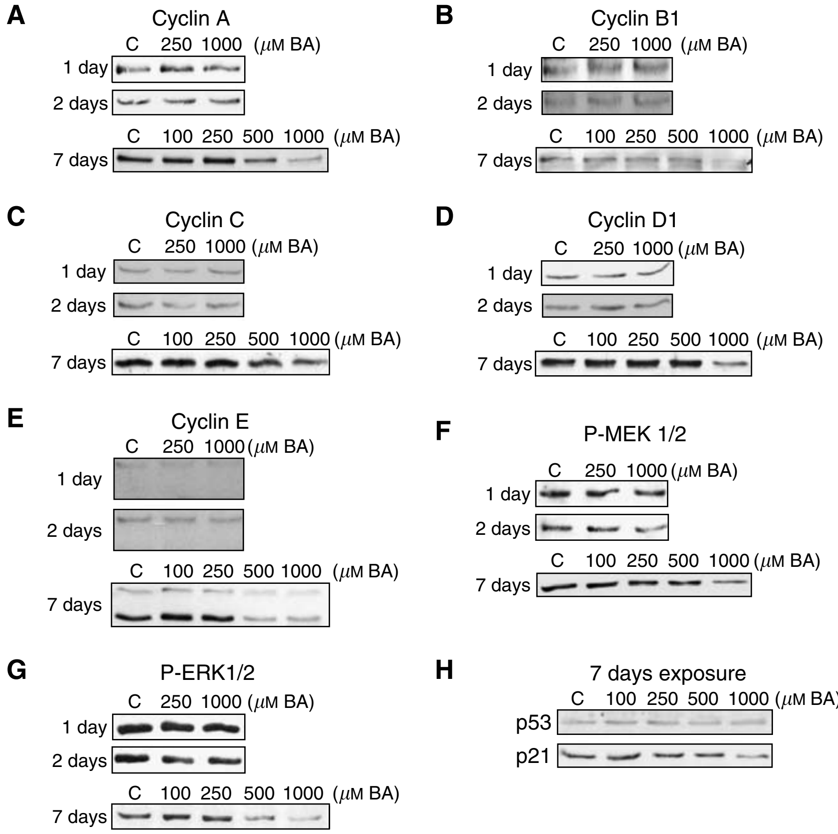

Figure 2 BA-induced alterations in proliferation-relevant protein expression, following 1, 2, and 7-day exposure, in DU-145 cells. (**A**–**E**) Western blots show dose-dependent BA-induced (0–1000 μM) expression changes of cyclin proteins, (**F**, **G**) P-MEK1/2 and P-ERK1/2, and (**H**) p53 and p21.

BA induces media acidosis and accumulation of acidic vesicles

Acidic yellowing of phenol red in culture media was more pronounced in BA treated cells. The pH of media was measured prior to (pH 7.4) and following exposure to DU-145 cells for 24 h, between the 7th and 8th days of culture. The pH for each concentration of BA (0, 250, and 1000 μM) was then converted into an acidic shift from pH 7.4 per cell value. Chronically BA-exposed DU-145 cells acidified the surrounding culture media in a dose-dependent manner (Figure 4A). The number of acidic vesicles (measured using Lysotracker fluorescent probe) also increased in a dose-dependent manner, but both the lysosome-specific LAMP-2 protein and early endosome marker EEA1 decreased (Figure 4B and C). The concentrations of BA used in culture media displays no significant effect on media pH (data not shown). To exclude the possibility that BA might alter the buffering capacity of densely populated culture plates, cells were cultured to near-confluence in control media before exposure to BA-supplemented media (250 and 1000 μM) for 24 h. The pH remained unchanged at all BA concentrations, showing acidity was not associated with the media, but instead with cell changes that occurred during the 7 day exposure (data not shown).

DISCUSSION

Boron has a high affinity for oxygen and is present in aqueous solution, depending on pH, as either BA ($B(OH)_3$) or borate ($(B(OH)_4)^-$). Since the pK_a of the equilibrium between $B(OH)_3$ and borate ($(B(OH)_4)^-$ is 9.2, at intracellular pH (7.4) free boron exists as the weak Lewis acid, BA. BA, a small molecule with a mass of 61.83, is rapidly absorbed from the human intestine and excreted via urine with a half-life of 21 h (Jansen *et al*, 1984, Schou *et al*, 1984). There is no evidence supporting metabolism of BA in any animal species (EPA, 1991). BA does bind to molecules with *cis*-hydroxyl groups, as established through mass spectrometry and NMR analysis identifying a high affinity for the ribose moieties of NAD^+, and a somewhat lower affinity for mononucleotides (Kim *et al*, 2003). Nucleotide phosphorylation and loss of charge greatly reduces substrate affinity for BA (Kim *et al*, 2004).

Morphology

Flow cytometry analysis showed that BA caused a reduction in cell volume, yet under light microcopic investigation cells appeared to have a larger diameter. We believe the DU-145 cell line is responding to higher concentrations of BA by rearranging its cell shape into a flattened, low-volume state (Figure 3A). These structural alterations in shape and size are likely contributing to the inability of the cells to proliferate, since increased cell volume and a rounding up from the attached substrate are both critical events during mitotic division (Lang *et al*, 2000; Fujibuchi *et al*, 2005). The observation that morphological alterations did not appear following 1 and 2 day BA exposures, but did at 8 days, argues the changes reflect secondary response of long-term treatment with BA.

The relative intensity of fluorescent staining for G- and F-actin was found to be unchanged, regardless of BA concentration, indicating a steady-state actin pool ratio. Although actin concentrations in general appear unaltered, F-actin-stained filopodia extending about the periphery of the cells was reduced by 1000 μM BA. With actin serving an important cytoskeletal factor

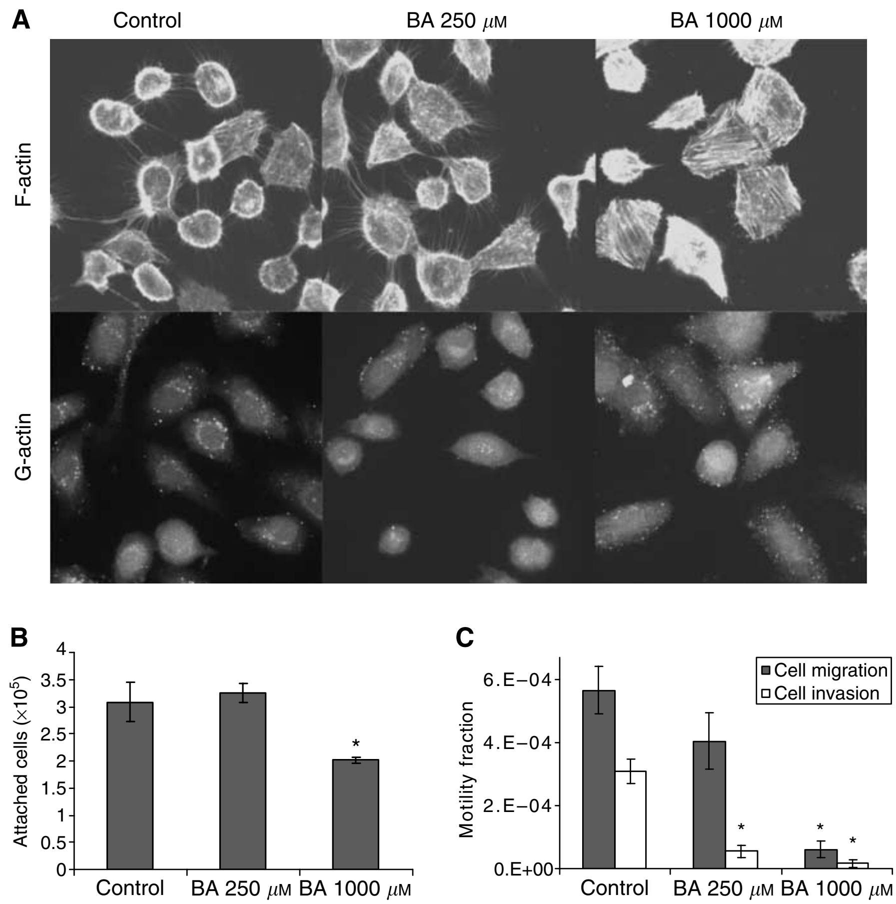

Figure 3 BA-induced changes in cell attachment, migration and invasion capacity, following 8-day exposure, in DU-145 cells. (**A**) Confocal images (63 ×) of BA-treated (0–1000 μM) cells showing F-actin filopodia retraction, yet no effect on G- or F-actin relative expression. (**B**) Reductions occurred in attachment efficiency. * Statistically significant from control exposures (P-value <0.04). (**C**) Migratory and invasive capacity was reduced in treated cells; mean ± s.e.m., $n=3$. * Statistically significant from control exposures (P-value <0.02).

in cell migration and invasion (Lambrechts *et al*, 2004), the observed F-actin retraction in BA-treated cells suggests a reduced capacity to perform either. This interpretation was reinforced by the analysis showing a dose-dependent inhibitory effect on motility and invasion capacity, along with incompetence for reattachment (Figure 3B and C). Together, these results suggest that BA reduces the metastatic potential of the DU-145 cell.

In BA-treated cells, granularity increased in proportion to exposure concentration, possibly due to the formation of intracellular vesicles (Figure 1A and B). The origin and content of these vesicles is unknown, since fluorescent probes for acidic compartments, tubulin, and intracellular calcium all failed to colocalise (data not shown).

Proliferation

The mechanism underlying the antiproliferative activity of BA has not been elucidated. One of the intriguing properties of BA is its ability to inhibit proliferation without causing a shift in cell cycle stage distribution or cell death (Barranco and Eckhert, 2004). In the current study, BA decreased the expression of five major cyclin proteins, all presumably playing significant roles in cell cycle progression (Figure 2A). Furthermore, the ability of antiproliferative agents to inhibit the expression of these proteins is important, since cyclins A, B1, E, and D1 have been correlated with prostate cancer aggressiveness (Mukhopadhyay *et al*, 2002; Maddison *et al*, 2004; Tsao *et al*, 2004).

The DU-145 cell line has a mutant p53 protein incapable of signalling through p21, so it was nonetheless surprising to see p21 expression reduced by BA exposure (Figure 2B) (Lecane *et al*, 2003). The downregulation of p21 helps to explain why BA does not shift DU-145 cell populations into a G1 arrest (Barranco and Eckhert, 2004, Shukla and Gupta, 2004).

BA's effects on growth has been shown to be parabolic in embryonic trout and zebrafish with poor embryonic growth occurring at very low and high concentrations (U-shaped curve) (Rowe *et al*, 1998). BA's growth effects are cell-type dependent with maximum growth occurring in *Saccharomyces cerevisiae* cells at $<0.8\,\mu$M BA, whereas 500 μM of BA maximised proliferation in HeLa cervical cancer cells (Bennett *et al*, 1999; Park *et al*, 2004). Furthermore, in HeLa cells BA (300 μM) was shown to stimulate the MAPK pathway in a bell-shaped fashion, with an initial induction of P-MEK1/2 and P-ERK1/2, followed by a decline in expression of P-MEK1/2 over time. In the present study, BA reduced P-MEK1/2 expression in a dose-dependent manner, yet increased P-ERK1/2 moderately at 250 μM (Figure 2F and G). By way of Ras/Raf signalling, the phosphorylated form of MEK phosphoylates ERK, which then translocates to the nucleus and activates transcription factors relevant in proliferative induction. Thus, by upregulation of this pathway's activity, it appears that DU-145 cells are attempting to counter the BA-induced growth inhibition (Giehl, 2005). Expression of MEK, ERK, and all cyclins were not altered following 1 and 2 day treatments suggesting, as observed with cell morphological changes, these were not the primary effect of BA.

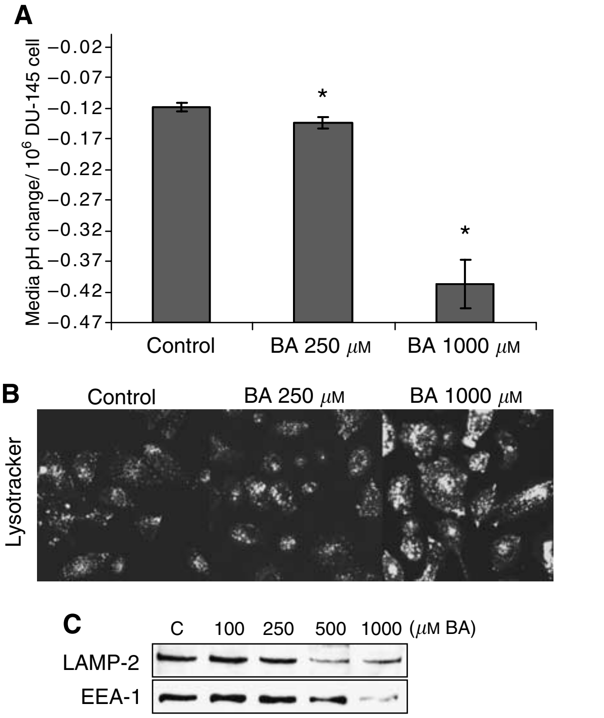

Figure 4 BA-induced media pH shifts and acidic vesicle accumulation, following 8-day exposure, in DU-145 cells. (**A**) pH shifts from 7.4 (per 10^6 cells) recorded in BA-supplemented (0–1000 μM) culture media, following overnight exposure, subsequent to 8-day treatment; mean $\pm$ s.e.m., $n = 3$. *Statistically significant from control exposures (P-value < 0.009). (**B**) Confocal microscopic images of BA-treated cells with Lysotracker (fluorescent marker of intracellular acidic compartments). (**C**) 7-day BA treatments (0–1000 μM) led to downregulation of lysosome (LAMP-2) and the early endosome (EEA1) markers, as shown in Western blots.

Senescence

DU-145 cells were evaluated for β-galactosidase activity, a marker of senescence or reversible cellular quiescence (Coates, 2002). When enzymatic activity is measured at pH 4.0, it is thought to indicate an increase in lysosomal enzyme concentration, whereas enhanced activity at pH 6.0 reflects an increased lysosomal mass (Kurz *et al*, 2000). In our study, BA treatment increased the activity of β-galactosidase in a dose-dependent manner at pH 4.0, yet no activity was apparent at pH 6.0. However, the dose-dependent increase recorded at pH 4.0 suggests the BA induces some 'senescent-like' characteristics.

Accumulation of acidic intracellular vesicles

A peculiar manifestation of BA treatment was discovered when the media of chronically exposed DU-145 cells became increasingly acidic (Figure 4A). This effect was dose-dependent and not due to changes in the buffering capacity of the media or BA itself. The documented accumulation of acidic intracellular compartments is supportive of an affiliation with the media pH shift, by either contributing directly to the environmental acidification, or rather resulting from it, as seen in breast cancer cells (Glunde *et al*, 2003). Initially, we believed the upregulation of acidic vesicles reflected an increase in lysosome organelles, yet the LAMP-2 protein, expressed on lysosomal membranes in prostate tissue, decreased in expression (Figure 4C) (Furuta *et al*, 1999). It was also possible that the acidic vesicles were early endosomes, yet the protein expression of early endosome marker EEA-1 was likewise reduced (Eskelinen *et al*, 2003). Further studies are needed to determine if this response is unique to cancer cells or a universal response to BA (Gatenby and Gillies, 2004). Interestingly, metabolic acidosis has been reported in a case of fatal BA poisoning (Restuccio *et al*, 1992).

Conclusion

The rationale for this study was based on the fact that BA is (i) a natural constitute of human blood, (ii) readily absorbed with plasma levels determined by dietary intake, and (iii) there is epidemiological, animal, and cell culture evidence supporting its antiproliferative capacity in prostate cancer. In this report, we show that pharmacologically-relevant BA treatment causes DU-145 prostate cancer cells to convert to highly granular, low-volume, flattened cells that have a marked reduction in their capacity to migrate, invade matrigel, and attach to synthetic substrates. Reduction in the expression of proliferation-relevant proteins, along with the upregulation of β-galactosidase activity, ultimately leads to a nonproliferating entity reminiscent of a senescent-like cell. Finally, the resulting cell accumulates intracellular acidic vesicles, while acidifying its extracellular environment.

ACKNOWLEDGEMENTS

We thank Dr Allan Pantuck and Randy Kallilew for their expertise concerning cell culture. With the help of Michael Gulrajani, flow cytometry was performed in the UCLA Jonsson Comprehensive Cancer Center (JCCC) and Center for AIDS Research Flow Cytometry Core Facility that is supported by National Institutes of Health awards CA-16042 and AI-28697, and by the JCCC, the UCLA AIDS Institute, and the David Geffen School of Medicine at UCLA. Grant support: DOD prostate idea Grant DAMD17-03-1-0067 (CD Eckhert) and UC TRS&TP (WT Barranco).

REFERENCES

Barranco WT, Eckhert CD (2004) Boric acid inhibits human prostate cancer cell proliferation. *Cancer Lett* **216:** 21–29

Bennett A, Rowe RI, Soch N, Eckhert CD (1999) Boron stimulates yeast (*Saccharomyces cerevisiae*) growth. *J Nutr* **129:** 2236–2238

Bone R, Shenvi AB, Kettner CA, Agard DA (1987) Serine protease mechanism: structure of an inhibitory complex of alpha-lytic protease and a tightly bound peptide boronic acid. *Biochemistry* **26:** 7609–7614

Chen X, Schauder S, Potier N, Van Dorsselaer A, Pelczer I, Bassler BL, Hughson FM (2002) Structural identification of a bacterial quorum-sensing signal containing boron. *Nature* **415:** 545–549

Coates PJ (2002) Markers of senescence? *J Pathol* **196:** 371–373

Cui Y, Winton MI, Zhang ZF, Rainey C, Marshall J, De Kernion JB, Eckhert CD (2004) Dietary boron intake and prostate cancer risk. *Oncol Rep* **11:** 887–892

Dimri GP, Lee X, Basile G, Acosta M, Scott G, Roskelley C, Medrano EE, Linskens M, Rubelj I, Pereira-Smith O, Peacocke M, Campisi J (1995) A biomarker that identifies senescent human cells in culture and in aging skin *in vivo*. *Proc Natl Acad Sci USA* **92:** 9363–9367

Environmental Protection Agency (1991) Health and environmental effects document for boron and boron compounds. Report EPA6008-91015; Order No. PB91-233635: 1–269

Eskelinen EL, Tanaka Y, Saftig P (2003) At the acidic edge: emerging functions for lysosomal membrane proteins. *Trends Cell Biol* **13:** 137–145

Fujibuchi T, Abe Y, Takeuchi T, Imai Y, Kamei Y, Murase R, Ueda N, Shigemoto K, Yamamoto H, Kito K (2005) AIP1/WDR1 supports mitotic cell rounding. *Biochem Biophys Res Commun* **327:** 268–275

Furuta K, Yang XL, Chen JS, Hamilton SR, August JT (1999) Differential expression of the lysosome-associated membrane proteins in normal human tissues. *Arch Biochem Biophys* **365:** 75 – 82

Gallardo-Williams MT, Chapin RE, King PE, Moser GJ, Goldsworthy TL, Morrison JP, Maronpot RR (2004) Boron supplementation inhibits the growth and local expression of IGF-1 in human prostate adenocarcinoma (LNCaP) tumors in nude mice. *Toxicol Pathol* **32:** 73 – 78

Gallardo-Williams MT, Maronpot RR, Wine RN, Brunssen SH, Chapin RE (2003) Inhibition of the enzymatic activity of prostate-specific antigen by boric acid and 3-nitrophenyl boronic acid. *Prostate* **54:** 44 – 49

Gatenby RA, Gillies RJ (2004) Why do cancers have high aerobic glycolysis? *Nat Rev Cancer* **4:** 891 – 899

Giehl K (2005) Oncogenic Ras in tumour progression and metastasis. *Biol Chem* **386:** 193 – 205

Glunde K, Guggino SE, Solaiyappan M, Pathak AP, Ichikawa Y, Bhujwalla ZM (2003) Extracellular acidification alters lysosomal trafficking in human breast cancer cells. *Neoplasia* **5:** 533 – 545

Jansen JA, Andersen J, Schou JS (1984) Boric acid single dose pharmacokinetics after intravenous administration to man. *Arch Toxicol* **55:** 64 – 67

Kim DH, Faull KF, Norris AJ, Eckhert CD (2004) Borate-nucleotide complex formation depends on charge and phosphorylation state. *J Mass Spectrom* **39:** 743 – 751

Kim DH, Marbois BN, Faull KF, Eckhert CD (2003) Esterification of borate with NAD+ and NADH as studied by electrospray ionization mass spectrometry and 11B NMR spectroscopy. *J Mass Spectrom* **38:** 632 – 640

Kurz DJ, Decary S, Hong Y, Erusalimsky JD (2000) Senescence-associated (beta)-galactosidase reflects an increase in lysosomal mass during replicative ageing of human endothelial cells. *J Cell Sci* **113:** 3613 – 3622

Lambrechts A, Van Troys M, Ampe C (2004) The actin cytoskeleton in normal and pathological cell motility. *Int J Biochem Cell Biol* **36:** 1890 – 1909

Lang F, Ritter M, Gamper N, Huber S, Fillon S, Tanneur V, Lepple-Wienhues A, Szabo I, Gulbins E (2000) Cell volume in the regulation of cell proliferation and apoptotic cell death. *Cell Physiol Biochem* **10:** 417 – 428

Lecane PS, Kiviharju TM, Sellers RG, Peehl DM (2003) Leptomycin B stabilizes and activates p53 in primary prostatic epithelial cells and induces apoptosis in the LNCaP cell line. *Prostate* **54:** 258 – 267

Maddison LA, Huss WJ, Barrios RM, Greenberg NM (2004) Differential expression of cell cycle regulatory molecules and evidence for a ‘cyclin switch’ during progression of prostate cancer. *Prostate* **58:** 335 – 344

Mukhopadhyay A, Banerjee S, Stafford LJ, Xia C, Liu M, Aggarwal BB (2002) Curcumin-induced suppression of cell proliferation correlates with down-regulation of cyclin D1 expression and CDK4-mediated retinoblastoma protein phosphorylation. *Oncogene* **21:** 8852 – 8861

Park M, Li Q, Shcheynikov N, Zeng W, Muallem S (2004) NaBC1 is a ubiquitous electrogenic Na+-coupled borate transporter essential for cellular boron homeostasis and cell growth and proliferation. *Mol Cell* **16:** 331 – 341

Price CJ, Strong PL, Murray FJ, Goldberg MM (1997) Blood boron concentrations in pregnant rats fed boric acid throughout gestation. *Reprod Toxicol* **11:** 833 – 842

Restuccio A, Mortensen ME, Kelley MT (1992) Fatal ingestion of boric acid in an adult. *Am J Emerg Med* **10:** 545 – 547

Rowe RI, Bouzan C, Nabili S, Eckhert CD (1998) The response of trout and zebrafish embryos to low and high boron concentrations is U-shaped. *Biol Trace Elem Res* **66:** 261 – 270

Schou JS, Jansen JA, Aggerbeck B (1984) Human pharmacokinetics and safety of boric acid. *Arch Toxicol Suppl* **7:** 232 – 235

Semmelhack MF, Campagna SR, Hwa C, Federle MJ, Bassler BL (2004) Boron binding with the quorum sensing signal AI-2 and analogues. *Org Lett* **6:** 2635 – 2637

Shukla S, Gupta S (2004) Molecular mechanisms for apigenin-induced cell-cycle arrest and apoptosis of hormone refractory human prostate carcinoma DU145 cells. *Mol Carcinog* **39:** 114 – 126

Sobel RE, Sadar MD (2005) Cell lines used in prostate cancer research: a compendium of old and new lines – part 1. *J Urol* **173:** 342 – 359

Takano J, Noguchi K, Yasumori M, Kobayashi M, Gajdos Z, Miwa K, Hayashi H, Yoneyama T, Fujiwara T (2002) Arabidopsis boron transporter for xylem loading. *Nature* **420:** 337 – 340

Tsao AS, Kim ES, Hong WK (2004) Chemoprevention of cancer. *CA Cancer J Clin* **54:** 150 – 180

JOURNAL OF MASS SPECTROMETRY
J. Mass Spectrom. 2004; **39**: 743–751
Published online in Wiley InterScience (www.interscience.wiley.com). DOI: 10.1002/jms.645

JMS

Borate–nucleotide complex formation depends on charge and phosphorylation state

Danny H. Kim,[1] Kym F. Faull,[2] Andrew J. Norris[3] and Curtis D. Eckhert[1]*

[1] Department of Environmental Health Sciences, University of California 10833 Le Conte Avenue, Los Angeles, California 90095, USA
[2] Pasarow Mass Spectrometry Laboratory, Departments of Psychiatry and Biobehavioral Sciences, Chemistry and Biochemistry and the Neuropsychiatric Institute, University of California, 10833 Le Conte Avenue, Los Angeles, California 90095, USA
[3] UCLA Johnson Comprehensive Cancer Center, University of California, 10833 Le Conte Avenue, Los Angeles, California 90095, USA

Received 22 December 2003; Accepted 1 April 2004

Flow injection analysis with electrospray ionization mass spectrometry was used to investigate borate–nucleotide complex formation. Solutions containing 100 μM nucleotide and 500 μM boric acid in water–acetonitrile–triethylamine (50 : 50 : 0.2, v/v/v; pH 10.3) showed that borate complexation with nicotinamide nucleotides was significantly influenced by the charge on the nicotinamide group and the number of phosphate groups on the adenine ribose. Borate binding decreased in the order of NAD$^+$, NADH, NADP$^+$ and NADPH. To investigate the relationship between complex formation and phosphorylation, association constants (K_A) of borate–adenine (AMP, ADP, ATP), –guanine (GMP, GDP, GTP), –cytidine (CMP, CDP, CTP) and –uridine (UMP, UDP, UTP) complexes were compared. The results showed that the number of nucleotide phosphate groups was inversely proportional to the relative abundance of the borate complexes, with the K_A of borate–nucleotide complex decreasing in the order mono-, di- and tri-phosphates (AMP $\approx$ GMP $\approx$ CMP $\approx$ UMP > ADP $\approx$ GDP $\approx$ CDP $\approx$ UDP > GTP > ATP $\approx$ CTP $\approx$ UTP). At pH 7.4, using ammonium bicarbonate buffer, only borate–NAD$^+$ complex was observed. This indicates that the borate–NAD$^+$ complex may be the most physiologically relevant of those studied. Copyright © 2004 John Wiley & Sons, Ltd.

KEYWORDS: borate–nucleotide complexation; nucleotide; association constant; dissociation constant

INTRODUCTION

In aqueous solution, boron exists as either boric acid ($B(OH)_3$) or borate ($B(OH)_4^-$) ions, as shown in Eqn (1). Since the pK_a of boric acid is 9.2, at intracellular pH, nearly all free boron exists as boric acid. Boric acid reacts with polyhydroxy compounds, leading to a decrease in pH (Eqn (2)).[1–4] Complex formation between boric acid and polyhydroxy compounds depends on the pH of the solution and the structure of the polyhydroxy compounds, and we have previously shown that this is true for boric acid and NAD$^+$.[5] Van den Berg *et al* showed that in the case of diols, *cis*-1,2- are favored over *trans*- or 1,3-diols, and five-membered ring are preferred over six-membered ring 1,2-diols.[6] Therefore, a ribose ring with 2,3-*cis*-diol may be an important reactive site for interaction with boric acid.

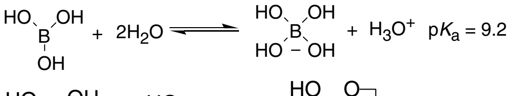

(1)

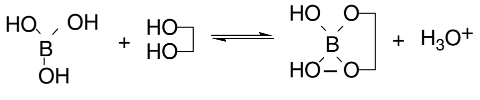

(2)

*Correspondence to: Curtis D. Eckhert, Department of Environmental Health Sciences, Box 957772, University of California, 10833 Le Conte Avenue, Los Angeles, California 90095, USA. E-mail: ceckhert@ucla.edu
Contract/grant sponsor: UC Toxic Substances Research and Teaching Program.
Contract/grant sponsor: US Borax.

Boron is ubiquitous in the environment and is present in all living organisms. In 1923, boron was shown to be an essential nutrient for plants,[7] but it was not until 1996 that it was discovered to be structural component of the cell wall.[8,9] Recently a transport mechanism for boron in plant roots was identified that has low homology to certain kidney transport proteins.[10,11] Boron has also been shown to be a component of autoinducer (AI-2), a signaling compound regulating colony-wide gene expressions in Gram-positive and -negative bacteria.[12] Boron was recently shown to promote embryonic growth[13] and to be essential for post-fertilization cell growth in fish[14] and frogs.[15] Human studies suggest that boron may be important for bone strength,[16] cognitive performance[17] and serum 17β-estradiol levels.[18] Dietary boron intake has also been reported to reduce the risk of prostate cancer.[19] However, toxic effects of excess boron have also been reported. At high concentrations of oral intake, boric acid caused degeneration of seminiferous epithelium of rodents.[20] Although the mechanisms for these effects remain obscure, the long-known complexation of boric acid to the *cis*-diol moiety of ribose sugars suggests that a similar reaction may underlie its biological effects in animals. Since nucleotides are among the most abundant and metabolically important molecules containing the ribose *cis*-diol moiety, a ranking of borate–nucleotide complex by association constants could provide insight for understanding the physiological effects of borate.

Briefly, in our previous work, we determined that boric acid bound to the *cis*-diol on the ribose moiety rather than the phosphate groups using GDP and deoxy-GDP. At pH 10.3, all the boric acid–nucleotide complex detected by flow injection analysis with electrospray ionization mass spectrometry (ESI-MS) was a fragment of borate–nucleotide complex due to a loss of a hydroxyl group in the gas phase.[5] Henceforth, most of the nucleotide complexes in solution prior to ionization are assumed to be borate–nucleotide complexes.

In the past, investigation of borate complexation was largely studied by indirect methods that relied on changes in pH, UV absorption or conductivity.[21–23] However, direct measurements by ESI-MS is superior to those methods.[5] Because of the sensitivity and resolution, it is possible to use concentrations that are physiologically more relevant to investigate the complexation. In the present study, we extended our previous work with a direct determination and comparison of the association constants (K_A) of different borate–nucleotide complexes. Fundamental characteristics of borate–nucleotide complex formation were established which are broadly applicable to the study of the interaction between borate and a wide variety of biochemical targets that contain *cis*-diols.

EXPERIMENTAL

Chemical reagents

Enriched $^{11}B(OH)_3$ (99.27% purity) was purchased from Eagle-Picher Technologies (Quapaw, OK, USA). Analytical-grade or higher NAD^+, NADH, $NADP^+$, NADPH, adenosine, AMP, ADP, ATP, guanosine, GMP, GDP, GTP, cytidine, CMP, CDP, CTP, uridine, UMP, UDP and UTP were purchased from Sigma Aldrich (St. Louis, MO, USA). All other reagents and solvents were of analytical grade or higher. Ultrapure water (<10 nM boron) was prepared by ion-exchange treatment, and the boron content was checked by quantitative inductively coupled plasma mass spectrometry as described previously.[24]

Sample preparation for ESI-MS analysis

All aqueous solutions were prepared fresh in ultrapure water. For experiments at pH 10.3, water–acetonitrile–triethylamine mixtures (WAT) (50 : 50 : 0.2, v/v/v) were used as the solvent. For experiments at pH 7.4, 50 mM aqueous ammonium bicarbonate (pH adjusted with 0.1 N acetic acid)–acetonitrile (50 : 50, v/v) was used as the solvent. The borate complexes (esters) were prepared by mixing equal volumes of boric acid and nucleotide solutions, yielding final concentrations of 100–600 and 100 μM, respectively. Volumes of 10 μL of these samples were analyzed by ESI-MS. For each nucleotide, a minimum of 12 different (made on three separate occasions, each time with different sample preparations) measurements were made and analyzed for the determination of K_A.

ESI-MS

A Perkin-Elmer Sciex (Thornhill, ON, Canada) API III triple-quadrupole mass spectrometer fitted with an Ionspray source was tuned and calibrated in the positive ion mode as described previously.[25] The instrument resolution allowed for a 15–20% valley between the ^{13}C-containing satellites of the polypropylene glycol/NH_4^+ singly charged calibrant ion at m/z 906. For analysis of borate esterification to the nucleotides, the instrument polarity was reversed and the ionspray voltage lowered to −3.5 kV. Samples dissolved in prepared solvents were introduced (10 μl per injection) into a stream of the same solvent entering the ion source (10 μl min^{-1}). Normal spectra were collected (profile mode) while the instrument was scanning a 100 m/z range (0.1 Da step size, 6 ms dwell time, 6.66 s per scan, orifice −60 V).

Data processing

Representative spectra were computed as the average of all the spectra accrued from each injection using instrument-supplied software (MacSpec, version 3.3; Perkin-Elmer Sciex). For the measurement of nucleotides and their complex concentrations, the spectra were smoothed and the relative peak areas were measured after exporting the data to the IGOR Pro program (version 4, WaveMetrics, Lake Oswego, OR, USA).

RESULTS

ESI-MS analysis of borate complexed with *NAD*$^+$, NADH, *NADP*$^+$ and NADPH

In WAT solvent (pH 10.3), negative ion ESI-MS of 100 μM solutions of NAD^+ revealed a prominent molecular anion for the singly charged, alkali metal-free molecule $[M-H]^-$ at m/z 661.8 (Scheme 1, **I**, calcd 662.1 Da). Following the addition of $^{11}B(OH)_3$ (100–500 μM final concentration), the spectra revealed additional signals at m/z 687.8, assigned as the singly charged boric acid–NAD^+ complex[5] (calcd 688.1 Da for $[M-H]^-$), m/z 705.8, assigned as a borate–NAD^+ complex[5] (calcd 706.1 Da for $[M-H]^-$), m/z 713.8, assigned as a diboric acid–NAD^+ complex (calcd 714.1 Da for $[M-H]^-$), and m/z 749.8, assigned as a

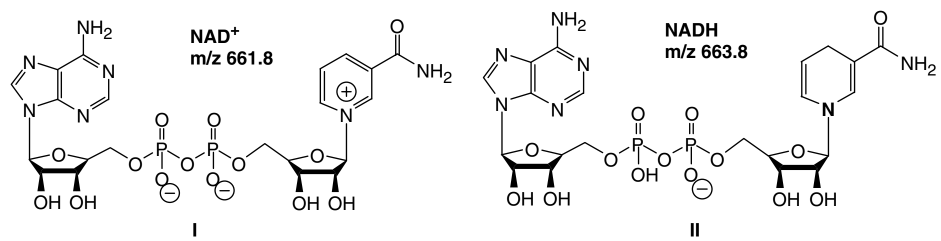

Scheme 1. Proposed structures of deprotonated NAD^+ and NADH.

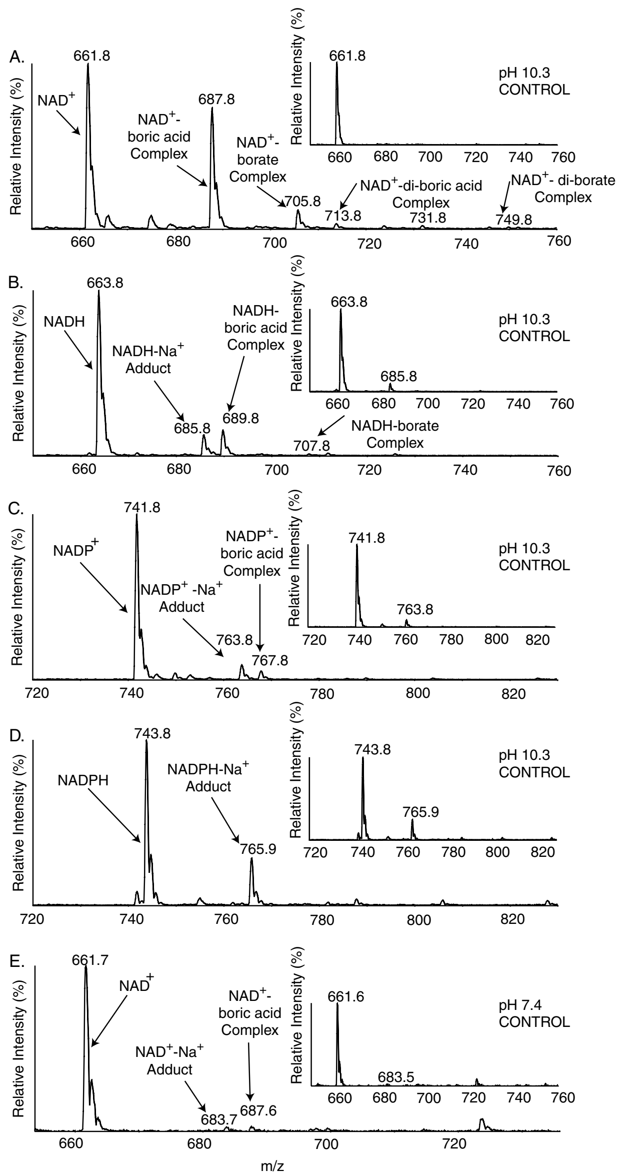

Figure 1. Negative ion ESI mass spectra of NAD^+, NADH, $NADP^+$ and NADPH (100 μM) and their complexes with borate (500 μM) in WAT at pH 10.3 (A–D) and in ammonium bicarbonate buffer at pH 7.4 (E). Although all peaks are anionic, they are labeled by their molecular name for simplification. (A) NAD^+ showing an intense $[M-H]^-$ signal at *m/z* 661.8 (calcd 662.1 Da), boric acid–NAD^+ complex at *m/z* 687.8 (calcd 688.1 Da), borate–NAD^+ complex at *m/z* 705.8 (calcd 706.1), diboric acid–NAD^+ complex at *m/z* 713.8 (calcd 714.1 Da) and diborate–NAD^+ complex at *m/z* 749.8 (calcd 750.1 Da). (B) Free NADH at *m/z* 663.8 (calcd 664.1 Da), NADH–Na^+ adduct at *m/z* 685.8 (calcd 686.1 Da), boric acid–NADH complex at *m/z* 689.8 (calcd 690.1 Da) and borate–NADH complex at *m/z* 707.8 (calcd 708.1 Da). (C) Free $NADP^+$ at *m/z* 741.8 (calcd 742.1 Da), $NADP^+$–Na^+ adduct at *m/z* 763.8 (calcd 764.1 Da) and boric acid–$NADP^+$ complex at *m/z* 767.8 (calcd 768.1 Da). (D) Free NADPH at *m/z* 743.8 (calcd 744.1 Da) and NADPH–Na^+ adduct at *m/z* 765.8 (calcd 766.1 Da). (E) In ammonium bicarbonate buffer at pH 7.4, free NAD^+ at *m/z* 661.7 (calcd 662.1 Da), NAD^+–Na^+ adduct at *m/z* 683.7 (calcd 684.1 Da) and boric acid–NAD^+ complex at *m/z* 687.6 (calcd 688.1 Da).

diborate–NAD^+ complex[5] (calcd 750.1 Da for $[M-H]^-$) (Fig. 1(A)).

The sum areas of the m/z 661.8, 687.8, 705.8, 713.8 and 749.8 peaks correspond to the total mass spectrometric response from the NAD^+ injected (1×10^{-9} mol). From the known concentrations of NAD^+ and boric acid, and the measured relative areas of free nucleotide and borate–complexed nucleotide, the concentration of the boric acid/borate–NAD^+ complexes was then calculated. Since the concentrations of all the different species in equilibrium were either known or could be estimated, it was possible then to calculate the K_A according to Eqn (3), where $[\mathrm{BNuc_{free}}]$ = borate–NAD^+ complex, $[\mathrm{B_{free}}]$ = free boric acid/borate, and $[\mathrm{Nuc_{free}}]$ = free NAD^+ in solution. According to Eqn (3), the ratio of complex to free nucleotide) was plotted against free boric acid (Fig. 2). The calculated slope or K_A was $1840 \pm 110\ \mathrm{l\,mol^{-1}}$. K_A of the borate–NAD^+ complex was also calculated from single boric acid and nucleotide concentrations, 500 and 100 μM, respectively. From the average of data collected from 18 separate spectra, representing 18 injections of three different sample preparations carried out on three different days, the calculated K_A was $1770 \pm 180\ \mathrm{l\,mol^{-1}}$.

$$K_A = \frac{[\mathrm{BNuc_{complex}}]}{[\mathrm{B_{free}}][\mathrm{Nuc_{free}}]}; \quad [\mathrm{B_{free}}] = K_A \frac{[\mathrm{BNuc_{complex}}]}{[\mathrm{Nuc_{free}}]} \qquad (3)$$

Substitution of NADH for NAD^+ gave rise to ions at m/z 663.8, corresponding to the free NADH (Scheme 1, **II**, calcd 664.1 Da for $[M-H]^-$), m/z 685.8, assigned as NADH–Na^+ adduct (calcd 686.1 Da), m/z 689.8, assigned as a boric acid–NADH complex (calcd 690.1 Da for $[M-H]^-$), and m/z 707.8, assigned as a borate–NADH complex (calcd 708.1 Da for $[M-H]^-$) (Fig. 1(B)). Due to ion suppression at elevated boric acid concentrations, the titration method was not employed for the remainder of the nucleotides. K_A was calculated from single concentration boric acid (500 μM) and nucleotide (100 μM). The sum of free NADH and NADH–Na^+ was assumed to be the total amount of free NADH at equilibrium. Using the relative

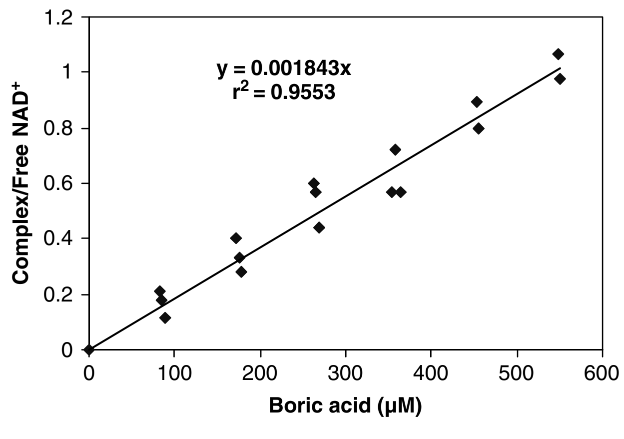

Figure 2. K_A of for boric acid and NAD^+ were determined by holding the NAD^+ concentration at 100 μM and titrating boric acid from 100 to 600 μM. The linear regression fit gives a correlation of 0.955. $K_A = 1840 \pm 110\ \mathrm{l\,mol^{-1}}$. WAT (50 : 50 : 0.2, v/v/v), was used as the solvent.

JMS

Table 1. K_A of borate–nicotinamide nucleotide complexes measured using concentrations of 500 μM boric acid and 100 μM nucleotide

Name	Complex	K_A (l mol^{-1}) pH 10.3	pH 7.4
NAD$^+$	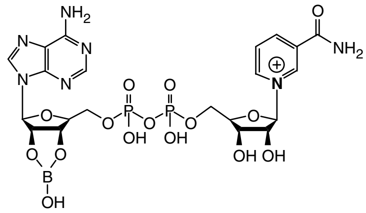	1770 ± 180	46 ± 7
NADH	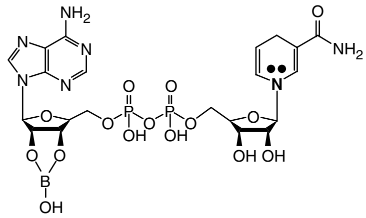	240 ± 35	Not observed
NADP$^+$	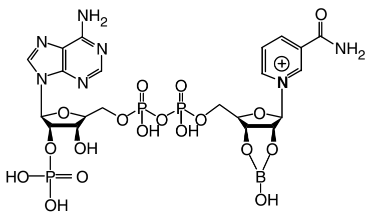	75 ± 6	Not observed
NADPH	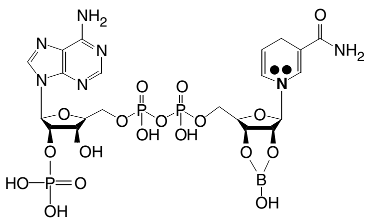	Not observed	Not observed

peak areas of the free NADH, NADH–Na$^+$ adduct and boric acid/borate–NADH complexes, the calculated K_A was 240 ± 35 l mol^{-1}.

Substitution with NADP$^+$ gave rise to ions at m/z 741.8, corresponding to free NADP$^+$ (calcd 742.1 Da for [M − H]$^-$), m/z 763.8 (calcd 764.1 Da), assigned as an NADP$^+$–Na$^+$ adduct, and m/z 767.8 (calcd 768.1 Da for [M − H]$^-$), assigned as a boric acid–NADP$^+$ complex (Fig. 1(C)). Using the relative peak areas of free NADP$^+$, NADP$^+$–Na$^+$ adduct and boric acid–NADP$^+$ complex, the calculated K_A was 75 ± 6 l mol^{-1}.

Substitution with NADPH gave rise to ions at m/z 743.8, corresponding to free NADPH (calcd 744.1 Da for [M − H]$^-$), and m/z 765.8 (calcd 766.1 Da), corresponding to an NADPH–Na$^+$ adduct. With an addition of 500 μM boric acid, the boric acid–NADPH complex was not observed (Fig. 1(D)).

We have shown previously that borate binding to NAD$^+$/NADH increased at higher pH.[5] Therefore, borate binding to NAD$^+$, NADH, NADP$^+$ and NADPH was repeated at physiological pH (7.4) using ammonium bicarbonate buffer–acetonitrile (50 : 50, v/v). The results showed that only boric acid–NAD$^+$ complex could be detected at this pH. Boric acid (500 μM) and NAD$^+$100 μM at pH 7.4 produced ions at m/z 661.7, corresponding to the free NAD$^+$ (calcd 662.1 Da for [M − H]$^-$), m/z 683.7, assigned as an NAD$^+$–Na$^+$ adduct (calcd 684.1 Da), and m/z 687.6, assigned as a boric acid–NAD$^+$ complex (calcd 688.1 Da for [M − H]$^-$) (Fig. 1(F)). The calculated K_A was 46 ± 7 l mol^{-1}. Table 1 summarizes the calculated K_A for all the borate–nicotinamide nucleotide complexes.

ESI-MS analysis of borate complexed with adenine and guanine nucleotides

In Fig. 3, spectra of 100 μM AMP, ADP, ATP, GMP, GDP and GTP with 500 μM boric acid at pH 10.3 in WAT are shown. In Fig. 3(A), a free AMP peak was observed at m/z 346.0 (calcd 346.0 Da for [M − H]$^-$). Subsequent addition of boric acid gave rise to a boric acid–AMP complex (Scheme 2, III) at m/z 371.9 (calcd 372.0 Da for [M − H]$^-$). The calculated K_A for the boric acid–AMP complex was 270 ± 50 l mol^{-1}. In Fig. 3(B), ADP and ADP–Na$^+$ adduct peaks were observed at m/z 425.9 (calcd 426.0 Da for [M − H]$^-$) and m/z 447.9 (calcd 448.0 Da), respectively. Subsequent addition of boric

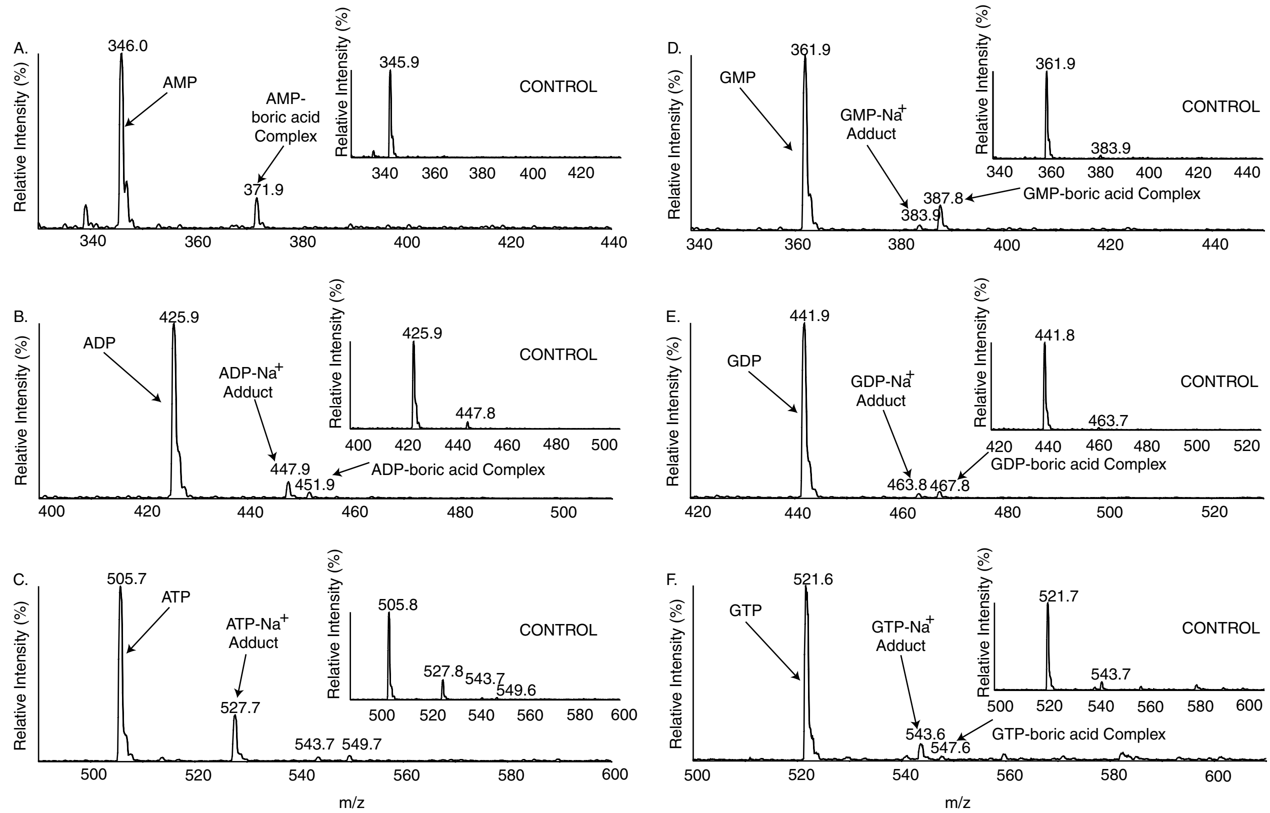

Figure 3. Negative ion ESI mass spectra of AMP, ADP, ATP, GMP, GDP and GTP (100 μM) and their complexes with borate (500 μM) in WAT at pH 10.3. Although all peaks are anionic, they are labeled by their molecular name for simplification. (A) Free AMP at *m/z* 346.0 (calcd 346.0 Da) and boric acid–AMP complex at *m/z* 371.9 (calcd 372.0 Da). (B) Free ADP at *m/z* 425.9 (calcd 426.0 Da), ADP–Na^+ adduct at *m/z* 447.9 (calcd 448.0 Da), and boric acid–ADP complex at *m/z* 451.9 (calcd 452.0 Da). (C) Free ATP at *m/z* 505.7 (calcd 506.0 Da) and ATP–Na^+ at *m/z* 527.7 (calcd 528.0 Da). (D) Free GMP at *m/z* 361.9 (calcd 362.0 Da), GMP–Na^+ at *m/z* 383.9 (calcd 384.0 Da) and boric acid–GMP complex at *m/z* 387.8 (calcd 388.0 Da). (E) Free GDP at *m/z* 441.9 (calcd 442.0 Da), GDP–Na^+ adduct at *m/z* 463.8 (calcd 464.0 Da) and boric acid–GDP complex at *m/z* 467.8 (calcd 468.0 Da). (F) Free GTP at *m/z* 521.6 (calcd 522.0 Da), GTP–Na^+ adduct at *m/z* 543.6 (calcd 544.0 Da) and boric acid–GTP complex at *m/z* 547.6 (calcd 548.0 Da).

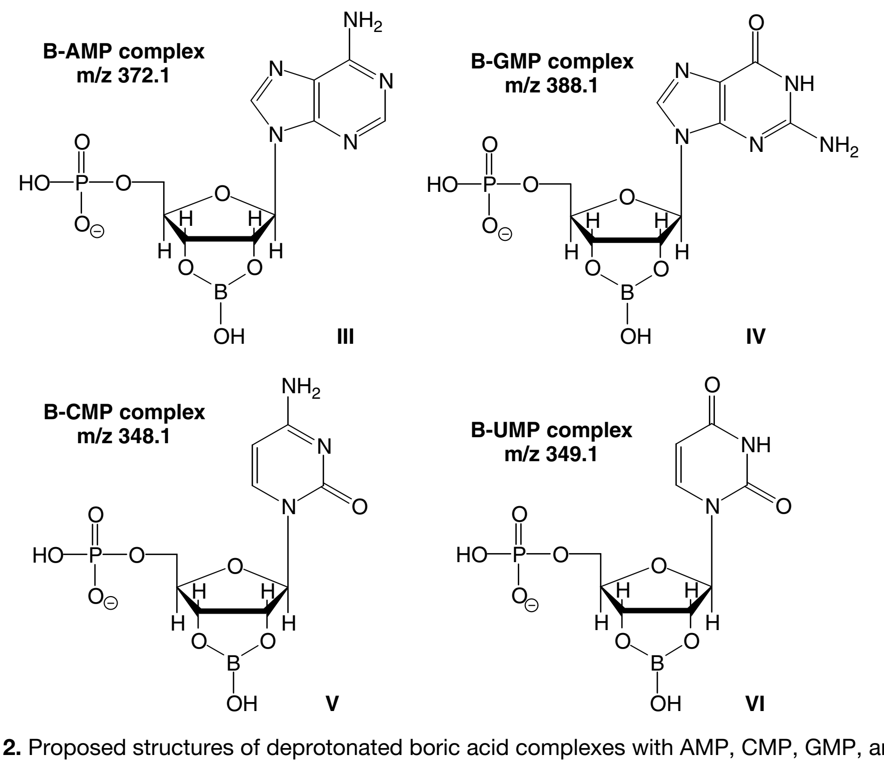

Scheme 2. Proposed structures of deprotonated boric acid complexes with AMP, CMP, GMP, and UMP.

JMS

acid gave rise to a boric acid–ADP complex at m/z 451.9 (calcd 452.0 Da for $[M-H]^-$). The calculated K_A for the boric acid–ADP complex was $44 \pm 5\,l\,mol^{-1}$. In Fig. 3(C), free ATP and ATP–Na^+ adduct peaks were observed at m/z 505.7 (calcd 506.0 Da for $[M-H]^-$) and m/z 527.7 (calcd 528.0 Da), respectively. Subsequent addition of boric acid did not result in new peaks; therefore, under these conditions, a boric acid–ATP complex was not observed. In Fig. 3(D), free GMP and GMP–Na^+ peaks were observed at m/z 361.9 (calcd 362.0 Da for $[M-H]^-$) and m/z 383.9 (calcd 384.0 Da), respectively. Subsequent addition of boric acid gave rise to a boric acid–GMP complex (Scheme 2, **IV**) at m/z 387.8 (calcd 388.0 Da for $[M-H]^-$). The calculated K_A for the boric acid–GMP complex was $230 \pm 30\,l\,mol^{-1}$. In Fig. 3(E), GDP and GDP–Na^+ adduct peaks were observed at m/z 441.9 (calcd 442.0 Da for $[M-H]^-$) and m/z 463.8 (calcd 464.0 Da), respectively. Subsequent addition of boric acid gave rise to a boric acid–GDP complex at m/z 467.8 (calcd 468.0 Da for $[M-H]^-$). The calculated K_A for the boric acid–GDP complex was $53 \pm 6\,l\,mol^{-1}$. In Fig. 3(F), free GTP and GTP–Na^+ adduct peaks were observed at m/z 521.6 (calcd 522.0 Da for $[M-H]^-$) and m/z 543.6 (calcd 544.0 Da), respectively. Subsequent addition of boric acid gave rise to the boric acid–GTP complex at m/z 547.6 (calcd 548.0 Da for $[M-H]^-$). The calculated K_A for the boric acid–GTP complex was $36 \pm 3\,l\,mol^{-1}$.

ESI-MS analysis of borate complexed with cytidine and uridine nucleotides

In Fig. 4, spectra of 100 μM CMP, CDP, CTP, UMP, UDP and UTP with 500 μM boric acid at pH 10.3 in WAT are shown. In Fig. 4(A), the free CMP peak was observed at m/z 321.8 (calcd 322.0 Da for $[M-H]^-$). Subsequent addition of boric acid gave rise to a boric acid–CMP complex (Scheme 2, **V**) at m/z 347.8 (calcd 348.0 Da for $[M-H]^-$). The calculated K_A for the boric acid–CMP complex was $200 \pm 30\,l\,mol^{-1}$. In Fig. 4(B), CDP and CDP–Na^+ adduct peaks were observed at m/z 401.8 (calcd 402.0 Da for $[M-H]^-$) and m/z 423.8 (calcd 424.0 Da), respectively. Subsequent addition of boric acid gave rise to a boric acid–CDP complex at m/z 427.8 (calcd 428.0 Da for $[M-H]^-$). The calculated K_A for the boric acid–CDP complex was $54 \pm 9\,l\,mol^{-1}$. In Fig. 4(C), free CTP and CTP–Na^+ adduct peaks were observed at m/z 482.1 (calcd 482.0 Da for $[M-H]^-$) and m/z 504.0 (calcd 504.0 Da), respectively. Subsequent addition of boric acid did not result in new peaks; therefore, under these

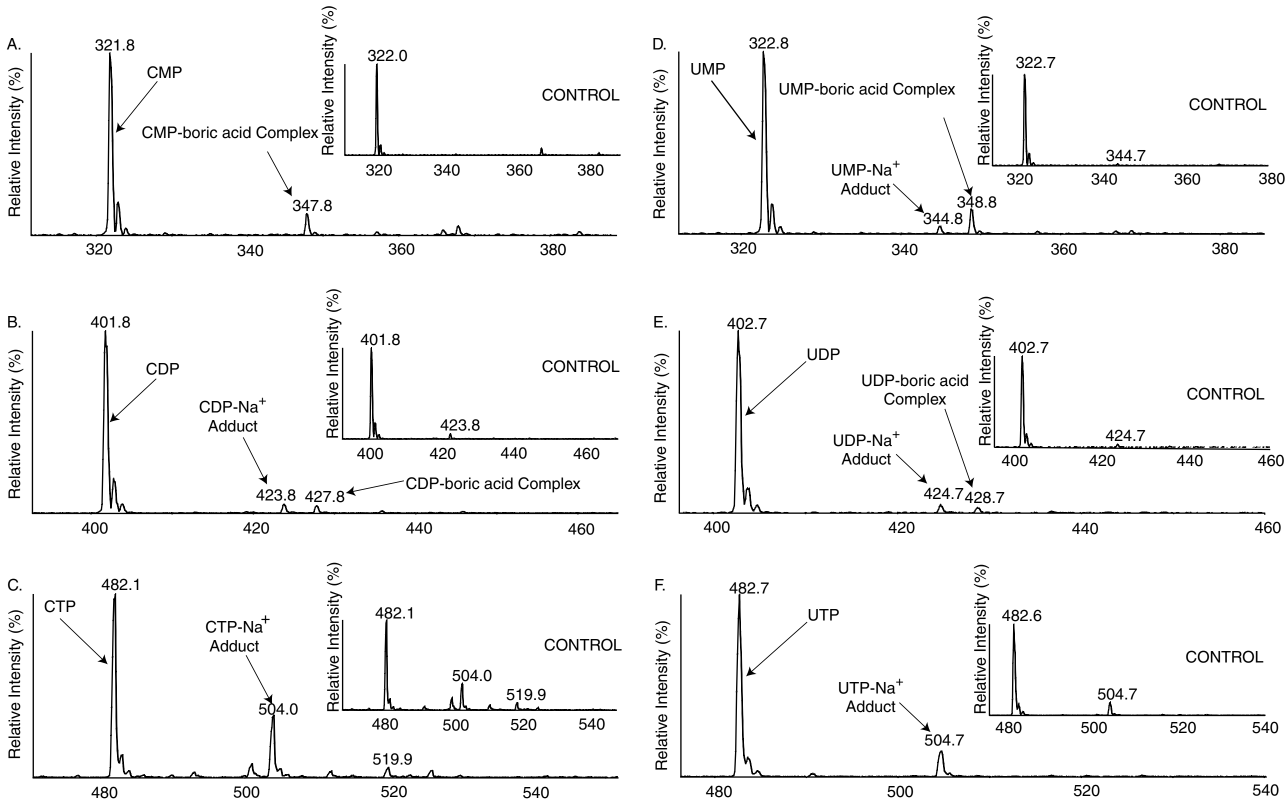

Figure 4. Negative ion ESI mass spectra of CMP, CDP, CTP, UMP, UDP and UTP (100 μM) and their complexes with borate (500 μM) in WAT at pH 10.3. Although all peaks are anionic, they are labeled by their molecular name for simplification. (A) Free CMP at m/z 321.8 (calcd 322.0 Da) and boric acid–CMP complex at m/z 347.8 (calcd 348.0 Da). (B) CDP at m/z 401.8 (calcd 402.0 Da), CDP–Na^+ adduct at m/z 423.8 (calcd 424.0 Da) and boric acid–CDP complex at m/z 427.8 (calcd 428.0 Da). (C) Free CTP at m/z 482.1 (calcd 482.0 Da) and CTP–Na^+ adduct at m/z 504.0 (calcd 504.0 Da). (D) Free UMP at m/z 322.8 (calcd 323.0 Da), UMP–Na^+ at m/z 344.8 (calcd 345.0 Da) and boric acid–UMP complex at m/z 348.8 (calcd 349.0 Da). (E) Free UDP at m/z 402.7 (calcd 403.0 Da), UDP–Na^+ adduct at m/z 424.7 (calcd 425.0 Da) and boric acid–UDP complex at m/z 428.7 (calcd 429.0 Da). (F) Free UTP at m/z 482.7 (calcd 483.0 Da) and UTP–Na^+ adduct at m/z 504.7 (calcd 505.0 Da).

JMS

Table 2. K_A of various borate–nucleotide complexes at pH 10.3 using measured concentrations of 500 μM boric acid and 100 μM nucleotide

Nucleotide	K_A (l mol^{-1})	Nucleotide	K_A (l mol^{-1})	Nucleotide	K_A (l mol^{-1})
AMP	270 ± 50	ADP	44 ± 5	ATP	Not observed
CMP	200 ± 30	CDP	54 ± 9	CTP	Not observed
GMP	230 ± 30	GDP	53 ± 6	GTP	36 ± 3
UMP	220 ± 50	UDP	51 ± 8	UTP	Not observed

conditions, a boric acid–CTP complex was not observed. In Fig. 4(D), free UMP and UMP–Na$^+$ peaks were observed at m/z 322.8 (calcd 323.0 Da for $[M - H]^-$) and m/z 344.8 (calcd 345.0 Da), respectively. Subsequent addition of boric acid gave rise to a boric acid–UMP complex (Scheme 2, **VI**) at m/z 348.8 (calcd 349.0 Da for $[M - H]^-$). The calculated K_A for the boric acid–UMP complex was 220 ± 50 l mol^{-1}. In Fig. 4(E), UDP and UDP–Na$^+$ adduct peaks were observed at m/z 402.7 (calcd 403.0 Da for $[M - H]^-$) and m/z 424.7 (calcd 425.0 Da), respectively. Subsequent addition of boric acid gave rise to a boric acid–UDP complex at m/z 428.7 (calcd 429.0 Da for $[M - H]^-$). The calculated K_A for the boric acid–UDP complex was 51 ± 8 l mol^{-1}. In Fig. 4(F), free UTP and UTP–Na$^+$ adduct peaks were observed at m/z 482.7 (calcd 483.0 Da for $[M - H]^-$) and m/z 504.7 (calcd 505.0 Da), respectively. Subsequent addition of boric acid did not result in new peaks; therefore, under these conditions, a boric acid–UTP complex was not observed. Table 2 summarizes the K_A values for these borate–nucleotide complexes.

DISCUSSION

In most cases, the best way to determine the K_A of a complex is by titrating a ligand (e.g. boric acid) up to or through the expected dissociation concentration. In Fig. 2, a plot of free boric acid versus the ratio of complex to free NAD$^+$ through the expected dissociation concentration (500–600 μM) was used to determine the slope or K_A, which was 1840 ± 110 l mol^{-1}. Unfortunately, the titration method could not be used for the rest of the nucleotides, because at pH 10.3 boric acid is equilibrated to anionic borate, which causes ion suppression of signals in elevated concentrations. In order to titrate these nucleotides through the expected dissociation concentration, the boric acid concentration has to be elevated to above 4 mM. We have determined that during ESI-MS ion suppression occurs at boric acid concentrations >600 μM. Additionally, the relative intensity of the complex peaks for nucleotides, excluding NAD$^+$, were small and, therefore, the uncertainty in the ratio of complex to free nucleotide was high. In order to overcome this, we also determined the K_A of the borate–NAD$^+$ complex using single concentrations, 500 μM boric acid and 100 μM NAD$^+$, which was 1770 ± 180 l mol^{-1}. Since these two K_A values are approximately the same, we used single concentrations, 100 μM nucleotide and 500 μM boric acid, to determine the K_A for the remainder of the nucleotides.

Using the single concentration method, the K_A values for borate complexation to different nucleotides are summarized in Tables 1 and 2. From these data, we propose that the amount of complexation between borate and nucleotide is heavily influenced by the pH of the solution, with alkaline conditions strongly favoring complexation, and by two nucleotide characteristics: (i) charge and (ii) phosphorylation state.

There is a substantial difference in K_A between charged NAD$^+$ (1770 ± 180 l mol^{-1}) and uncharged NADH (240 ± 35 l mol^{-1}), as shown in Table 1. Similarly, there is a reduction in K_A from NADP$^+$(75 ± 6 l mol^{-1}) to NADPH (complex not observed). Smith and Johnson hypothesized that the difference in complexation between NAD$^+$ and NADH to borate is due to the fact that borate ion with a negative charge is attracted to the positive charge on NAD$^+$ and hence enhances the binding to NAD$^+$.[2] Our results show that the charge on the nucleotide contributes to the stability of the borate–nucleotide complex.

There is also a large reduction in K_A from NAD$^+$ to NADP$^+$ and from NADH to NADPH. The ribose adjacent to the adenine group in NADP$^+$ and NADPH nucleotides is phosphorylated compared with NAD$^+$ and NADH. This phosphorylation contributes to the destabilization of borate–nicotinamide nucleotide complexes. Using adenine, guanine, cytidine and uridine nucleotides, we confirmed that phosphorylation destabilized borate–nucleotide complexes. We found that the length of the phosphate group on the nucleotide influences the complexation between borate and nucleotides. The K_A of the borate–nucleotide complex decreases in the order mono-, di-, triphosphates (Table 2). All the monophosphate nucleotides including AMP (270 ± 50 l mol^{-1}), CMP (200 ± 30 l mol^{-1}), GMP (230 ± 30 l mol^{-1}) and UMP (220 ± 50 l mol^{-1}) have similar K_A values that are not significantly different from one another. The stability of borate complexation with monophosphate nucleotides is about four times higher than that of diphosphate nucleotides, which include ADP (44 ± 5 l mol^{-1}), CDP (54 ± 9 l mol^{-1}), GDP (53 ± 6 l mol^{-1}) and UDP (51 ± 8 l mol^{-1}). Once again these complexes have K_A values that are not significantly different from one another. Finally, among all the triphosphate nucleotides, only borate–GTP (36 ± 3 l mol^{-1}) complex was observed. Therefore, the stability of the borate–nucleotide complex is inversely proportional to the length of the phosphate group, where AMP > ADP > ATP, CMP > CDP > CTP, GMP > GDP > GTP and UMP > UDP > UTP. Our data contradict those of Ralston and Hunt,[1] who observed *S*-adenosylmethionine > diadenosine polyphosphates > NAD$^+$ > NADH > ATP > ADP > AMP > cAMP using capillary electrophoresis. Since the ESI-MS method gives a direct measure of the complexes rather than electrophoretic retention times, and shows satisfactory agreement among the four different types of nucleotides studied, it is reasonable to suggest that our results provide a more accurate measure of the complexes formed between borate and nucleotides.

Borate complexation with nucleotides was also measured at pH 7.4 in ammonium bicarbonate buffer. At 500 μM boric acid and 100 μM nucleotide concentrations, of all the nucleotides tested only the boric acid–NAD^+ complex was observed. The K_A of this complexation was 46 ± 7 l mol^{-1} and indicates that borate complexation with NAD^+ is relevant at physiological pH. From this it is reasonable to suggest that some of the effects of borate can be contributed to the *in vivo* formation of an NAD^+–borate complex.

The inverse relationship between complex stability and length of phosphate groups can be explained by electrostatic and physical interactions of phosphate groups and borate bound to the ribose group. First, at elevated pH, the deprotonated phosphate groups electrostatically repel borate ions from complexing with the nucleotides. Second, our previous experiment with borate–NAD^+ complex demonstrated that the phosphate backbone is sufficiently flexible to interact with the ribose group. We showed that one of the MS/MS fragments of NAD^+ is a borate diester that connects two ribose groups linked by two phosphate groups to form a cyclic molecule.[5] In the light of this, we propose that the hydroxyls on the phosphate groups can physically interact near the ribose ring to destabilize the borate binding. As result, the complex stability between borate and nucleotides is inversely proportional to the length of the phosphate group. Therefore, the K_A of borate complexes decreases in the order mono-, di- and triphosphate nucleotides.

In order to use MS for quantitative purposes, the ionization efficiencies of the species compared must be similar. Unfortunately, because elevated boric acid concentrations (>600 μM) cause ion suppression of signals, we cannot shift the equilibrium between two extreme conditions to examine the ionization efficiencies of the borate–nucleotide complex and the free nucleotide. Moreover, a standard for borate–nucleotide complexes is unavailable, owing to the reactivity of borate with hydroxyl groups in solvents including water and alcohol. However, it seems reasonable to assume that the ionization properties of the free nucleotides and borate–nucleotide complex species are similar for the following reasons. (i) At high pH, both complexed and free nucleotide species are already ionized in solution owing to deprotonation of the phosphate group on the nucleotides ($pK_a = 6–7$).[26] Therefore, both the free nucleotide and borate–nucleotide complex are ionized prior to electrospray. (ii) The change in the mass due to borate complexation is small compared with the mass of the free nucleotides (<10% difference). (iii) The complex is covalently bound and therefore it is less susceptible to collision-induced dissociation in the gas phase. (iv) MS analysis in water-ammonium hydroxide at pH 10, instead of WAT solvents, also showed consistent borate–nucleotide complex formation but with lower sensitivity. The complexation of borate–nucleotide does not depend on the organic solvents. (v) Johnson and Smith[27] studied the kinetics of borate–NAD^+ complex formation by stopped-flow spectrophotometry and determined that the K_A for NAD^+ (44 mM) and boric acid (2.5 mM) at pH 10.4 was 1500 ± 400 l mol^{-1}. Using ESI-MS, we determined that the K_A for boric acid (0.5 mM) complexation with NAD^+ (0.1 mM) was 1840 ± 110 l mol^{-1} at pH 10.3. Since these two K_A values are in reasonable agreement, we believe that the ionization efficiencies between the borate–nucleotide complex and free nucleotide are similar. Therefore, ESI-MS is a valid method for determining the K_A for borate complexation with nucleotides.

The K_A values for different nucleotides were calculated from the peak areas of the signals for complexed and free nucleotides. The total concentration of the nucleotide (Nuc_{total}) is constant and is equivalent to the sum of all the nucleotide-associated peak areas. The sodium-adducted nucleotides also complex with boric acid at elevated concentrations (data not shown). The concentration of the free boric acid is then derived. Using this method, the concentration of all the species at equilibrium is determined. The K_A is then calculated using Eqn (3). This method assumes that the ESI-MS peak areas are proportional to concentration, a stipulation that has been repeatedly verified both here (unpublished data) and elsewhere[28] and, as already stated, we believe that the efficiencies of ionization of the free nucleotides and the borate–nucleotide complexes are not significantly different from one another.

We also investigated the stability of other borate–nucleoside complexes including those with adenosine, cytidine, guanosine and uridine. The complex stability with these nucleosides fits into the trend described above. Since these nucleosides are not phosphorylated, they have higher K_A values than the monophosphate nucleotides. We believe that only qualitative comparisons can be made with these nucleosides because there might be a difference in ionization efficiency between negatively charged complexed nucleoside and uncharged free nucleosides. Unlike mono-, di- and triphosphate nucleotides, these non-phosphorylated nucleosides will have neutral charge even at pH 10.3. With this caveat in mind, the K_A for adenosine, cytidine, guanosine and uridine analyzed by ESI-MS were 1150 ± 110, 1900 ± 170, 800 ± 100 and 970 ± 130 l mol^{-1}, respectively.

In conclusion, we have examined the K_A values of borate complexation with 16 nucleotides at pH 10.3 and 7.4 using ESI-MS. We demonstrated that the stability of borate–nucleotide complex is predicted by the charge and phosphorylation state of the nucleotide and by the pH of the solution. The cationic charge on the nicotinamide group increases the K_A as compared with the neutral nicotinamide group. Also the length of the phosphate group is inversely proportional to the K_A of borate complexation with nucleotides.

Acknowledgements

We thank Alex Dooley for assistance with ESI-MS and Beth Marbois for continual guidance. This work was supported by UC Toxic Substances Research and Teaching Program and US Borax.

REFERENCES

1. Ralston NVC, Hunt CD. Diadenosine phosphates and S-adenosylmethionine: novel boron binding biomolecules detected by capillary electrophoresis. *Biochim. Biophys. Acta* 2001; **1527**: 20.

2. Smith KW, Johnson SL. Borate inhibition of yeast alcohol dehydrogenase. *Biochemistry* 1976; **15**: 560.
3. Penn SG, Hu H, Brown PH, Lebrilla CB. Direct analysis of sugar alcohol borate complexes in plant extracts by matrix-assisted laser desorption/ionization Fourier transform mass spectrometry. *Anal. Chem.* 1997; **69**: 2471.
4. Chapelle S, Verchere JF. A boron-11 and carbon-13 NMR determination of the structures of borate complexes of pentoses and related sugars. *Tetrahedron* 1988; **44**: 4469.
5. Kim D, Marbois B, Faull K, Eckhert C. Esterification of borate with NAD^+ and NADH as studied by electrospray ionization mass spectrometry and ^{11}B NMR spectroscopy. *J. Mass Spectrom.* 2003; **38**: 632.
6. van den Berg R, Peters JA, van Bekkum H. The structure and (local) stability constants of borate esters of mono- and di-saccharides as studied by ^{11}B and ^{13}C NMR spectroscopy. *Carbohydr. Res.* 1995; **253**: 1.
7. Warington K. The effect of boric acid and borax on the broad bean and certain other plants. *Ann. Bot.* 1923; **40**: 27.
8. Kobayashi M, Matoh T, Azuma JI. Two chains of rhamnogalacturonan II are cross-linked by borate–diol ester bonds in higher plant cell walls. *Plant Physiol.* 1996; **110**: 1017.
9. Pellerin P, Doco T, Vidal S, Williams P, Brillouet JM, O'Neill M. Structural characterization of red wine rhamnogalacturonan II. *Carbohydr. Res.* 1996; **290**: 183.
10. Takano J, Noguchi K, Yasumorl M, Kobayashi M, Gajdos Z, Miwa K, Hayashi H, Yoneyama T, Fujiwara T. Arabidopsis boron transporter for xylem loading. *Nature* 2002; **420**: 337.
11. Frommer WB, von Wirén N. Ping-pong with boron. *Nature* 2002; **410**: 282.
12. Chen X, Schauder S, Potier N, Van Dorsselaer A, Pelczer I, Bassier BL, Hughson FM. Structural identification of a bacterial quorum-sensing signal containing boron. *Nature* 2002; **415**: 545.
13. Eckhert CD. Boron stimulates embryonic trout growth. *J. Nutr.* 1998; **128**: 2488.
14. Rowe R, Eckhert C. Boron is required for zebrafish embryogenesis. *J. Exp. Biol.* 1999; **202**: 164.
15. Fort D, Stover E, Strong P, Murray F. Effects of boron deprivation on reproductive parameters in *Xenopus laevis*. *J. Trace Elem. Exp. Med.* 1999; **12**: 187.
16. McCoy H, Kenney M, Montgomery C, Irwin A, Williams L, Orrell R. Relation of boron to the composition and mechanical properties of bone. *Environ. Health Perspec.* 1994; **102**(Suppl. 7): 49.
17. Penland J. Dietary boron, brain function, and cognitive performance. *Environ. Health Perspec.* 1994; **102**(Suppl. 7): 65.
18. Nielsen F. Biochemical and physiologic consequences of boron deprivation in humans. *Environ. Health Perspec.* 1994; **102**(Suppl. 7): 59.
19. Zhang Z-F, Winton MI, Rainey C, Eckhert CD. Boron is associated with decreased risk of human prostate cancer. *FASEB J.* 2001; **15**: 834.3.
20. Treinen KA, Chapin RE. Development of testicular lesions in F344 rats after treatment with boric acid. *Toxicol. Appl. Pharmacol.* 1991; **107**: 325.
21. Schummer D, Irschik H, Reichenbach H, Hoefle G. Tartrolons: new boron-containing macrodiolides from *Sorangium cellulosum*. *Liebigs Ann. Chem.* 1994; **3**: 283.
22. Bell CF, Beauchamp RD, Short EL. A study of the complexes of borate ions and some cyclitols using boron-11 NMR spectroscopy. *Carbohydr. Res.* 1986; **147**: 191.
23. Ferrier RJ. Carbohydrate boronates. *Adv. Carbohydr. Chem. Biochem.* 1978; **35**: 31.
24. Rowe R, Eckhert C. Boron is required for zebrafish embryogenesis. *J. Exp. Biol.* 1999; **202**: 164.
25. Glasgow BJ, Abduragimov AR, Yusifov TN, Gasymov OK, Horwitz J, Hubbell WL, Faull KF. A conserved disulfide motif in human tear lipocalins influences ligand binding. *Biochemistry* 1998; **37**: 2215.
26. Rösch P, Kalbitzer R, Goody R. ^{31}P NMR Spectra of thiophosphate analogues of guanosine nucleotides pH dependence of chemical shifts and coupling constants. *FEBS Lett.* 1980; **121**: 211.
27. Johnson SL, Smith KW. The interaction of borate and sulfite with pyridine nucleotides. *Biochemistry* 1976; **15**: 553.
28. Gabelica V, Galic N, Rosu F, Houssier C, De Pauw E. Influence of response factors on determining equilibrium association constants of non-covalent complexes by electrospray ionization mass spectrometry. *J. Mass Spectrom.* 2003; **38**: 491.


Volume 1115, Issues 1–2, 19 May 2006 ISSN 0021-9673
Complete in one issue

JOURNAL OF CHROMATOGRAPHY A

INCLUDING ELECTROPHORESIS, MASS SPECTROMETRY AND OTHER SEPARATION AND DETECTION METHODS

Available online at www.sciencedirect.com

Available online at www.sciencedirect.com

SCIENCE DIRECT®

Journal of Chromatography A, 1115 (2006) 246–252

JOURNAL OF CHROMATOGRAPHY A

www.elsevier.com/locate/chroma

Boric acid inhibits adenosine diphosphate-ribosyl cyclase non-competitively

Danny H. Kim [a], Shane Que Hee [a], Andrew J. Norris [b,c], Kym F. Faull [b], Curtis D. Eckhert [a,*]

[a] Department of Environmental Health Sciences, Box 951772, University of California, 650 Charles E Young Dr South, Los Angeles, CA 90095-1772, USA

[b] Pasarow Mass Spectrometry Laboratory, Departments of Psychiatry & Biobehavioral Sciences and the Jane and Terry Semel Institute for Neuroscience and Human Behavior, University of California, 10833 Le Conte Avenue, Los Angeles, CA 90095, USA

[c] UCLA Johnson Comprehensive Cancer Center, University of California, 10833 Le Conte Avenue, Los Angeles, CA 90095, USA

Received 5 January 2006; received in revised form 15 February 2006; accepted 21 February 2006
Available online 20 March 2006

Abstract

Adenosine diphosphate-ribosyl cyclase (ADP-ribosyl cyclase) is a ubiquitous enzyme in eukaryotes that converts NAD^+ to cyclic-ADP-ribose (cADPR) and nicotinamide. A quantitative assay for cADPR was developed using capillary electrophoresis to separate NAD^+, cADPR, ADP-ribose, and ADP with UV detection (254 nm). Using this assay, the apparent K_m and V_{max} for *Aplysia* ADP-ribosyl cyclase were determined to be 1.24 ± 0.05 mM and 131.8 ± 2.0 μM/min, respectively. Boric acid inhibited ADP-ribosyl cyclase non-competitively with a K_i of 40.5 ± 0.5 mM. Boric acid binding to cADPR, determined by electrospray ionization mass spectrometry, was characterized by an apparent binding constant, K_A, of 655 ± 99 L/mol at pH 10.3.

Keywords: ADP-ribosyl cyclase; Boron; Capillary electrophoresis; cADPR; NAD; Mass spectrometry; Enzyme kinetics

1. Introduction

Adenosine diphosphate-ribosyl cyclase (ADP-ribosyl cyclase) is widely distributed in nature and is expressed in over 40 different species of protists, plants, and animals [1–5]. The enzyme cyclizes NAD^+ to produce cyclic-ADP-ribose (cADPR) with the release of nicotinamide (Fig. 1) [6]. cADPR acts as a second messenger that mobilizes Ca^{2+} from the endoplasmic reticulum via activation of ryanodine receptors [7]. Three homologs of the cyclase with 30% sequence identity have now been identified [8–12]. There is a soluble cyclase present in the sea hare *Aplysia*, the membrane-bound lymphocyte antigen CD38, and another antigen BST-1. Mammalian CD38 is a multiple function cell surface molecule possessing both cyclase activity that converts NAD^+ to cADPR, and hydrolase activity that converts cADPR to ADPR. At pH 4.5, CD38 also converts $NADP^+$ to nicotinic acid adenine dinucleotide phosphate (NAADP), another second messenger that also triggers Ca^{2+} release from intracellular stores. However, these stores are different from those affected by cADPR [13].

The soluble *Aplysia* cyclase has been recombinantly produced in yeast and crystallized [14]. This enzyme only catalyzes the synthesis of cADPR. Lee [8] has proposed a catalytic model for the CD38 type based on an active site that consists of a highly conserved sequence containing 10 cysteine residues and three other critical residues: glutamate 179, which is the catalytic residue and lies in the catalytic pocket, and two tryptophan residues. The model proposes that the two tryptophan residues bind and fold the linear NAD^+ molecule, while glutamate attack releases the nicotinamide moiety. The adenine ring then reacts with the terminal ribose to form cADPR [8]. According to this model, disruption of NAD^+ folding in the active site may slow the catalytic activity of the enzyme. The CD38 type has about 25% sequence identity with the *Aplysia* type. Boron as boric acid and borate binds to NAD^+ [15] and therefore may affect the activity of ADP-ribosyl cyclase.

Boric acid has affinity for diol-containing compounds such as carbohydrates, where its strong complexation is now being

* Corresponding author. Tel.: +1 310 825 8429; fax: +1 310 825 8429.
E-mail address: ceckhert@ucla.edu (C.D. Eckhert).

0021-9673/$ – see front matter
doi:10.1016/j.chroma.2006.02.066

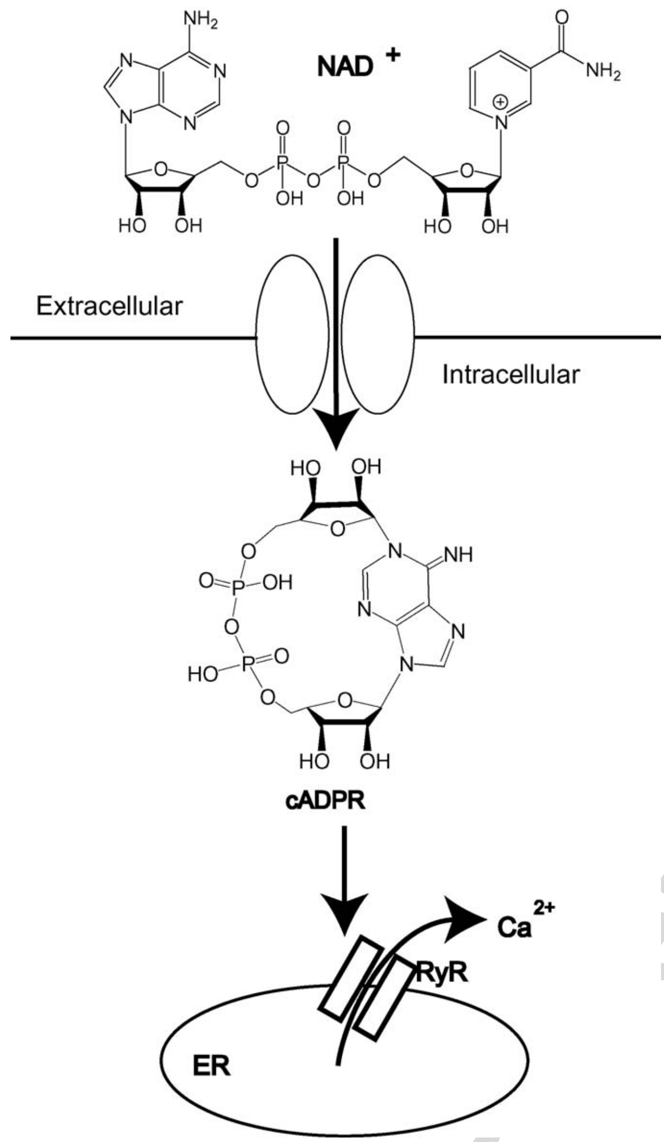

Fig. 1. Schematic view of the cADPR signaling pathway. NAD^+ is converted to cADPR, which interacts with the ryanodine receptor (RyR) through an unknown mechanism. cADPR mobilizes Ca^{2+} from endoplasmic reticulum (ER) stores by activation of RyR.

used for the fabrication of carbohydrate sensors and transporters (Eq. (1)) [16–18].

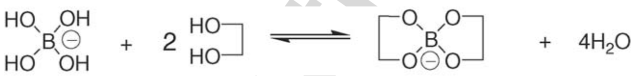

(1)

Diols are also present in the carbohydrate moieties of nucleosides and nucleotides including NAD^+, NADH, $NADP^+$, adenosine, and guanosine. Previously, we used electrospray ionization mass spectrometry (ESI-MS) to demonstrate that boric acid binds to *cis*-diols on both ribose groups on NAD^+ [15]. A comparison of 16 different nucleotides containing *cis*-diols determined that NAD^+ had highest affinity for boric acid [19]. NAD^+ affinity was about seven times greater than NADH. Migaud et al. [20] described that the ribosyl diol moiety adjacent to the nicotinamide group is important in binding NAD^+ in the active site of ADP-ribosyl cyclase. Since boric acid can bind to this diol, such binding may influence the conversion of NAD^+ to cADPR through ADP-ribosyl cyclase.

In recent years, capillary electrophoresis (CE) has emerged as a powerful separation technique to measure water-soluble metabolites, including nucleotides, for several reasons: analysis without derivatizations; simple sample preparation, short analysis time; and small sample quantity as compared to high-performance liquid chromatography (HPLC) [21,22]. On the other hand, previous assays for ADP-ribosyl cyclase mostly relied on reverse phase and anion-exchange HPLC [23–26]. In order to take advantages of this alternate separation technique, for the first time, CE was utilized to investigate the enzyme kinetics of ADP-ribosyl cyclase. The objective of the present study was to determine if boric acid binds directly to cADPR and to assess the impact of boric acid on ADP-ribosyl cyclase kinetics. The results suggest that boric acid may be involved in modulating Ca^{2+} mobilization. Ca^{2+} serves as a communicating signal that initiates a myriad of changes including control of muscle contraction and neurotransmitter release, cell migration [27], cell cycle progression [28,29], angiogenesis [30], apoptosis [31], and proliferation [32].

2. Materials and methods

2.1. Chemicals and reagents

ADP-ribosyl cyclase purified from *Aplysia californica*, nicotinamide adenine dinucleotide, oxidized form (NAD^+) (free acid), cADPR, adenosine 5′-diphosphate (ADP) (sodium salt), ADP-ribose (ADPR), boric acid, and tris(hydroxymethyl) aminomethane (Tris) were purchased from Sigma Aldrich (St. Louis, MO, USA). Enriched $^{11}B(OH)_3$ (99.27% purity) was purchased from Eagle-Picher Technologies (Quapaw, OK, USA). Ultrapure water containing <10 nM boron was used for all the experiments. Ultrapure water was prepared by ion-exchange treatment, and the boron content was checked by inductively coupled plasma mass spectrometry as previously described [33]. All other reagents and solvents were of analytical grade or higher.

2.2. Enzyme reactions

To investigate the effect of boric acid on the synthesis of cADPR, ADP-ribosyl cyclase was incubated with various concentrations of NAD^+ and boric acid in 200 mM Tris buffer (pH 7.4). Each reaction tube contained Tris (pH 7.4) and NAD^+ (0.5, 0.75, 1, 1.5, 2, 3, 4, or 5 mM) in 300 μL. Reactions were started by addition of 0.156 units of ADP-ribosyl cyclase (100 μL) and incubated at 37 °C for 0, 60, 90, and 120 s. Reactions were terminated by mixing 120 μL of the reaction mixture with 360 μL of cold 90% acetonitrile containing 97 μM ADP (73 μM final concentration) as internal standard. Each sample was centrifuged (14,000 × *g*, 4 °C, 10 min), and before analysis by CE, 200 μL was removed and added to 200 μL of 100 mM borate buffer (pH 9.2), which was used as a background electrolytes for the electrophoretic separation of cADPR. Schmitt-Kopplin et al. [34] and Hoffstetter-Kuhn et al. [35] showed that borate buffer enhanced peak shape and changed migration time by forming a complex with the substrates. For blank and standard samples, the enzyme was denatured prior to the addition of the substrate mixture followed by the same methodology as above to determine the standard curve. For the inhibition analysis, NAD^+ was varied from 0, 0.75, 1, 1.5, 2, or 4 mM, and the boric acid concentration was varied between 0, 30, 35, and 40 mM for each NAD^+ concentration.

2.3. Capillary electrophoresis

Using an Agilent HP-CE model G1600AX (Waldbronn, Germany) CE system equipped with a diode array detector, a 50 μm i.d. × 56 cm bulbed glass capillary was pretreated with 0.1 M KOH for 10 min and then equilibrated with 100 mM borate buffer of pH 9.2 for 5 min before loading each sample. Samples were loaded by hydrostatic pressure at 50 mbar for 15 s and separations were performed at 20 °C using 20 kV producing about 24 mA of current, for 25 min duration. The effluent was monitored by absorption at 254 nm. A solution of acetone was used as an electroosmotic flow marker. One hundred and twenty microliters of standard samples containing varying amounts of cADPR (0, 12.5, 25, 50, 125, 250, and 375 μM) in the reaction mixture were mixed with 360 uL of 97 μM ADP (73 μM final concentration) in 90% cold acetonitrile and separated with CE. cADPR and ADP peak areas were computed using a program supplied with the instrument (3D-CE Chemstation, rev. A. 10.01, Waldbronn, Germany). A calibration curve was constructed by plotting the cADPR/ADP peak area ratio against amount of cADPR for the standard samples. The concentration of cADPR in the reaction samples was computed by interpolation from the standard curve.

2.4. Sample preparation for ESI-MS analysis

All solutions were prepared fresh in ultrapure water, then diluted to the desired concentration in water/acetonitrile/triethylamine (WAT, 50/50/0.2, v/v/v, pH 10.3). The borate complexes were prepared by mixing equal volumes of boric acid and cADPR solutions, yielding final concentrations of 500 and 100 μM, respectively. To determine the apparent K_A, a minimum of 12 different measurements (made on three separate occasions, each time with fresh sample preparations) were made and analyzed. The mean and standard deviation were computed.

2.5. ESI-MS

A Perkin-Elmer Sciex (Thornhill, Canada) API III triple quadrupole mass spectrometer fitted with an Ionspray™ source was tuned and calibrated in the positive ion mode as previously described [36]. Instrument resolution allowed for a 15–20% valley between the ^{13}C-containing satellites of the polypropylene glycol/NH_4^+ singly charged calibrant ion at m/z 906. For analysis of borate esterification to the nucleotides, the instrument polarity was reversed and the ion spray voltage was lowered to −3.5 kV. Samples dissolved in WAT were introduced (10 μL/injection) into a stream of the same solvent entering the ion source (10 μL/min). Spectra were collected (profile mode) while the instrument was scanning from *m/z* 520–620 (0.1 Da step size, 6 ms dwell time, 6.66 s/scan, orifice −60 V). Representative spectra were computed as the average of all the spectra accrued from each injection using instrument-supplied software (MacSpec, version 3.3 PE Sciex, Ontario, Canada).

3. Results

3.1. Michaelis–menten plot of ADP-ribosyl cyclase

CE gave clear separation of cADPR, ADP and the other nucleotides tested, with typical migration times for NAD^+, cADPR, and ADP of 13.7, 15.7, and 22.3 min, respectively. The response at 254 nm was quantitative as demonstrated by the linear standard curve ($y = 2.362x$, $r^2 = 0.999$, $p < 0.001$) across the 0–400 μM concentration range. The incubation times were adjusted such that less than 20% of the substrates were converted. The apparent K_m and V_{max} for ADP-ribosyl cyclase for NAD^+ were calculated to be 1.24 ± 0.05 mM and 131.8 ± 2.0 μM/min (r^2 of 0.999, $p < 0.001$), respectively, through nonlinear regression of the data fit to the Michaelis–Menten equation (Fig. 2). Likewise, using a Lineweaver and Burk plot, the apparent K_m and V_{max} were determined to be 1.12 ± 0.05 mM and 126.3 ± 5.3 μM/min with r^2 of 0.991, $p < 0.001$.

3.2. Inhibition of ADP-ribosyl cyclase by boric acid

With an initial NAD^+ concentration of 1 mM and boric acid concentrations between 0–40 mM, CE revealed peaks at 13.7, 15, and 22 min representing NAD^+, cADPR, and ADP, respec-

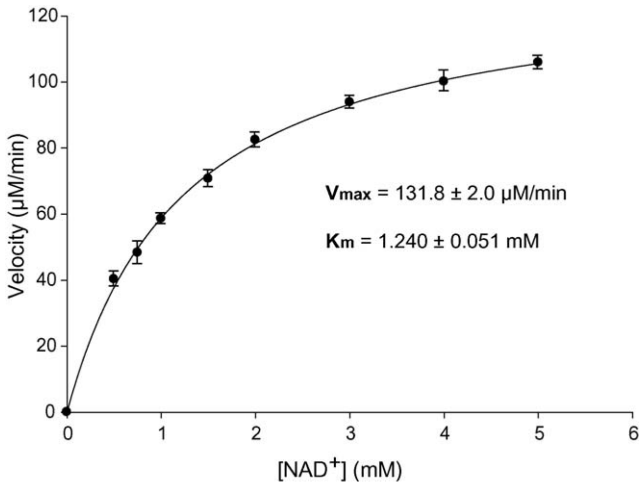

Fig. 2. Michaelis–Menten plot of ADP-ribosyl cyclase activity with NAD^+ substrate using capillary electrophoresis for separation of the reaction components and detection by absorption at 254 nm. The samples were incubated in 37 °C at pH 7.4 in Tris buffer. Nonlinear regression of the data fitted to the Michaelis–Menten equation was used to determine the K_m (1.240 ± 0.051 mM) and V_{max} (131.8 ± 2.0 μM/min).

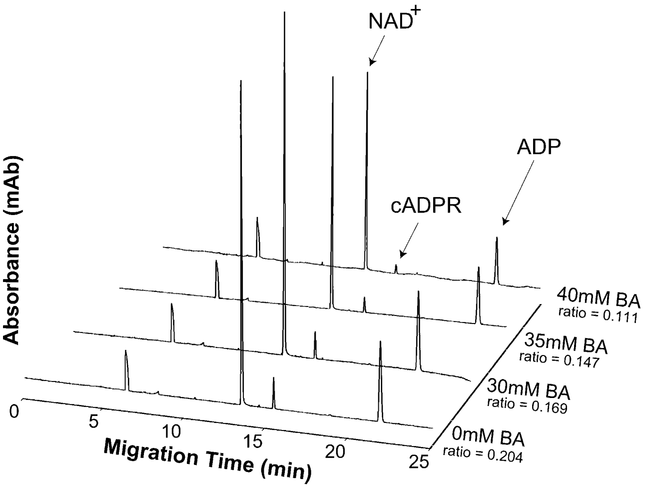

Fig. 3. Capillary electrophoretograms of the ADP-ribosyl cyclase assay in the presence of increasing boric acid concentrations. ADP was used as an internal standard. NAD^+ (1 mM) and various boric acid concentrations were reacted at 37 °C and pH 7.4 for 90 s. The area ratio of cADPR/ADP decreased as boric acid concentration increased.

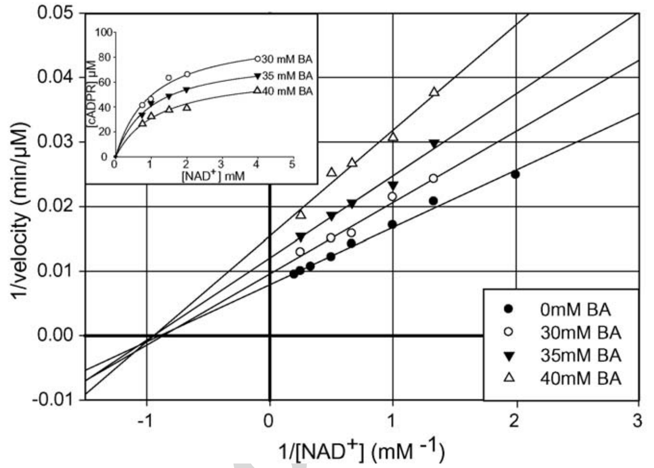

Fig. 5. Lineweaver and Burk plots reveal that the inhibition of ADP-ribosyl cyclase by boric acid (BA) is non-competitive. At the various NAD^+ concentrations, reactions occurred at 37 °C and pH 7.4. Inset: Michaelis–Menten plots at 30, 35, 40 mM BA are shown. Nonlinear regression of the data fit to the Michaelis–Menten equation revealed that K_m were similar but V_{max} decreased.

tively (Fig. 3). The ratio of cADPR to ADP decreased as boric acid concentration increased from 0 to 40 mM, showing that boric acid slowed the conversion of NAD^+ to cADPR (Fig. 4). At 40 mM, boric acid caused a 52% decrease in the activity of ADP-ribosyl cyclase.

Methyl boric acid was used as a negative control for boric acid in the inhibition of ADP-ribosyl cyclase (Fig. 4). At 40 mM, methyl boric acid had no detectable effect on the rate of cADPR formation (Fig. 4). In fact, methyl boric acid partially rescued the activity of ADP-ribosyl cyclase when both boric acid and methyl boric acid were added together as compared to boric acid alone (Fig. 4).

The Lineweaver and Burk plots of ADP-ribosyl cyclase inhibition by boric acid revealed extrapolated intercepts near the x-axis, implying that the inhibition of ADP-ribosyl cyclase by

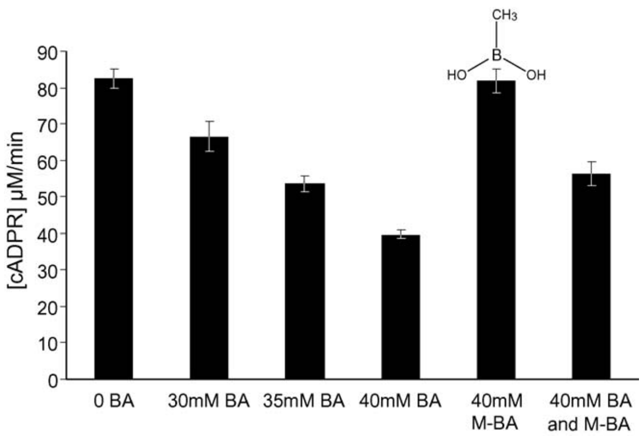

Fig. 4. Methyl boric acid (M-BA) does not inhibit ADP-ribosyl cyclase. The structure of methyl boric acid is shown in the figure. Boric acid (BA) inhibits the enzyme in a dose dependent manner (30–40 mM). The activity of the enzyme inhibited by BA is partially rescued by addition of M-BA ($n = 3$). $[NAD^+] = 2$ mM and reaction time = 0–2 min.

boric acid is mostly non-competitive (Fig. 5). Nonlinear regression of the curves fitted to the Michaelis–Menten equation showed that the K_m remained constant but that V_{max} changed, confirming that non-competitive inhibition occurred (Fig. 5, insert). The apparent K_i was determined to be 40.5 ± 0.5 mM (Eq. (2)).

$$K_i' = \frac{[I]}{(V_{max}/V_{max}') - 1} \tag{2}$$

3.3. ESI-MS analysis of borate complexed with cADPR

In WAT solvent (pH 10.3) the negative ion ESI-MS spectra of 100 μM solutions of cADPR revealed a prominent molecular anion for the singly charged, alkali metal-free molecule $[(M-H)^-]$ at m/z 539.8 (calc. 540.0 Da) (Fig. 6A). Following the addition of $^{11}B(OH)_3$ (500 μM final concentration), the spectra revealed additional signals at m/z 565.7, assigned as the singly charged boric acid-cADPR complex (calc. 566.0 Da for $(M-H)^-$), and m/z 583.7, assigned as a borate-cADPR complex (calc. 584.0 Da for $(M-H)^-$)(Fig. 6B). The sum areas of the m/z 539.8, 565.7, and 583.7 peaks correspond to the mass spectrometric response from the cADPR injected (1×10^{-9} mol). From the known concentrations of cADPR and boric acid, and the measured relative areas of free nucleotide and borate-complexed nucleotide, the concentration of the boric acid/borate-cADPR complex was calculated. Since the concentrations of all the different species in equilibrium (Eq. (3)) were known, the equilibrium constant was calculated (Eq. (4)). The calculated apparent K_A for borate-cADPR complex was 655 ± 99 L/mol.

$$K_{equ} = \frac{[B_{complex}]}{[B_{free}][Nuc_{free}]} \tag{3}$$

$$[Nuc_{total}] = [Nuc_{free}] + [Nuc_{adduct}] + [Nuc_{complexed}] \tag{4}$$

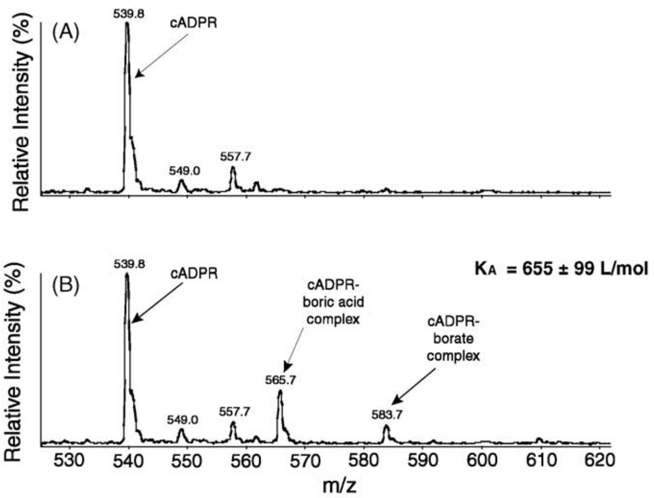

Fig. 6. Negative ion ESI-mass spectra of cADPR and cADPR–boric acid complexes in water:acetonitrile:triethylamine mixtures at pH 10.3. (A) 100 μM cADPR showing an intense $(M-H)^-$ signal at *m/z* 539.8 (calc. 540.0 Da). The signals at *m/z* 549.0 and 557.7 are assigned as unknown impurities in the cADPR sample. (B) A mixture of 100 μM cADPR and 500 μM $^{11}B(OH)_3$ produced signals corresponding to the cADPR–boric acid complex at *m/z* 585.7 (calc. 586.0 Da), and the cADPR–borate complex at *m/z* 583.7 (calc. 584.0). Apparent binding constant, K_A, for the complex formation was calculated to be 655 ± 99 L/mol.

4. Discussion

The source of the cyclase used in this study was *A. californica*, a herbivorous sea hare that lives in protected coves along the California coast. This creature normally inhabits the land-side of wave action in seaweed beds that protect it from predators and furnish a food supply. Fecal pellet analysis have determined that *A. californica* prefers to eat dark brown and green seaweeds pulverized by wave action [37]. Sea water on average contains 4.6 mg B/L [38], and seaweeds bioaccumulate boron, averaging about 94 mg B/kg, a value substantially higher than the boron concentration of more familiar leafy plants like lettuce which contain 1.0 mg B/kg.

In the present study, CE was used for the first time to determine and characterize the inhibition of ADP-ribosyl cyclase by boric acid. In the presence of boric acid, ADP-ribosyl cyclase was non-competitively inhibited, slowing the production of the Ca^{2+} mobilizing cADPR. The high concentrations of boric acid required to inhibit the cyclase in this study may reflect the sea hare's environmental adaptation and preference for consuming and living in a plume of fine sea weed particles. Furthermore, in previous work we showed by ESI-MS and ^{11}B NMR that the binding of boric acid to nucleotides is pH dependent and is significantly increased under more basic conditions [15]. If the pH near the binding site becomes more basic, a lower boric acid concentration would be required to inhibit the enzyme. Studies from CD38, a mammalian homolog of ADP-ribosyl cyclase, have suggested that cADPR production may be involved in regulating insulin secretion [39], muscarinic receptor-mediated Ca^{2+} signaling in pancreatic acinar cells [40], and in chemotaxis in response to the f-met-leu-phe peptide in neutrophils [41]. Furthermore, since cADPR is a Ca^{2+} mobilizing agent, it may even be involved in general biochemical processes such as muscle movement, neurotransmitter release, and cell proliferation [32]. The fact that the production of cADPR by *Aplysia* cyclase can be disrupted by boric acid suggest that the cyclase may be involved in boric acid anti-proliferation effect in human prostate cancer cell [42].

Methyl boric acid was used as a negative control for boric acid. The specificity of boric acid as an inhibitor of the cyclase was apparent as methyl boric failed to inhibit enzyme activity at equivalent concentrations. Furthermore, the use of methyl boric acid allowed controls for ionic strength and other unwanted changes due to the addition of boric acid. Boric acid-inhibited enzyme could be partially rescued by methyl boric acid, suggesting that the two compounds compete for the same binding site on the enzyme. Methyl boric acid has three hydroxyl groups in anionic form (Eq. (5)), and forms monoester bonds with single *cis*-diol groups, whereas boric acid can bind two *cis*-diol groups to form diester bonds (Eq. (1)). This difference is important in plants where a borate atom crosslinks polysaccharide chains through diester bonds formed between opposing apiose residues. This suggests that boric acid inhibition of ADP-ribosyl cyclase may require the formation of a diester bond near the active site.

(5)

Lineweaver and Burk plots were used to show that boric acid inhibited ADP-ribosyl cyclase non-competitively. Cornish-Bowden and Eisenthal plots were also used to confirm that the mode of inhibition was non-competitive (plot not shown) [43,44]. Boric acid has been shown to inhibit several oxidoreductase enzymes all of which use NAD^+ as a co-factor, including alcohol [45], lactate [46], phosphogluconate [47], glucose-6-phosphate [48], glyceraldehyde-3-phosphate [49], and succinate dehydrogenases [50]. The present work adds to this list ADP-ribosyl cyclase, an enzyme that uses NAD^+ as a substrate. The mammalian cyclase, CD38, is a multifunctional enzyme, with both cyclase and hydrolysis activity [6], whereas *Aplysia* ADP ribosyl-cyclase only has cyclase activity [10]. We used standard ADPR and determined its CE migration time to be 19.0 min (data not shown). The absence of a peak at this position in the electrophoretograms showed that the enzyme had no detectable hydrolase activity under the conditions of the assay. The inhibition of cADPR production by boric acid therefore cannot be attributed to alterations in the hydrolase activity of the enzyme.

Nicotinamide, a byproduct of the cyclase reaction, is a known inhibitor of ADP-ribosyl cyclase [51]. The linearity of the initial rate curves from 0 to 2 min showed that nicotinamide did not appreciably inhibit ADP-ribosyl cyclase as the concentration increased over time (data not shown). Upon addition of boric acid, initial rate curves remained linear, revealing that the presence of nicotinamide did not alter the inhibition of ADP-ribosyl cyclase by boric acid. We previously used ESI-MS/MS to observe fragments of the NAD^+-boric acid complex and determined that the binding sites were *cis*-diol groups on the riboses, and not the nicotinamide group [15]. The boric acid would therefore not be expected to interfere with the inhibition activity of nicotinamide on the cyclase. Therefore, these data support an interpretation that boric acid inhibited ADP-ribosyl cyclase directly.

In investigating the inhibitory effect of boric acid on the enzymatic activity of ADP-ribosyl cyclase, the K_m value was calculated to be 1.24 ± 0.05 mM. The apparent K_m derived in this study is greater than those reported by Migaud et al. (135 μM) [20] and Graeff et al. (39 μM) [52]. The reasons for this disparity are unclear. It is possible that the incubation temperature, buffer pH, and buffer concentration may have caused variation in the K_m value. Migaud et al. used 17 °C, Graeff et al. used ambient temperature (23–25 °C), and this study used 37 °C incubation temperatures. Since this enzyme is derived from a sea hare, it is possible that temperatures lower than the body temperature may increases the efficacy of the enzyme. In addition, Migaud et al. used 25 mM HEPES (pH 8) and Graeff et al. used 20 mM Tris (pH 7). In this study, 200 mM Tris (pH 7.4) was used because the high buffer concentration was necessary to control for the pH change after the addition of boric acid. Although there is a variation in the K_m value among these three studies, this study showed that boric acid inhibits ADP-ribosyl cyclase.

Boric acid binds to NAD^+ (1840 ± 110 L/mol) [15] as well as cADPR (655 ± 99 L/mol) (Fig. 6). In most cases, the best way to determine the apparent K_A of a complex formation is by titrating a ligand (i.e. boric acid) up to or through the expected dissociation concentration. In previous work, titration of boric acid to NAD^+ was used to determine that the apparent K_A was 1840 ± 110 L/mol [19], but the titration method could not be used for cADPR because of ion suppression at higher boric acid concentrations. We showed that the apparent K_A determination using a single concentration with $n = 12$ for NAD^+ complexation with boric acid gave a similar value as the titration method. Alkaline pH was employed to optimize the complexation of boric acid to cADPR. For comparison purposes with other nucleotides, the apparent K_A of cADPR with boric acid was also measured in alkaline pH.

The inhibition of ADP-ribosyl cyclase by boric acid is different from general inhibition because the boric acid–NAD^+ complex serves as an inhibitor. We have modified the general non-competitive inhibition model to construct a new model to fit the data (Fig. 7). Methyl boric acid did not inhibit the enzyme but rescued boric acid inhibition because of its competition with boric acid to form a complex with NAD^+ reduced the overall concentration of the boric acid–NAD^+ complex. The mechanism of the inhibition may be further complicated by the fact that boric acid binds cADPR. Since ADP-ribosyl cyclase does not have hydrolase activity the increase in cADPR is proportional to the increase in cADPR–boric acid complex. The increase in cADPR in the presence of boric acid did not cause deviation from the linearity at different reaction time points suggesting that cyclase inhibition was not associated with the formation of a cADPR–boric acid complex. Nevertheless, since cADPR interacts with the ryanodine receptor to release Ca^{2+}, cADPR–boric acid complex could affect its ability to trigger Ca^{2+} release from endoplasmic reticulum.

In order to determine if the high boric acid K_i is an adaptation of the *Aplysia* cyclase it will be necessary to evaluate CD38. The source of the enzyme was *A. californica*, a sea hare that feeds on seaweeds containing high concentrations of boron. Human cell-surface antigen CD38 is a 46 kDa type II glycoprotein with a single transmembrane domain [53]. In contrast to ADP-ribosyl cyclase, CD38 is an ectoenzyme with both NAD^+ glycohydrolase (NADase) and cADPR hydrolase activities that produce ADP-ribose from cADPR. Since CD38 is an ectoenzyme with catalytic domains facing away from the cytoplasm, it would encounter boric acid in the extracellular environment, but this would be expected to be in the micromolar range rather than the millimolar range experienced by *Aplysia*.

In conclusion, the present study determined that boric acid inhibits ADP-ribosyl cyclase non-competitively and binds directly to cADPR. CE proved to be an attractive alternative to HPLC for the analysis of cADPR. The results suggest that boric acid or NAD^+–boric acid complex inhibits ADP-ribosyl cyclase directly, possibly by forming a diester bond near the active site. To determine if the high boric acid K_i is the result of adaptation of *Aplysia* to a high boron environment, it will be necessary to study boric acid inhibition in the mammalian enzyme CD38, which is exposed to lower boron concentrations.

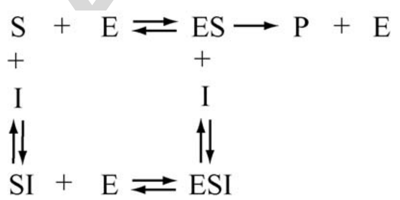

Fig. 7. Non-competitive inhibition model for ADP-ribosyl cyclase inhibition by boric acid. S = NAD^+, E = ADP-ribosyl cyclase, I = boric acid, and P = cADPR.

Acknowledgements

Contract/grant sponsor: UC Toxic Substances Research and Training Grant. Gift from US Borax. We thank Wade Barranco and Kim Henderson for advice and guidance.

References

[1] N. Rusinko, H.C. Lee, J. Biol. Chem. 264 (1989) 11725.
[2] H.C. Lee, R. Aarhus, Biochim. Biophys. Acta 1164 (1993) 68.
[3] W. Masuda, S. Takenaka, S. Tsuyama, H. Inui, K. Miyatake, Y. Nakano, J. Biochem. 125 (1999) 449.
[4] J. Sánchez, P. Duque, N.H. Chua, Plant J. 38 (2004) 381.
[5] H.C. Lee, Biol. Chem. 380 (1999) 785.
[6] H.C. Lee, R. Aarhus, Cell Regul. 2 (1991) 203.
[7] H. Higashida, M. Hashii, S. Yokoyama, N. Hoshi, X.L. Chen, A. Egorova, M. Noda, J.-S. Zhang, Pharmacol. Ther. 90 (2001) 283.
[8] H.C. Lee, Chem. Immunol. 75 (2000) 39.
[9] M. Howard, J.C. Grimaldi, J.F. Bazan, F.E. Lund, L. Santos-Argumendo, R.M. Parkhouse, T.F. Walseth, H.C. Lee, Science 262 (1993) 1056.
[10] E. Zocchi, L. Franco, L. Guida, U. Benatti, A. Bargellesi, F. Malavasi, H.C. Lee, A. De Flora, Biochem. Biophys. Res. Commun. 196 (1993) 1459.
[11] Y. Hirata, N. Kimura, K. Sato, Y. Ohsugi, S. Takasawa, H. Okamoto, J. Ishikawa, T. Kaisho, K. Ishihara, T. Hirano, FEBS Lett. 356 (1994) 244.

[12] M. Itho, K. Ishihara, H. Tomizawa, H. Tanaka, Y. Kobune, J. Ishikawa, T. Kaisho, T. Hirano, Biochem. Biophys. Res. Commun. 203 (1994) 1309.
[13] R. Aarhus, R.M. Graeff, D.M. Dickey, T.F. Walseth, H.C. Lee, J. Biol. Chem. 270 (1995) 30327.
[14] G.S. Prasad, D.E. McRee, E.A. Stura, Nat. Struct. Biol. 3 (1996) 957.
[15] D. Kim, B. Marbois, K. Faull, C. Eckhert, J. Mass Spectrom. 38 (2003) 630.
[16] R. Badugu, J.R. Lakowicz, C.D. Geddes, Bioorg. Med. Chem. 13 (2005) 113.
[17] W. Wang, X. Gao, B. Wang, Curr. Org. Chem. 6 (2002) 1285.
[18] N.D. Winblade, I.D. Nikolic, A.S. Hoffman, J.A. Hubbell, Biomacromolecules 1 (2000) 523.
[19] D. Kim, K. Faull, A. Norris, C. Eckhert, J. Mass Spectrom. 39 (2004) 743.
[20] M.E. Migaud, R.L. Pederick, V.C. Bailey, B.V. Potter, Biochemistry 38 (1999) 9105.
[21] P. Kießling, G.K. Scriba, F. Süß, G. Werner, H. Knoth, M. Hartmann, J. Pharm. Biomed. Anal. 36 (2004) 535.
[22] J.M. Fujima, N.D. Danielson, J. Capillary Electrophor. 7 (2002) 19.
[23] R.M. Graeff, T.F. Walseth, H.K. Hill, H.C. Lee, Biochemistry 35 (1996) 379.
[24] A.A. Suave, C. Munshi, H.C. Lee, V.L. Schramm, Biochemistry 37 (1998) 13239.
[25] K. Schweitzer, G.W. Mayr, A.H. Guse, Anal. Biochem. 299 (2001) 218.
[26] L. Sternfeld, E. Krause, A.H. Guse, I. Schulz, J. Biol. Chem. 278 (2003) 33629.
[27] D.M.F. Savarese, J.T. Russel, A. Fatatis, L.A. Liotta, J. Biol. Chem 267 (1992) 21928.
[28] A.R. Means, FEBS Lett. 347 (1994) 1.
[29] A.D. Short, J. Bian, T.K. Gosh, R.T. Waldron, S.L. Rybak, D.L. Gill, Proc. Natl. Acad. Sci. U.S.A. 90 (1993) 4986.
[30] E. Kohn, R. Allessandro, J. Spoonster, R. Wersto, L. Liotta, Proc. Natl. Acad. Sci. U.S.A. 92 (1995) 1307.
[31] P. Nicotera, B. Zhivotovsky, S. Orrenius, Cell Calcium 16 (1994) 279.
[32] M.J. Berridge, J. Physiol. 499 (1997) 291.
[33] R. Rowe, C. Eckhert, J. Exp. Biol. 202 (1999) 1649.
[34] P. Schmitt-Kopplin, N. Hertkorn, A.W. Garrison, D. Freitag, A. Kettrup, Anal. Chem. 70 (1998) 3798.
[35] S. Hoffstetter-Kuhn, A. Paulus, E. Gassmann, H. Widmer, Anal. Chem. 63 (1991) 1541.
[36] B.J. Glasgow, A.R. Abduragimov, T.N. Yusifov, O.K. Gasymov, J. Horwitz, W.L. Hubbell, K.F. Faull, Biochemistry 37 (1998) 2215.
[37] I. Kato, Y. Yamamoto, M. Fujimura, N. Noguchi, S. Takasawa, H. Okamoto, J. Biol. Chem. 274 (1999) 1869.
[38] Y. Fukushi, I. Kato, S. Takasawa, T. Sasaki, B.H. Ong, J. Biol. Chem. 276 (2001) 649.
[39] S. Partida-Sanchez, D.A. Cockayne, S. Monard, E.L. Jacobson, N. Oppenheimer, Nat. Med. 7 (2001) 1209.
[40] L.R. Winkler, The biology of California sea hares of the genus *Aplysia*, Ph.D. Dissertation, University of Southern California, Los Angeles, CA, 1957.
[41] R.W. Sprague, The Ecological Significance of Boron, U.S. Borax Research Corp., Anaheim, CA, 1972, p. 58.
[42] W.T. Barranco, C.D. Eckhert, Cancer Lett. 216 (2004) 21.
[43] A. Cornish-Bowden, R. Eisenthal, Biochem. J. 139 (1974) 721.
[44] A. Cornish-Bowden, R. Eisenthal, Biochim. Biophys. Acta 523 (1978) 268.
[45] A.H. Roush, B.B. Gowdy, Biochim. Biophys. Acta 52 (1961) 200.
[46] K.W. Smith, S.L. Johnson, Biochemistry 15 (1976) 560.
[47] S. Lee, S. Aronoff, Science 158 (1967) 798.
[48] M.Y. Shkol'nik, N.L. Il'inskaya, Fiziol. Rastenii. 22 (1975) 801.
[49] T. Misawa, H. Kaneshima, M. Akagi, Chem. Pharm. Bull. 14 (1966) 467.
[50] C.J. Shepherd, Biochem. J. (Tokyo) 48 (1951) 483.
[51] J.K. Sethi, R.M. Empson, A. Galione, Biochem. J. 319 (1996) 613.
[52] R. Graeff, T. Walseth, K. Fryxell, W. Branton, H.C. Lee, J. Biol. Chem. 269 (1994) 30260.
[53] D.G. Jackson, J.I. Bell, J. Immunol. 144 (1990) 2811.

Cancer Causes Control
DOI 10.1007/s10552-006-0077-8

ORIGINAL PAPER

Evaluation of ecological and in vitro effects of boron on prostate cancer risk

Wade T. Barranco · Paul F. Hudak · Curtis D. Eckhert

Received: ■ / Accepted: 24 August 2006

Abstract

Objective To determine: (1) the correlation of prostate cancer incidence and mortality with groundwater boron and selenium concentrations; and (2) the impact of boron on prostate cancer cell proliferation during co-treatment with alternative chemo-preventative agents, along with boron pre-treatment effects on cell sensitivity to ionizing radiation.

Methods For regression analysis, data on prostate cancer incidence and mortality were obtained from the Texas Cancer Registry, while groundwater boron and selenium concentrations were derived from the Texas Water Development Board. Cultured DU-145 prostate cancer cells were used to assess the impact of boric acid on cell proliferation when applied in combination with selenomethionine and genistein, or preceding radiation exposure.

Results Groundwater boron levels correlated with a decrease in prostate cancer incidence ($R = 0.6$) and mortality ($R = 0.6$) in state planning regions, whereas selenium did not ($R = 0.1$; $R = 0.2$). Growth inhibition was greater during combined treatments of boric acid and selenomethionine, or boric acid and genistein, versus singular treatments. 8-day boric acid pre-exposure enhanced the toxicity of ionizing radiation treatment, while dose-dependently decreasing the expression of anti-apoptotic protein Bcl-2.

Conclusions Increased groundwater boron concentrations, across the state of Texas, correlate with reduced risk of prostate cancer incidence and mortality. Also, boric acid improves the anti-proliferative effectiveness of chemo-preventative agents, selenomethionine and genistein, while enhancing ionizing radiation cell kill.

Keywords Boron · Selenium · Prostate cancer · Texas · Groundwater · Ionizing radiation · Bcl-2 · Genistein · Ecological

Introduction

The development of public health strategies, for the prevention and control of prostate cancer, has been hindered by a gap in our understanding of factors responsible for the large geographical disparity in disease risk. It is estimated that there will be 232,090 new U.S. cases in 2005, along with significant regional variability in incidence and mortality [1].

Environmental exposure, by way of dietary intake, is receiving much attention as a contributor to prostate cancer prevention [2]. Several natural, plant-derived products are currently in clinical prevention trials, including: (n–3) polyunsaturated fatty acids, flaxseed, vitamin E, selenomethionine (SeM), soy protein isolate, isoflavones, genistein, lycopene and low-fat diets [3–5]. The largest prostate cancer clinical trial, SELECT, will determine the effectiveness of SeM and

W. T. Barranco · C. D. Eckhert (✉)
Department of Environmental Health Sciences, University of California, Los Angeles, CA 90095-1772, USA
e-mail: ceckhert@ucla.edu

P. F. Hudak
Department of Geography and Environmental Science Program, University of North Texas, Post Office Box 305279, Denton, TX 76203-5279, USA
e-mail: hudak@unt.edu

Journal : 10552 Dispatch : 20-9-2006 Pages : 7
Article No. : 0077 ☐ LE ☐ TYPESET
MS Code : CACO548R2 ☑ CP ☑ DISK

vitamin E supplementation in 35,000 men, over a 12-year period [2, 4].

Recently, boron (B), a metalloid element like selenium (Se), has been identified as a prostate cancer chemo-preventative agent. In a study based on the NHANES III database, the risk of prostate cancer was reported to be inversely proportional to dietary intake of B [6]. Studies have also shown that boric acid (BA), the chemical form of B in physiological fluids, reduced the growth of LNCaP-seeded tumors in nude mice, along with IGF-1 tissue concentrations and serum levels of prostate specific antigen (PSA) [7, 8]. Finally, using human prostate cancer cell lines, BA inhibited cell proliferation dose-dependently in androgen-dependent (LNCaP) and androgen-independent (DU-145 and PC-3) cells, without inducing cell death [9].

The B content of plants reflects both the soil concentrations in which they are grown, and the B levels of water applied during irrigation. B serves as an essential nutrient for plant growth, pollen tube formation and flowering, with deficiencies contributing to crop failures worldwide. B essentiality in plants is based on its role in maintaining the structure of scaffolding polysaccharides in the pectin of the cell wall that enable cells to resist the high turbid pressure associated with cell elongation. Monomers of the complex carbohydrate, rhamnogalacturonan, are cross-linked using borate-diol diester linkages between the two hydroxyl groups, located on apiose sugars of opposing polysaccharide chains [10, 11]. The rhamnogalacturonan II (RG-II) dimer is present in all human food plants, while being particularly abundant in vegetables and seed crops (legumes, nuts and carrots), as well as plant-based beverages (wine, fruit drinks and coffee). Furthermore, a borate transporter has been identified which traffics BA from plant roots to shoots [12].

In U.S. adult males, 31–70 years of age, the average daily intake of B from foods is 1.4 mg/day. Drinking water can contribute significantly to this value; yet unlike diet, groundwater chemistry at a particular location may be stable for long time periods, and its usage is often restricted to narrow geographical areas, thus making it a reputable data source [13, 14]. A recent study documented high B and Se concentrations in South Texas groundwater supplies, prompting us to correlate statewide groundwater B and Se levels with geographically variant prostate cancer risk [15]. In addition, we explored the biological relevance of this observation in studies comparing the anti-proliferative properties of BA exposure, in combination with SeM, genistein and radiation treatments, in human prostate cancer cells.

Materials and methods

B and Se water sampling

Data for linear regression analysis of average B and Se, in groundwater samples of Texas counties and state planning regions, was derived from the Groundwater Database of the Texas Water Development Board, http://www.twdb.state.tx.us. Sampling dates varied at wells evaluated for dissolved B (1939–2004) and dissolved Se (1964–2004). Multi-sampled wells were included in the analysis. The template for the B groundwater distribution map was acquired from the Texas Association of Regional Councils (TARC) website, http://www.txregionalcouncil.org.

Texas cancer statistics

Cancer incidence and mortality data have been provided by the Texas Cancer Registry, Cancer Epidemiology and Surveillance Branch, Texas Department of State Health Services, 1100 W. 49th Street, Austin, Texas, 78756, http://www.dshs.state.tx.us/tcr, or (512) 458–7,523. Prostate cancer incidence and mortality rates (1997–2001), for each county and state planning region were derived from the Texas Cancer Registry.

Cell culture

DU-145 prostate cancer cells, donated by Dr. Allan Pantuck, were cultured in RPMI 1640 media (Invitrogen) supplemented with 10% FBS, penicillin/streptomysin (100 U/ml; 100 μg/ml), and L-glutamine (200 mM) (Gemini Bioproducts, Woodlands, CA).

Experimental culture

BA and SeM stock solutions were prepared in ultrapure water. Genistein stock was prepared in DMSO, while solvent concentration in media (0.1%) was predetermined to be nontoxic. Prior toxicity evaluation of reagents, for doses imposing a 25–50% reduction in cell growth, led to the concentrations applied during experimentation. Experimental cells were cultured for eight days in treated media, with media replacement occurring daily. On day 8, cells were counted with a hemacytometer, while utilizing Trypan blue (Invitrogen) for exclusion of dead cells.

Ionizing radiation exposure

DU-145 cells were cultured in BA-supplemented media (0, 100, and 500 μM) for 8 days, in 12-well

Journal : 10552 Dispatch : 20-9-2006 Pages : 7
Article No. : 0077 ☐ LE ☐ TYPESET
MS Code : CACO548R2 ☑ CP ☑ DISK

culture plates (Fisher), with daily media replacement. On day 8, media was aspirated partially and adherent cells were exposed to 1, 3 and 5 Gy's of ionizing radiation from a ^{137}Cs gamma ray source. Following exposure, cells were trypsinized, re-seeded onto 601×5 mm plates ($1–3 \times 10^4$ cells/plate), and cultured for nine days in low-B media. Adherent colonies were washed with PBS, fixed in methanol (10 min), allowed to air-dry following methanol removal, submerged in Giemsa stain (30 s), washed with PBS (8 min), and rinsed with de-ionized water. Stained colonies were counted without microscopic aid.

Western blot

DU-145 cells, in the presence of BA (0–1,000 (M), were cultured for seven days on 100×20 mm tissue culture plates, with daily media replacement. On day seven, near-confluent monolayers were washed with PBS, scraped off with a rubber policeman, and centrifuged for 5 min at 1,200 rpm. Pellets were lysed (250 mM NaCl, .1% NP40, 50 mM HEPES (pH 7.0), 5 mM EDTA, 1 mM DTT, 10% protease inhibitor mixture (Sigma # P8340)), sonicated, and incubated for 40 min at 4°C for protein extraction. 30 μg of protein was loaded per lane and separated on a 10% stacking, 12% separating (SDS-PAGE) gels for 30 min at 100 V, followed by 1 h at 200 V. Proteins were transferred onto nitrocellulose membranes for 4 h at 40 V, 4°C. Following overnight blocking of membranes (4 g nonfat dry milk, 38 mM Tris base, 125 mM NaCl 2.5, 100 μl Tween 20, 100 ml ddH_2O), a 2-hour primary antibody exposure (1/800 dilution) was applied, with nitrocellulose membranes subsequently being washed for 10 min in PBS/Tween 20 (0.1%). Membranes were then probed with a secondary antibody for 1 h (1/1,000 dilution), followed by 3×10 min washes in PBS/Tween 20 (0.1%). Membranes were subsequently submerged in ECL detection reagent (Amersham Int), wrapped in cellophane and exposed to X-ray film (Fuji). Bcl-2 and B-actin antibodies were purchased from Santa Cruz Biotechnology (Santa Cruz, CA).

Statistical analysis

SigmaStat 3.1 statistical software (Systat Software, Point Richmond, CA) was utilized for the following analyses: one-way analysis of variance, paired *t*-test, and linear regression analysis with correlation.

Results

Texas B and Se groundwater levels & prostate cancer rates

Linear regression analysis of prostate cancer incidence and mortality rates, as a function of average B and Se groundwater levels per state planning region, is shown in Fig. 3. Prostate cancer incidence and mortality is inversely correlated with B groundwater levels, with R values of 0.63 and 0.598, respectively (Fig. 1A, B). The predicted linear regression passed both ANOVA and *t*-tests (*P*-value < 0.002). In contrast, linear regression analysis of prostate cancer incidence and mortality, as a function of groundwater Se levels (Fig. 1C, D), showed no statistically relevant correlation, with *R* values of 0.144 and 0.154, respectively; while failing both ANOVA and *t*-tests (*P*-value > 0.4).

Cell proliferation

BA (250 μM) was evaluated singularly and in combination with SeM (15 μM) and genistein (15 μM), with respect to proliferative inhibition of DU-145 cells (Fig. 2). Cell proliferation, when cultured in the presence of SeM and BA, was significantly reduced relative to either compounds treatment alone; while pre- and post-treatment with BA had negligible inhibitory effects, relative to one another. As with SeM, BA and genistein co-administration induced a semi-additive proliferative inhibition; whereas pretreatment with BA sensitized cells to genistein toxicity, while the reverse treatment was less toxic.

Ionizing radiation sensitivity

DU-145 cells exposed to ionizing radiation (1, 3, and 5 Gy), following 8-days in culture with 0–500 μM BA, displayed enhanced sensitivity to induced gross toxicity (Fig. 3A). Relative to control cells, BA pre-treatment dose-dependently reduced the number of viable cells capable of seeding and proliferating into detectable colonies. Also, following a 7-day exposure to BA (0–1,000 μM), DU-145 cells displayed a dose-dependent reduction in Bcl-2 protein expression (Fig. 3B).

Discussion

The consistent quality of groundwater, in equilibrium with its environment, makes it an attractive choice for assessing health effects displaying strong geographic

Journal : 10552 Dispatch : 20-9-2006 Pages : 7
Article No. : 0077 LE TYPESET
MS Code : CACO548R2 CP DISK

Fig. 1 Scatter plots of mean groundwater B (**A**, **B**) and Se (**C**, **D**) concentrations in Texas state planning regions, as a function of prostate cancer incidence and mortality. *y*-axis represents the average annual age-adjusted (to the 2,000 U.S. standard population) prostate cancer incidence and mortality rates per 100,000 people. Dotted line represents 95% confidence interval, while solid line represents the linear regression

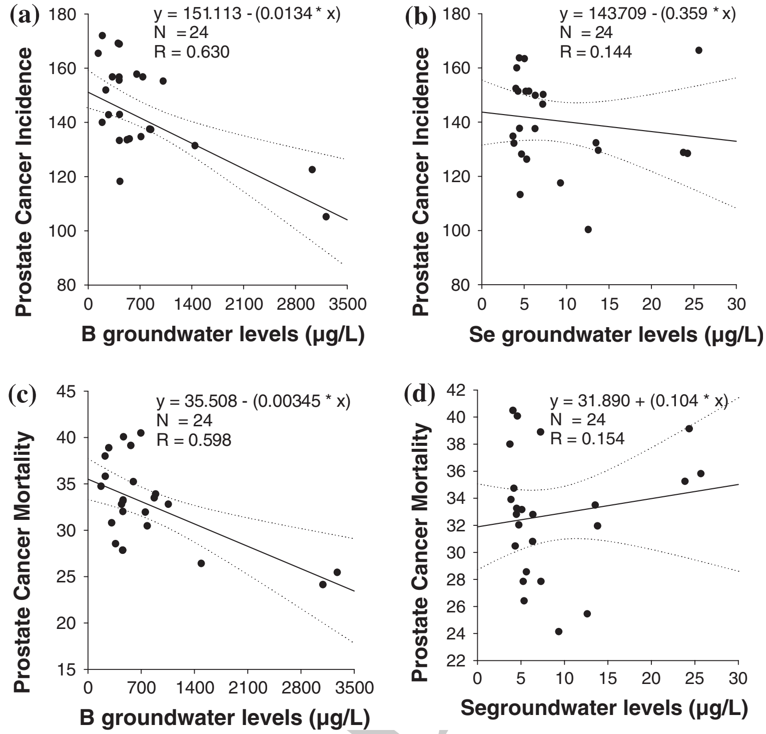

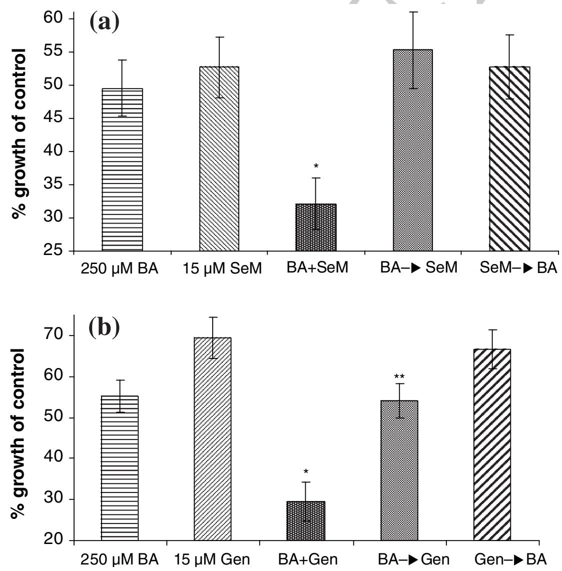

Fig. 2 Effects of 8-day exposure to 250 μM BA, in combination with 15 μM selenomethionine (SeM), (**A**) and 60 μM genistein (Gen), (**B**), on the proliferation of cultured DU-145 prostate cancer cells. Cells were treated with BA alone (BA); with the alternative compound alone (SeM or Gen); with both compounds simultaneously (BA + SeM or Gen); and in sequence, with BA treatment for the 1st 4 days followed by alternative compound for the last 4 days (BA ►SeM or Gen), and the reverse sequence (SeM or Gen ►BA). Mean (sem, $n = 6$. *Statistically significant from single exposures (P-value < 0.003). **Statistically significant from reverse sequence exposure (P-value < 0.04)

associations. In Texas, groundwater provides 60% of the water supply for drinking and irrigation, and varies in B concentration across the state (30–16,200 μg B/L) [5]. This wide range provided an opportunity to assess prostate cancer risk, as a function of groundwater B concentrations. The geographical distribution of groundwater B across the state of Texas is indicated with regions of higher B in darker hues (Fig. 4). Areas with relatively high groundwater B concentrations occupy portions of central and south Texas. These central

Journal : 10552 Dispatch : 20-9-2006 Pages : 7
Article No. : 0077 LE TYPESET
MS Code : CACO548R2 CP DISK

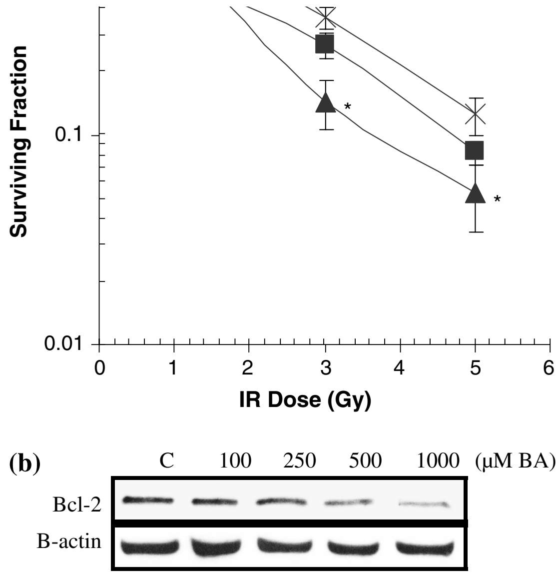

Fig. 3 Effects of 8-day BA pre-treatment on the killing efficiency of ionizing radiation, and Bcl-2 protein expression, in DU-145 prostate cancer cells. (**A**), BA pre-treatments of 0 μM (X), 100 μM (■), and 500 μM (▲) were applied prior to ionizing radiation exposure (0–5 Gy); mean ± sem, $n = 4$. *Statistically significant from 0 μM pre-treatment at like radiation exposure (P-value > .005). (**B**) Cells given 7-day treatments of BA (0–1,000 μM) were evaluated for Bcl-2 protein expression by western blot

and southern areas overlap portions of the Trinity Group and Gulf Coast Aquifers, respectively. Both aquifers comprise sediment deposited in fluvial, deltaic, and shallow marine environments. Portions of the Trinity Group also contain carbonates and evaporites. Brackish seawater trapped in marine sediment and evaporites are possible sources of B [16]. A previous investigation attributed high groundwater B concentrations in south Texas to naturally occurring, brackish water in the Gulf Coast Aquifer [15].

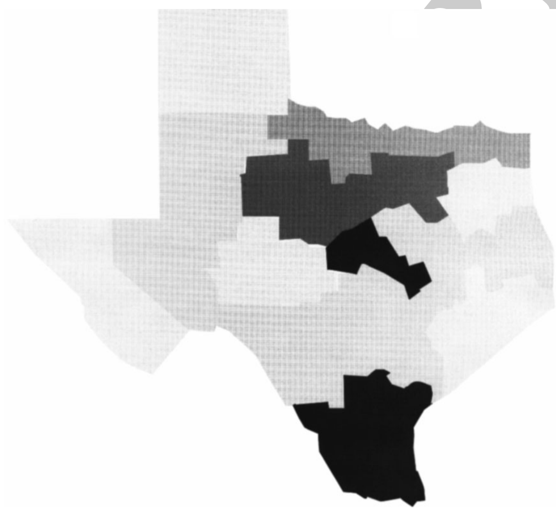

Fig. 4 Geographical distribution of groundwater B concentrations across Texas, relative to state planning regions. Groundwater B levels: 100–400 μg/l ( ), 400–600 μg/l ( ), 600–800 μg/l ( ),800–1,000 μg/l (■), > 1,000 μg/l (■).

One of the limitations of this study was that large cities, including Houston, Dallas-Fort Worth and Austin, receive the majority of their drinking water from surface sources of inconsistent quality. A second limitation was the number of Afro-American and Hispanic men residing in rural counties and planning regions was too small to allow analysis of prostate cancer rates in ethnic sub-populations, as a function of the state's groundwater geography. Higher rates of prostate cancer were not observed in areas of low median family income in south Texas were groundwater levels of boron were high. In addition to potential ethnic and demographic cofounders, environmental factors could also contribute to the observed cancer rates. For example, poor air quality in the Houston area of southeast Texas could contribute to higher observed cancer rates in that region.

In Texas, counties are grouped into state planning regions for the purpose of water supply and quality planning, health resource distribution, and assessment of the geographic adequacy of facilities, providers, and cancer services [17]. We compiled prostate cancer incidence and mortality rates using data from the Texas Cancer Registry [18], and B groundwater concentrations from the Texas Water Development Board [19], for the 24 planning regions of the state. When groundwater concentrations were plotted relative to the state planning regions, statistical analysis showed the data were normally distributed, and the inverse correlations of prostate cancer incidence ($R = 0.6$) and mortality ($R = 0.6$), with groundwater B, were highly significant ($P < 0.002$). Planning region B groundwater concentrations, along with the empirically-derived water consumption values of 3.6 l/d for males between 51 and 70 y, predict a B intake ranging from 619 μg B/d to 11,979 μg B/d in regions utilizing groundwater as their major drinking water source [20]. This 19-fold variance in B intake coincided with a 37% difference in prostate cancer incidence, and falls within the safe range of B ingestion even after adding in the dietary component of 1.4 mg B/d [14].

The correlation between groundwater Se and prostate cancer incidence and mortality rates was non-significant. Consumption of 3.6 l/d would have provided a mean inorganic Se intake of 36 μg/day with a range of 10–98.6 μg/day. The recommended dietary intake of Se is 55 μg/day so this range should have provided a sufficient gradient to observe an effect of inorganic Se on prostate cancer incidence should one exist [21]. Others have reported a de-

Journal : 10552 Dispatch : 20-9-2006 Pages : 7
Article No. : 0077 □ LE □ TYPESET
MS Code : CACO548R2 ✔ CP ✔ DISK

crease in the incidence of prostate cancer in men living in regions of low soil Se content subsequent to dietary supplementation with an organic form of Se, SeM [22]. Until the mechanism is discovered through which Se achieves its protective effect, a more explicit explanation for the absence of an effect cannot be provided. The favored explanation, at present, is that Se protects through its antioxidant enzymes, primarily the glutathione peroxidases. However, Se is also anti-angiogenic and protects against basement membrane thickening [2, 23].

Knowledge of the relative effectiveness of anticancer agents is important for understanding both their mode of action, and identifying possible inhibitory interactions with alternative treatments. The potential of BA to interfere with SeM and genistein's capacity to inhibit cell proliferation was studied using DU-145 human prostate cancer cells. Rather than blocking their induced growth inhibition, BA exhibited a semi-additive effect when administered simultaneously with SeM and genistein. Although sequential treatments with SeM and BA did not display statistical differences in effectiveness, BA treatment followed by genistein enhanced proliferative inhibition. Radiation therapy is frequently used, alone and in combination with chemical reagents, for treatment of both localized and metastatic prostate tumors [24]. Cell kill resulting from gamma irradiation of DU-145 prostate cancer cells has been shown to be enhanced when cells are pre-treated with genistein and selenite [25, 26]. The same positive effect occurred when cells were pretreated with BA, prior to ionizing radiation exposure. Because a ^{137}Cs source of gamma irradiation was utilized for exposures, rather than a pulse of neutrons, ^{10}B nuclei fractionization was not a contributor to the observed toxicity, as occurs during the administration boron neutron capture therapy [27].

Bcl-2 has been established as an anti-apoptotic protein and one that conveys resistance to radiotherapy in prostate cancer patients [28, 29]. Supporting Bcl-2's role in ionizing radiation-induced cell death, curcumin acts both as a down-regulator of Bcl-2 expression and a sensitizer to ionizing radiation kill in PC-3 prostate cancer cells [30]. We examined Bcl-2 expression in DU-145 cells subjected to prolonged BA treatments, and found protein concentrations to be reduced in a dose-dependent manner. This suggests that BA functions as a sensitizer to radiation treatment by inhibiting Bcl-2. The cell death most likely occurred through a pathway that did not involve Bcl-2 because DU-145 cells treated with either a Bcl-2 antisense oligonucleotide or BA undergo proliferation inhibition without cell death [9, 31, 32].

In conclusion, groundwater B concentrations are inversely correlated with prostate cancer incidence and mortality rates in the state of Texas. When applied in combination with SeM and genistein, BA enhances the ability of either reagent to inhibit DU-145 cell proliferation, while prior treatment of cells with BA sensitizes to ionizing radiation kill.

Acknowledgments We thank Dr. Allan Pantuck and Randy Kallilew for their expertise concerning the culturing of prostate cancer cells, along with Kurt Hafer and Cecelia Chan for aiding in the administration of ionizing radiation. Funding for this research was provided by: DOD prostate idea grant DAMD17–03-1-0067 (CD Eckhert) and UC TRS&TP (WT Barranco). In the spirit of full disclosure, we declare that since 1997 the National Institutes of Health has without exception declined funding of all grant applications submitted by CE on the role of boron in biology or cancer with recent applications triaged prior to full review.

References

1. Jemal A, Murray T, Ward E, et al. (2005). Cancer statistics. CA Cancer J Clin 55(1):10–30
2. Willis MS, Wians FH (2004) The role of nutrition in preventing prostate cancer: a review of the proposed mechanism of action of various dietary substances. Clinica Chimica Acta 330: 57–83
3. Djavan B, Zlotta A, Schulman C, et al. (2004) Chemotherapeutic prevention studies of prostate cancer. J Urol 171(2 Pt 2): S10–S13
4. Klein EA, Thompson IM, Lippman SM, et al. (2001) SELECT: the next prostate cancer prevention trial. Selenium and Vitamin E Cancer Prevention Trial. J Urol 166(4): 1311–1315
5. http://www.clinicaltrials.gov
6. Cui Y, Winton MI, Zhang ZF et al. (2004) Dietary boron intake and prostate cancer risk. Oncol Rep 11(4): 887–892
7. Gallardo-Williams MT, Chapin RE, King PE, et al. (2004) Boron supplementation inhibits the growth and local expression of IGF-1 in human prostate adenocarcinoma (LNCaP) tumors in nude mice. Toxicol Pathol 32: 73–78
8. Gallardo-Williams MT, Maronpot RR, Wine RN, Brunssen SH, Chapin RE (2003) Inhibition of the enzymatic activity of prostate specific antigen by BA and 3-nitrophenyl boronic acid. Prostate 54: 44–49
9. Barranco WT, Eckhert CD (2004) BA inhibits human prostate cancer cell proliferation. Cancer Lett 216(1): 21–9
10. Kobayashi M, Matoh T, Azuma J (1996) Two chains of rhamnogalacturonan II are cross-linked by borate-diol ester bonds in higher plant cell walls. Plant Physiol 110(3): 1017–1020
11. O'Neill MA, Warrenfeltz D, Kates K, et al. (1997) Rhamnogalacturonan-II, a pectic polysaccharide in the walls of growing plant cell, forms a dimer that is covalently cross-linked by a borate ester. In vitro conditions for the formation and hydrolysis of the dimer. J Biol Chem 271(37): 22923–22930
12. Takano J, Noguchi K, Yasumori M, et al. (2002) Arabidopsis boron transporter for xylem loading. Nature 420(6913): 337–340

Journal : 10552 Dispatch : 20-9-2006 Pages : 7
Article No. : 0077 □ LE □ TYPESET
MS Code : CACO548R2 ✔ CP ✔ DISK

13. Anderson DL, Cunningham WC, Lindstrom TR (1994) Concentrations and intakes of H, B, S, K Na, Cl, and NaCl in foods. J Food Comp Anal 7: 59–82
14. Dietary reference intakes for vitamin A, vitamin K, arsenic, boron, chromium, copper, iodine, iron, manganese, molybdenum, nickel, silicon, vanadium, and zinc. A report of the panel on micronutrients, subcommittees on upper reference levels of nutrients and of interpretation and use of dietary reference intakes, and the standing committee on the scientific Evaluation of dietary reference Intakes. (2001) Food and Nutrition Board, Institute of Medicine, National Academy Press, Washington, D.C., p C-13
15. Hudak PF (2004) Boron and selenium contamination in south Texas groundwater. J Environ Sci Health A Tox Hazard Subst Environ Eng 39(11–12):2827–2834
16. Hem JD (1985) Study and interpretation of the chemical characteristics of natural water. U.S. Geological Survey Water Supply Paper 2254
17. http://www.tcc.state.tx.us/tcplan/goal2/goal2_obje_frames.html
18. http://www.dshs.state.tx.us/tcr, accessed May 31, 2005
19. http://www.twdb.state.tx.us, accessed May 31, 2005
20. Panel on Dietary Reference Intakes for Electrolytes and Water. (2004) Dietary reference intakes for water, potassium, sodium, chloride, and sulfate. National Academies Press, Washington, D.C., p 494.
21. Dietary Reference Intakes for Vitamin C, Vitamin E, Selenium, and Carotenoids. (2000) Selenium. National Academies Press, Washington, D.C., p. 284.
22. Clark LC, Dalkin B, Krongrad A, et al. (1998) Decreased incidence of prostate cancer with selenium supplementation: results of a double-blind cancer prevention trial. Br J Urol 81: 730–734
23. Eckhert CD, Lockwood MK, Shen B (1993) Influence of selenium on the microvascular circulation of the retina. Microvas Res 45: 74–82
24. Bischof M, Abdollahi A, Gong P, et al. (2004) Triple combination of irradiation, chemotherapy (pemetrexed), and VEGFR inhibition (SU5416) in human endothelial and tumor cells. Int J Radiat Oncol Biol Phys 60(4):1220–1232
25. Yan SX, Ejima Y, Sasaki R, et al. (2004) Combination of genistein with ionizing radiation on androgen-independent prostate cancer cells. Asian J Androl 6(4): 285–290
26. Husbeck B, Peehl DM, Knox SJ (2005) Redox modulation of human prostate carcinoma cells by selenite increases radiation-induced cell killing. Free Radic Biol Med 38(1):50–57
27. Bendel P (2005) Biomedical applications of 10B and 11B NMR. NMR Biomed 18(2): 74–82
28. Rudner J, Jendrossek V, Belka C (2002) New insights in the role of Bcl-2 Bcl-2 and the endoplasmic reticulum. Apoptosis 7(5): 441–447
29. Rosser CJ, Reyes AO, Vakar-Lopez F et al (2003) Bcl-2 is significantly overexpressed in localized radio-recurrent prostate carcinoma, compared with localized radio-naive prostate carcinoma. Int J Radiat Oncol Biol Phys 56(1): 1–6
30. Chendil D, Ranga RS, Meigooni D, Sathishkumar S, Ahmed MM (2004) Curcumin confers radiosensitizing effect in prostate cancer cell line PC-3. Oncogene 23(8): 1599–1607
31. Campbell MJ, Dawson M, Koeffler HP (1998) Growth inhibition of DU-145 prostate cancer cells by a Bcl-2 antisense oligonucleotide is enhanced by N-(2-hydroxyphenyl) all-trans retinamide. Br J Cancer 77(5): 739–744
32. Raffo A, Lai JC, Stein CA, et al. (2004) Antisense RNA down-regulation of bcl-2 expression in DU145 prostate cancer cells does not diminish the cytostatic effects of G3139 (Oblimersen). Clin Cancer Res May 10(9): 3195–3206

Journal : 10552	Dispatch : 20-9-2006	Pages : 7
Article No. : 0077	☐ LE	☐ TYPESET
MS Code : CACO548R2	☑ CP	☑ DISK